INFORMATION TO USERS

This material was produced from a microfilm copy of the original document. While the most advanced technological means to photograph and reproduce this document have been used, the quality is heavily dependent upon the quality of the original submitted.

The following explanation of techniques is provided to help you understand markings or patterns which may appear on this reproduction.

1. The sign or "target" for pages apparently lacking from the document photographed is "Missing Page(s)". If it was possible to obtain the missing page(s) or section, they are spliced into the film along with adjacent pages. This may have necessitated cutting thru an image and duplicating adjacent pages to insure you complete continuity.

2. When an image on the film is obliterated with a large round black mark, it is an indication that the photographer suspected that the copy may have moved during exposure and thus cause a blurred image. You will find a good image of the page in the adjacent frame.

3. When a map, drawing or chart, etc., was part of the material being photographed the photographer followed a definite method in "sectioning" the material. It is customary to begin photoing at the upper left hand corner of a large sheet and to continue photoing from left to right in equal sections with a small overlap. If necessary, sectioning is continued again — beginning below the first row and continuing on until complete.

4. The majority of users indicate that the textual content is of greatest value, however, a somewhat higher quality reproduction could be made from "photographs" if essential to the understanding of the dissertation. Silver prints of "photographs" may be ordered at additional charge by writing the Order Department, giving the catalog number, title, author and specific pages you wish reproduced.

5. PLEASE NOTE: Some pages may have indistinct print. Filmed as received.

University Microfilms International
300 North Zeeb Road
Ann Arbor, Michigan 48106 USA
St. John's Road, Tyler's Green
High Wycombe, Bucks, England HP10 8HR

7822907

GUNNING, JOHN EDMUND
THE STRUCTURE OF AMORPHOUS ARSENIC AS
DETERMINED BY THERMAL NEUTRON SCATTERING.

THE UNIVERSITY OF MICHIGAN, PH.D., 1978

University
Microfilms
International 300 N. ZEEB ROAD, ANN ARBOR, MI 48106

THE STRUCTURE OF AMORPHOUS ARSENIC AS DETERMINED BY THERMAL NEUTRON SCATTERING

by

John Edmund Gunning

A dissertation submitted in partial fulfillment
of the requirements for the degree of
Doctor of Philosophy
(Nuclear Engineering)
in The University of Michigan
1978

Doctoral Committee:

John M. Carpenter, Co-chairman
Program Director: Intense Pulsed Neutron Source
Argonne National Laboratory
Professor Dietrich H. Vincent, Co-chairman
Assistant Professor Brenton Mattes
Professor George C. Summerfield
Charles Pelizzari
Assistant Scientist, Argonne National Laboratory

For Susan

ACKNOWLEDGEMENTS

The author would like to acknowledge the financial assistance provided by National Science Foundation Grant GK-35901 during his stay at the University of Michigan. He is also grateful to Argonne National Laboratory Center for Educational Affairs for its support in the form of a Laboratory Graduate Participantship.

Gratitude is due to Dr. Jack Carpenter for his continuing guidance during the pursuit of this thesis. Finally, I would like to thank Midge Thompson for her persistent typing of this manuscript.

TABLE OF CONTENTS

DEDICATION ii

ACKNOWLEDGEMENTS iii

LIST OF APPENDICES vi

CHAPTER

I. INTRODUCTION 1

II. THEORY 8

2.1 Introduction
2.2 Static Structure Factor
2.3 Double Differential Cross Section

III. EXPERIMENT 21

3.1 Single Wavelength Diffraction
3.2 The Single Wavelength Diffractometer
3.3 Time of Flight Diffraction
3.4 The CPS Time of Flight Diffractometer
3.5 The ZING-P Time of Flight Diffractometer

IV. ANALYSIS 36

4.1 Introduction
4.2 Cross Sections
4.3 Multiple Scattering and Attenuation Corrections
4.4 Inelastic Scattering Corrections
4.4.1 Introduction
4.4.2 Form of Correction Factors
4.4.3 Model of the Scattering Law
4.4.3.1 General
4.4.3.2 Model Density of States
4.4.3.3 Debye Waller Factor
4.4.3.4 Elastic Scattering
4.4.3.5 One Phonon Scattering
4.4.3.6 Multiphon Scattering
4.4.4 Results of the Model

V. RESULTS 92

5.1 General
5.2 Single Wavelength Diffraction
5.3 Time of Flight Diffraction
5.4 The Joined Result: Total Diffraction Pattern
5.5 Fourier Transform of the Structure Factor
5.6 Comparison to Existing Models

VI. CONCLUSIONS 133

APPENDIX 139

REFERENCES 149

LIST OF APPENDICES

I. Acoustic Velocity Determination of Amorphous Arsenic

II. Comparison of the Path Integral Method of Inelastic Scattering Correction to a Formulation by Sinclair and Wright

CHAPTER I

Introduction

Amorphous materials have become of increasing technological and theoretical interest in recent years. Everyone is familiar with glassware and window glass which are amorphous forms of silicon dioxide with other added materials--these are the technical glasses. Amorphous magnets and amorphous switching devices are presently being developed. The possibility of large scale use of amorphous silicon photoelectric cells has stirred the imagination of many people. Even though amorphous materials have been utilized extensively for a millenium of time, the theoretical understanding of their microscopic properties has lagged far behind that of crystalline materials.

The prime reason that the theory of crystalline properties has developed to such a high level is that most problems can be attacked by treating one unit cell of the material. This immediately reduces the problem by a factor of $\sim 10^{23}$ and makes it amenable to solution. Amorphous materials, on the other hand, do not consist of regular periodic arrays and thus cannot be treated so simply. The electronic structure theory of amorphous materials is still

in its infancy and it is not yet clear whether to treat the electronic structure from a band theory or chemical bond point of view. Independently of which point of view is taken, the physical structure of the material must always enter as an input. Similarly structural information must enter theories other than those relating to electronic properties, such as lattice vibrations and specific heats.

It is this need for high quality structural data that has initiated x-ray, electron, and neutron scattering experiments from these materials. The information that we may obtain is more limited than that available from a single crystal because the material as a whole is isotropic. The measurement we make is in effect an average over all directions. Thus, the diffraction pattern that we measure can have a functional dependence on only one variable, the magnitude of the wave vector transfer Q. (Q is a variable commonly used in diffraction that eliminates the need to specify both the wavelength and the angle at which a measurement was made. This quantity is defined as

$$Q = \frac{4\pi \sin(\Theta S/2)}{\lambda}$$

where Θ_S is the scattering angle and is the wavelength of the neutron.) If we take the Fourier transform of the diffraction pattern we obtain the radial density function as will be explained later. The radial density function (RDF) is a measure of the distribution of atom to atom distances. At this point we run into a problem if we have a

material that consists of more than one element. If a material is made of A and B it is difficult to determine directly from the measurement whether a peak in the RDF is an A-A distance, a B-B distance or an A-B distance. However, if a material is monoatomic this ambiguity does not arise. Thus, monoatomic materials are of large importance for fundamental studies because measurements from them give unique results. Polyatomic materials can be understood in detail with the assistance of models or in simple cases, with the assistance of only chemical information.

The elements in the IV, V, and VI groups of the periodic table tend to form semiconductors and semimetals because they are between the conducting metals and the insulating noble gases. Because of this midway point between a conductor and an insulator the properties of the materials are rather sensitive to the physical structure. The group VI elements (chalcogens), tend to be 2 coordinates and thus form long chains. They are also relatively easily made into a noncrystalline form. I did some initial experiments making amorphous sulfur, but quickly decided I was opening Pandora's box. Sulfur forms chains of length greater than 10^6 atoms and is thus not very amenable to a continuous random network modeling.

The group V elements (pnictides) are semimetals in their crystalline form. Phosphorous, arsenic, and antimony can be made amorphous without great difficulty. Amorphous phosphorous is in fact the most common form of phosphorous.

Indeed there are a number of different forms of amorphous phosphorous. Arsenic, of course, is the material of interest in this thesis. It is a semiconductor in its amorphous form.

Boron, although it is in group III, is of interest because it is also a semiconductor. Amorphous boron also can be made without difficulty. The possibility of using boron as the host material of a semiconduction junction, doping with beryllium and silicon, and then using as a neutron detector seems to be a po-sibility. Although this application is not necessarily dependent upon the amorphous phase of the material, it is of interest because of the possibility of thin, large area, high efficiency neutron detectors.

The materials that have generated the most interest are two members of group IV, silicon and germanium. Silicon in particular has come to dominate the semiconductor industry and thus has wide ranging technological applications. In its amorphous form silicon has lately become important because of the possibility of large scale manufacture of photovoltaic devices (Spear and LeComber, 1975; Speer et al, 1976; Carlson and Wronski, 1976). The properties of an amorphous material can be altered, and thus they can be tailored to fit the needs of the particular application desired. It also appears that the large scale manufacture of thin films of amorphous silicon would be much less expensive than the traditional method of solar cell manufacture from single crystals.

An interesting aspect of the problem of understanding the structure of amorphous silicon, from a neutronic point of view, is the role of hydrogen in the material. Amorphous silicon from which p-n junctions have been made is actually a silicon hybrid alloy. Because of the small atomic number of hydrogen in relationship to that of silicon, the hydrogen is invisible to scattering of x-rays. On the other hand, hydrogen is quite visible to neutrons. Silicon deuteride might be preferred in order to obtain coherent scattering information from the material.

Amorphous silicon was the primary choice as a sample material, but unfortunately bulk samples of this are not available. Silicon forms an amorphous material only reluctantly and thus only thin films can presently be made. Because of Nature's cross sections and the intensities of existing neutron sources, samples on the order of grams are required to do neutron scattering experiments.

Amorphous arsenic was then settled upon as the object of this investigation. It is readily obtainable from the Mining and Chemical Products Ltd., England, and thus one has reasonable assurance that one is not examining a unique sample. Arsenic is between the four coordinates silicon and germanium, and the two coordinates chalcogens. Silicon and the chalcogens have been rather extensively studied because of their technological interest. Thus arsenic is of interest because it has properties between the others.

This reasonable amount of theoretical interest is combined with a present distinct lack of technological application. In its crystalline phase it is a semimetal and in its amorphous form it is a semiconductor, with a difference in room temperature conductivity of 11 orders of magnitude. The properties of the material than are clearly closely linked with the physical structure. In fact this material may be quite useful for observing properties related to the onset of crystallization.

Some justification has been given as to why amorphous arsenic was worthy of investigation. The next obvious question is why use neutrons? The neutron scattering length does not fall off with angle and thus gives the possibility of going to larger wave vector transfer more easily. Neutrons probe the position of the nucleus and are unaffected by the shape of the electronic cloud as are x-rays. Large wave vector transfer information is necessary to accurately discern the shape and position of peaks in the radial density function.

In this thesis the neutron diffraction pattern of amorphous arsenic was measured to a modest wave vector transfer of $Q = 14.75\ \mathring{A}^{-1}$. At the time of measurement there was no published data regarding neutron scattering from amorphous arsenic. Multiple scatter and attenuation corrections were applied to this data to obtain the structure factor S(Q). This structure factor was then transformed

to the radial density function (RFD) with use being made of a novel method of termination and normalization error removal in the RDF. A method for making inelastic scattering (Placzek) corrections was developed, but the magnitude and reliability of these corrections deemed it best to not apply them to the data. The diffraction pattern of amorphous arsenic was also measured on a separate instrument to a maximum wave vector transfer of 25 $\mathring{A}^{-1}$. This measurement showed very interesting structure out to the longest wave vector transfer measured, but unfortunately background problems were present in the measurement. It was thus deemed inappropriate to make attenuation, multiple scattering, and inelastic scattering corrections to this data and was therefore analyzed minimally.

A general organizational explanation with respect to placement of figures is deemed appropriate here. All figures are placed at the end of the major chapter divisions. For example, all figures in section 4.4.3 will be found at the end of 4.4, where the first 4 is the chapter, the second 4 is the major chapter division, and the 3 is a chapter subdivision.

CHAPTER II

Theory

2.1 Introduction

In this section we briefly describe some of the fundamentals of thermal neutron scattering. It is not intended as an extensive presentation of scattering theory, for which any of the standard texts on the subject may be consulted. For example, one could see Bacon (1967), Marshall and Lovesey (1971), Egelstaff (1965), or Turchin (1963).

A summary of some useful properties of thermal neutrons is presented first. Next comes the development of the static structure factor and its relationship to the radial density function. This is followed by the presentation of the double differential cross section, scattering law, Van Hove space-time correlation function and the relationships between the double and single differential cross sections.

2.2 General Properties

Neutrons are well suited as a probe of condensed matter. The wavelength of neutrons in thermal equilibrium with surroundings that are at standard room temperature are on the order of nearest neighbor distances in a solid. The nearest neighbor distances in solid matter are on the order of 3 Å.

For

$$\lambda = \frac{h}{p} = \frac{h}{\sqrt{2m_n E}} \tag{2.1}$$

with

$m_n = 1.67 \times 10^{-27}$ kg

$E = .025$ eV

We find

$\lambda = 1.8$ Å.

Also, we might note that thermal neutrons are useful as a probe of collective excitations in condensed matter. Collective excitations are in a region of 1 to 100 meV. Since the energy of the neutron is 25 meV energy changes of the neutron produced by excitations in the solid are readily seen with moderate resolution. It is also to be noted that if one is attempting to observe only the static structure, this interaction ability can be more of a liability than an asset.

The description of thermal neutron scattering theory follows in many ways the formalism developed in x-ray scattering and crystal structure analysis.

The wave vector of a neutron is defined in terms of the direction and speed of the neutron.

$$\bar{k} = \frac{m\bar{v}}{h} \tag{2.2}$$

where $\bar{v}$ is the velocity of the neutron. Similarly a scalar k is defined as

$$k = \frac{m|\bar{v}|}{h} = \frac{2\pi}{\lambda} \tag{2.3}$$

For Bragg scattering from crystals no reflection occurs unless $\vec{Q} = 2\pi\vec{\tau}$ where $\vec{\tau}$ is a reciprocal lattice vector of the crystal and $\vec{Q}$ is the wave vector transfer.

$$\vec{Q} = \vec{k}_o - \vec{k}' \tag{2.4}$$

$\vec{k}_o$: incident neutron wave vector

$\vec{k}'$: outgoing wave vector

Alternately, one could write

$$\hbar Q = \hbar(k_o - k') \tag{2.5}$$

and then call the quantity $\hbar Q$ the momentum transfer.

If we assume that there is no interchange of energy with the system, then

$$|\vec{k}_o| = |\vec{k}'| = k \tag{2.6}$$

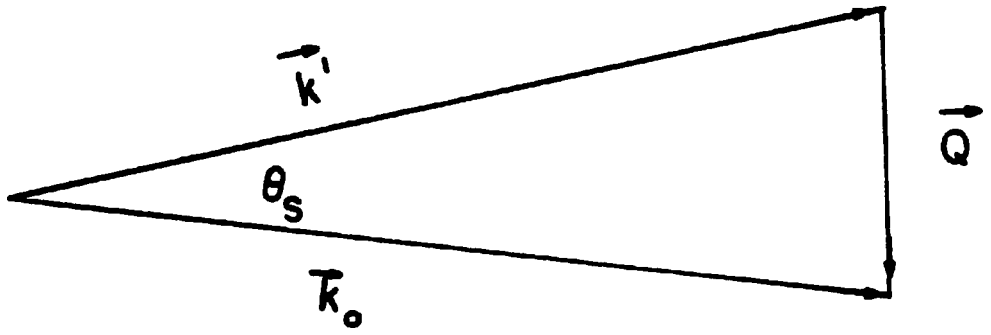

$$|\vec{Q}| = |\vec{k}_o - \vec{k}'| \tag{2.7}$$

$$Q = 2k \sin(\theta_s/2) \tag{2.8}$$

where θ_s is called the scattering angle and is the angle between the incident and scattered neutron.

Eq. (2.8) is often written as

$$Q = \frac{4\pi \sin(\theta_s/2)}{\lambda} \tag{2.9}$$

where λ is the wavelength of the incident neutron.

From (2.9) it is clear that we can find the diffracted intensity as a function of Q by holding λ fixed and varying θ_s, or by fixing θ_s and varying λ. Measurements taken with constant λ and variable θ_s are referred to as constant wavelength diffraction measurements.

Measurements made with θ_s fixed and λ variable are referred to as time of flight experiments. For this case it is convenient to rewrite (2.9) as

$$Q = \frac{2mL}{t} \sin(\theta_s/2) \tag{2.10}$$

where L is the total path length from the source to the detector and t is the time it takes a neutron of a particular wavelength to travel this distance.

It is also useful to note the relationship between flight time and energy which is

$$t = \frac{mL}{\sqrt{2mE}} \quad . \tag{2.11}$$

It is not necessary to restrict ourselves to the case of no energy transfer with the system. If there is energy

transfer with the system then the magnitude of the incident and scattered wave vector are different. The energy transfer, ε is then

$$\varepsilon = \frac{\hbar^2}{2m} (k_o^{\ 2} - k'^2) \tag{2.12}$$

$$\varepsilon = \hbar\omega \tag{2.13}$$

where ε is the energy gain by the system from the incident neutron, and ω is called the frequency transfer.

2.3 Static Structure Factor

Consider scattering from a monoisotopic static fluid. The scattering probability per unit solid angle, $\partial\sigma/\partial\Omega$, is composed of a coherent and an incoherent cross section.

$$\frac{\partial\sigma}{\partial\Omega}(Q)_{total} = \frac{\partial\sigma}{\partial\Omega}(Q)_{coherent} + \frac{\partial\sigma}{\partial\Omega}(Q)_{incoherent} \tag{2.14}$$

$$\frac{\partial\sigma}{\partial\Omega}(Q)_{incoherent} = Na_{inc}^{\ 2} \tag{2.15}$$

$$\frac{\partial\sigma}{\partial\Omega}(Q)_{coherent} = |f(\theta)|^2 \tag{2.16}$$

$f(\theta)$ = scattering amplitude.

Since we are concerned about the structure of a material and $\frac{\partial\sigma}{\partial\Omega}(Q)_{incoh}$ contains no such information, our interest in this quantity will be minimal. However, $f(\theta)$ contains structural information and is defined as

$$f(\theta) = \sum_{j=1}^{N} a_j \, e^{i\bar{Q}\cdot\bar{r}_j} \qquad (2.17)$$

where $\bar{r}_j$ and a_j are the position and coherent scattering length respectively of the jth atom. It follows then that

$$f(\theta) = a \sum_{j=1}^{N} e^{i\bar{Q}\cdot\bar{r}_j} \qquad (2.18)$$

since all a_j's are the same. Thus,

$$\frac{\partial\sigma}{\partial\Omega}(Q)_{coh} = a^2 \left| \sum_{j=1}^{N} e^{i\bar{Q}\cdot\bar{r}_j} \right|^2 \qquad (2.19)$$

and we define the structure factor, S(Q) as

$$S(Q) \equiv \frac{1}{N} \left| \sum_{j=1}^{N} e^{i\bar{Q}\cdot\bar{r}_j} \right|^2 . \qquad (2.20)$$

It is then straightforward to find the structure factor from the measured cross section by writing

$$S(Q) = \frac{1}{Na^2} \frac{\partial\sigma}{\partial\Omega}(Q)_{coh} \qquad (2.21)$$

We are now interested in the relationship between S(Q) and functions that may give us some physical understanding as to the structure of the system under investigation.

To this end, we expand Eq. (2.20) above.

$$S(Q) = \frac{1}{N} \left| \sum_{j=1}^{N} e^{i\bar{Q}\cdot\bar{r}_j} \right|^2$$

$$= \frac{1}{N} \left(N + \sum_{i \neq j}^{N} e^{i\bar{Q}\cdot(\bar{r}_i - \bar{r}_j)} \right) \qquad (2.22)$$

By noting that

$$e^{i\bar{Q}\cdot(\bar{r}_i - \bar{r}_j)} = \int d^3r \, \delta(\bar{r} - \bar{r}_i + \bar{r}_j) e^{i\bar{Q}\cdot\bar{r}} \qquad (2.23)$$

we can rewrite S(Q) as

$$S(Q) = 1 + \frac{1}{N} \int \sum_i \sum_j e^{-i\bar{Q}\cdot\bar{r}} \, \delta(\bar{r} - \bar{r}_i + \bar{r}_j) \, d^3r \qquad (2.24)$$

$$S(Q) = 1 + \int_v e^{i\bar{Q}\cdot\bar{r}} \rho(\bar{r}) d^3\bar{r}$$

where $\rho(\bar{r}) = \frac{1}{N} \sum_{i=1}^{N} \sum_{j=1}^{N} \delta(\bar{r} - \bar{r}_i + \bar{r}_j)$.

For an isotropic material $\rho(\bar{r})$ depends only on the magnitude of $\bar{r}$, and thus $\rho(\bar{r})$ can be written as $\rho(r)$.

$\rho(r)$ is called the static pair density. It is the average volume density of atoms at distance r from the origin, provided an atom is at the origin. One sometimes defines a static pair correlation function $\rho'(r) = \rho(r)/\rho_0$ where ρ_0 is the average density of the sample. A few properties of $\rho(r)$ are useful to note.

First, as r becomes large, $\rho(r)$ must approach the average atomic density of the system.

$$\lim_{r \to \text{large}} \rho(r) = \frac{N}{V} = \rho_0 \tag{2.25}$$

Secondly, as r becomes smaller than the nearest neighbor distance, $\rho(r) \to 0$.

$$\lim_{r \to 0} \rho(r) = 0$$

These properties are most helpful in normalizing the data.

It is now convenient to slightly rewrite S(Q), by adding and subtracting a constant.

$$\begin{aligned} S(Q) &= 1 + \int_V e^{i\bar{Q}\cdot\bar{r}}[\rho(r) + \rho_0 - \rho_0]d^3r \\ &= 1 + \int_V e^{i\bar{Q}\cdot\bar{r}}[\rho(r)-\rho_0]d^3r + \rho_0 \int e^{-i\bar{Q}\cdot\bar{r}}d^3r \\ &= 1 + \int_V e^{i\bar{Q}\cdot\bar{r}}[\rho(r)-\rho_0]d^3r + (2\pi)^2\rho_0\,\delta(Q) \end{aligned} \tag{2.26}$$

The term $(2\pi)^2\rho_0\cdot\delta(Q)$ is the forward scattering from the sample as a whole, which cannot be measured, and is therefore ignored.

Since we are dealing with isotropic materials, $\rho(r)$ is a function only of a scalar r so that the volume average of the function inside the integral may be carried out.

$$\int_V e^{i\bar{Q}\cdot\bar{r}}[\rho(r)-\rho_o]d^3r = \int_o^\infty r^2(\rho(r)-\rho_o)dr \int_o^{2\pi} d\phi \int_o^\pi \sin\theta e^{i\bar{Q}\cdot\bar{r}} d\theta \qquad (2.27)$$

The $d\theta$ integral is carried out by noting

$$\bar{Q}\cdot\bar{r} = Qr\cos\theta \qquad (2.28)$$

and thus

$$\int_o^\pi \sin\theta\, e^{iQr\cos} \, d\theta = \frac{1}{-iQr} e^{iQr\cos\theta}\Big|_o^\pi = \left[\frac{-e^{-iQr}+e^{+iQr}}{iQr}\right] \qquad (2.29)$$

$$= \frac{2\sin Qr}{Qr}$$

The $d\phi$ integral is merely 2π. It then follows that

$$S(Q)=1 + \int_V e^{i\bar{Q}\cdot r}[\rho(r)-\rho_o]d^3r = 4\pi\int_o^\infty r^2(\rho(r)-\rho_o)\frac{\sin Qr}{Qr}dr \qquad (2.30)$$

and finally rearranging

$$Q(S(Q)-1) = \int_o^\infty 4\pi r(\rho(r)-\rho_o)\sin Qr dr \qquad (2.31)$$

The above (2.31) is a Fourier sine transform of the function $4\pi r(\rho(r)-\rho_o)$. If we take the transform again, we obtain the argument before transformation on the right, and obtain

the transform with respect to Q accompanied by appropriate normalization on the left.

$$\frac{2}{\pi}\int_0^\infty Q(S(Q) - 1)\sin QrdQ = 4\pi r\,(\rho(r) - \rho_0) \qquad (2.32)$$

The formulas 2.31 and 2.32 are the standard ones derived by Zernike and Prins (1927).

Using the notation of Wright (1974), we define the differential radial correlation function, G(r).

$$G(r) = 4\pi r(\rho(r) - \rho_0) \qquad (2.33)$$

It is this function that will be used for most analyses of the correlation function. It is now clear that G(r) is readily obtainable from S(Q). S(Q) in turn follows directly from the differential cross section $\frac{\partial\sigma}{\partial\Omega}(Q)$.

We now define $\frac{\partial\sigma}{\partial\Omega}(Q)_{exact}$ as

$$\frac{\partial\sigma}{\partial\Omega}(Q)_{exact} \equiv Na^2\,S(Q) \quad . \qquad (2.34)$$

This is not, in general, what is measured and we must find a relationship between what actually is measured and $\frac{\partial\sigma}{\partial\Omega}(Q)_{exact}$.

2.4 Double Differential Cross Section

The double differential cross section $\frac{\partial^2\sigma}{\partial\Omega\partial\varepsilon}(Q,\varepsilon)$ is the probability that a neutron incident upon a sample will scatter through some wave vector transfer Q and some energy transfer ε, per unit energy per unit solid angle.

The point of introducing the double differential cross section is that the static approximation is not exactly valid. Atoms in the sample move and can recoil from the incident neutron. Proper accounting must be made for inelastic scattering, to relate

$$\left.\frac{\partial\sigma(Q)}{\partial\Omega}\right|_{\text{exact}} \quad \text{to} \quad \left.\frac{\partial\sigma(Q)}{\partial\Omega}\right|_{\text{meas}} .$$

The double differential cross section is related to a quantity called the scattering law $S(Q,\varepsilon)$ in the following manner.

$$\frac{\partial^2\sigma}{\partial\Omega\partial\varepsilon} = a^2 \frac{k'}{k} \; S(Q,\varepsilon) \tag{2.35}$$

The scattering law is a function of the microscopic properties of the material only and is independent of the method of measurement. The scattering law itself is defined in terms of a Van Hove space-time correlation function, $G(\bar{r},t)$.

$$S(Q,\varepsilon) = \frac{1}{2\pi\hbar} \int d\bar{r}dt \; e^{i(\bar{Q}\cdot\bar{r}-\varepsilon t/\hbar)} \; G(\bar{r},t) \tag{2.36}$$

$G(\bar{r},t)$ can be interpreted classically as the probability of finding a particle at $\bar{r}$ and t given that there was a particle at r = 0 at t = 0. However, we have no desire in this experiment to measure $G(\bar{r},t)$, but only to measure $\rho(r) = G(r,t=0)$. $\rho(r)$ depends on $S(Q)$, which in turn follows from $\frac{\partial\sigma}{\partial\Omega}(Q)_{\text{exact}}$. At this point we can relate the differential cross section to the double differential cross section in the following manner.

$$\frac{\partial\sigma}{\partial\Omega}(Q) = \int_{-\infty}^{+\infty} \frac{\partial^2\sigma}{\partial\Omega\partial\varepsilon}(Q_\varepsilon,\varepsilon)d\varepsilon = \int_{-\infty}^{\infty} a^2 \frac{k'}{k} S(Q_\varepsilon,\varepsilon)d\varepsilon \tag{2.37}$$

The differential cross section $\frac{\partial\sigma}{\partial\Omega}(Q)$ is the integral over all possible energy transfers, while Q_ε varies with ε in a way that depends on the details of the measurement.

The static structure factor assumes that the integration path in (Q, ε) space for a nominal Q is that of Q = constant. For x-rays and electrons, the assumption is quite valid. However because of the large mass of the neutron it is possible to transmit substantial momentum transfer with a relatively small energy transfer. For neutrons then, the static approximation is not necessarily valid.

At this point then we differentiate between the $\frac{\partial\sigma}{\partial\Omega}(Q)_{exact}$ and the result of a measurement $\frac{\partial\sigma}{\partial\Omega}(Q)_{meas}$ in the following manner:

$$\frac{\partial\sigma}{\partial\Omega}(Q)_{exact} = a^2 \int_{\text{const } Q} \frac{k'}{k} S(Q,\varepsilon)d\varepsilon \tag{2.38}$$

$$\frac{\partial\sigma}{\partial\Omega}(Q)_{meas} = a^2 \int_{\substack{\text{instrumental}\\ \text{integration}\\ \text{path}}} W(Q_\varepsilon,\varepsilon)\frac{k'}{k} S(Q_\varepsilon,\varepsilon)d\varepsilon \tag{2.39}$$

where $W(Q_\varepsilon,\varepsilon)$ is the weighting function of the instrument. When elastic scattering is assumed k'=k, $S(Q_\varepsilon,\varepsilon)$ is a delta function in ε, and the $\frac{\partial\sigma}{\partial\Omega}(Q)_{exact}$ reduces to

$$\frac{\partial\sigma}{\partial\Omega}(Q)_{exact} = a^2 \int S(Q,\varepsilon)d\varepsilon \tag{2.40}$$

If $S(Q,\varepsilon)$ were known precisely, there would be no trouble in determining $\frac{\partial\sigma}{\partial\Omega}(Q)$ exact.

However, $S(Q,\varepsilon)$ is not known and in fact is more difficult to determine than $S(Q)$. Reasonable models for $S(Q,\varepsilon)$ may be created, nevertheless, and used in conjunction with the measured $\frac{\partial\sigma}{\partial\Omega}(Q)_{meas}$ to yield the $\frac{\partial\sigma}{\partial\Omega}(Q)_{exact}$ that is desired. A more thorough description of the procedure used to accomplish this end is set forth in the section on inelastic scattering corrections.

The property of detailed balance is useful in placing restrictions on the scattering law. Detailed balance requires.

$$S(-Q,-\varepsilon) = e^{-\varepsilon/kT}S(Q,\varepsilon) \quad . \tag{2.41}$$

From this we can define a symmetrized scattering law $\tilde{S}(Q,\varepsilon)$ by

$$\tilde{S}(Q,\varepsilon) = e^{-\varepsilon/2kT}S(Q,\varepsilon) \tag{2.42}$$

which has the property that

$$\tilde{S}(-Q,-\varepsilon) = \tilde{S}(Q,\varepsilon) \quad .$$

Henceforth, all references to the scattering law will mean the symmetrized scattering law, but the tilda ($\sim$) will be dropped.

CHAPTER III

Experiment

3.1 Single Wavelength Diffraction

As noted by Eq. (2.9) in Chapter II, one way to carry out a neutron diffraction experiment is the single wavelength technique. In this method we take a wide energy spectrum neutron beam, for example from a reactor, and pass it through a single crystal of appropriate material to diffract out a beam of a single wavelength. A sample is then placed in this single wavelength beam and a detector positioned at some angle with respect to this beam to record any neutrons that are diffracted from the sample. The angle of the detector with respect to beam incident upon the sample is then varied and the intensity of neutrons diffracted from the sample is recorded as a function of angle.

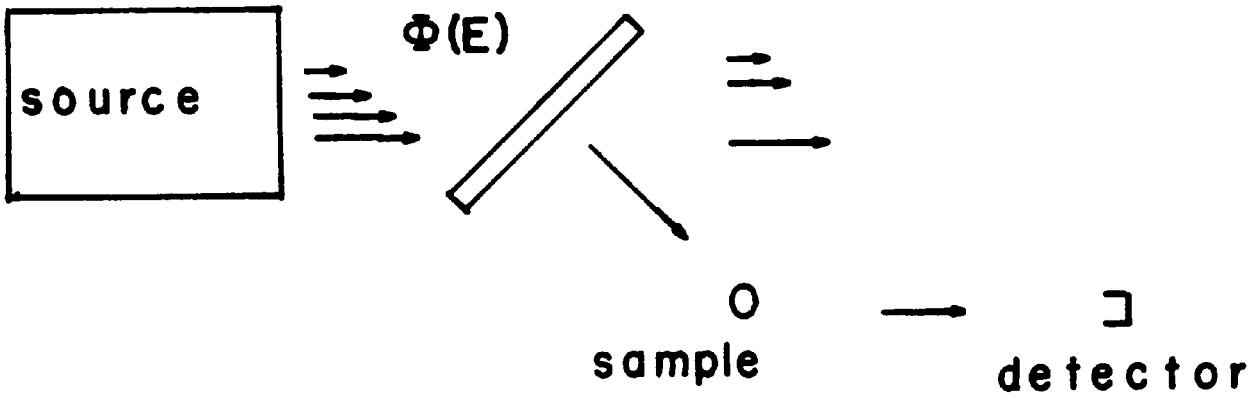

For an experiment with this arrangement combined with the static approximation and neglecting multiple scattering and attenuation effects, the counting rate of detected neutrons per unit solid angle as a function of scattering angle θ_s and incident neutron energy E_o, may be represented as follows.

$$C(\theta_s) = \eta(E_o)\,\phi(E_o)\,\frac{\partial\sigma}{\partial\Omega}(Q) \qquad (3.1)$$

where

$\eta(E_o)$ = detector efficiency at energy Eo

$\phi(E_o)$ = neutron flux of energy Eo incident upon the sample

$\frac{\partial\sigma}{\partial\Omega}(Q)$ = differential scattering cross section for wave vector transfer Q.

For this type of measurement, since Eo is fixed, $\eta(E_o)$ and $\phi(E_o)$ are constant throughout the range of the measurement and the only variable is θ_s. Thus, using the previously stated simplifying assumptions the functional dependence of $\frac{\partial\sigma}{\partial\Omega}(Q)$ on θ_s will be directly imaged by the measurement of $C(\theta_s)$.

Thus, provided E_o is fixed, the incident flux and the detector efficiency are independent of the wave vector transfer Q being measured. In this case it is easy to extract the differential cross section from the data.

For a cursory examination of thin samples this approach is often sufficient. However, there are three processes that have been neglected in this analysis. These are multiple scattering, attenuation, and inelastic scattering, each of which will be accounted for later.

3.2 The Single Wavelength Diffractometer

The instrument used for this part of the experiment was the Powder Diffractometer (Mueller, 1972) of M. H. Mueller and J. Faber, attached the the CP-5 reactor of Argonne National Laboratory. A LiF monochromator was used that gave a $\lambda = 1.05$ Å ($E_o = 74.18$ meV) neutron beam from the [222] planes with a $\lambda/2$ passage of .4%. The 2.368 gm of powdered amorphous arsenic (which will be denoded as aAs)sample was placed in a vanadium tube with length 1.00°, inside diameter of .252°, and wall thickness of .0008". The sample was positioned in the .5°x.75° neutron beam such that the axis of the tube was normal to the beam and in the same direction as the .5" dimension of the incident beam. Thus, 1.184 gm of sample and .309 gm of vanadium container were in the beam. At the given incident energy the sample had an attenuation of $\Sigma_T X = .127$ and a scattering probability $\Sigma_S X = .071$.

The scattered neutrons were detected by a 8" x 1" Reuter Stokes BF_3 (96% enriched in B^{10}) proportional counter with 100 cm pressure. The detector was viewed end on and had an efficiency of

$$n(E) = 1 - e^{-.419/E^{1/2}} \qquad (3.2)$$

where E is in electron volts.

At E_o = 74.18 meV, this yields an efficiency of 78.5%. Measurements were taken throughout the range of $5^o \leq \theta_s \leq 110^o$ in angular increments of $\theta_s = .5^o$. This corresponds to a wave vector transfer range of .52 $\text{Å}^{-1} \leq Q \leq 9.8\ \text{Å}^{-1}$ with a ΔQ range of $.052\ \text{Å}^{-1} \leq \Delta Q \leq .030\ \text{Å}^{-1}$.

Data was accumulated from the sample plus container for a uniform beam monitor count of 2×10^6 counts at each angular position. This gave a maximum of 1500 counts of data at $\theta = 35.5^o$ or $Q = 3.64\ \text{Å}^{-1}$. An average of $\sim$ 1000 counts of data was measured at each angular position. This corresponds to a statistical uncertainty of $\sim$ 3% at any given wave vector transfer. Data from the container alone was counted until an average of 150 counts per angular position was obtained and this corresponded to an accumulation time of half that required for the sample plus container. This represents only 8% statistical uncertainty, but the functional form of scattering from vanadium is known to be a smoothly varying function of θ_s, and thus the actual uncertainty after smoothing is less than 1%.
Similarly the statistical uncertainty in the sample plus container data after smoothing may be assumed to be less than the 3% previously stated, but a quantitative measure of the uncertainty is difficult to ascertain because no functional form for the data is previously known. The data is smoothed

using a cubic spline.

3.3 Time of Flight Diffraction

As mentioned in Chapter II an alternate method of diffraction is by time of flight. Here a pulse of neutrons with a continuous distribution in energy is directed towards the sample and counted by a detector at a fixed scatering angle. By knowing the scattering angle, the distance from the source to the detector, and time for a neutron to travel this distance, one can determine the wave vector transfer from eq. (2.10). Again assuming the static approximation and no multiple scattering we write the formulation for counting rate as:

$$C(t) = \eta(E)\,\phi(E)\,\frac{\partial\sigma}{\partial\Omega}(Q) \quad . \tag{3.3}$$

However in this case we fix θ_s and t varies. Since E depends on t as shown in (2.11) the incident flux and efficiency are no longer constant.

Extracting the differential cross section in a manner similar to before we find

$$\frac{\partial\sigma}{\partial\Omega}(Q) = \frac{1}{\eta(E)\ \phi(E)}\ C(t)$$

It is immediately apparent that we do not have the simplicity that was found in the single lambda experiment where the efficiency and incident flux were constants. If the detector efficiency η and incident flux ϕ are well

known functions of energy, the appropriate expression as a function of Q is readily divided out of C(Q) to obtain $\frac{\partial\sigma}{\partial\Omega}(Q)$. In practice this rarely the case. Detector of-ficiencies are of the form

$$\eta(E) = 1 - e^{-nx\sigma(E)} \tag{3.4}$$

where we see that σ itself varies with energy.

The incident flux $\phi(E)$ is an involved function of E and its shape depends on the source. If the source is a truely pulsed source the spectral shape is that of a Maxwellian combined with a 1/E tail arising from neutron slowing down. Alternately, if the source is continuous with the pulsing being done by a neutron chopper, then the spectral dependence is a product of the steady state spectrum of the reactor (for example) with the energy transmission function of the chopper. In either case the precise shape of the incident $\phi(E)$ is difficult to predetermine, and similarly the form of $\eta(E)$ is nontrivial to find. The method usually used to circumvent this problem is by use of the vanadium reference technique, which will be described shortly.

However, there are ways of solving the spectral shape problem other than using a reference scatterer and for some experiments these approaches should be taken. For example in carrying out the inelastic scattering

corrections on data taken by the vanadium reference technique we find the corrections tend to cancel out because of similarities in the model which is used both for the sample and the reference. Thus there is basically no way of checking the inelastic scattering model with data taken using the vanadium reference method.

A method other than using a vanadium reference is to use "black" detectors in combination with a "thin" beam monitor upbeam of the sample that is energy analyzed by time of flight. A beam monitor is a detector placed in the incident beam and can be used for monitoring the incident spectrum or fluence. By a "black" detector we mean one such that $nx\sigma(E)$ is large enough so that $\eta(E) \approx 1$ independent of E. This can be done by using detectors such as Li^6 loaded glass scintillators or high pressure He^3 proportional counters. The spectral shape of the flux $\phi(E)$ can be found by monitoring the time of flight intensity of the incident beam. A "thin" beam monitor is used such that

$$\eta(E) = 1 - e^{-nx\sigma(E)} \simeq nx\sigma(E) \qquad (3.5)$$

and also to prevent altering the spectrum incident upon the sample.

We see that the problem of $\sigma(E)$ is still present but this can be extracted if the functional form of the beam monitor detection material cross section is well known. For example the B^{10} neutron absorption [$B^{10}(n,\alpha)Li^{7}$] cross section is 1/v with no structure from E = .001 eV to in excess of 100 eV. In this case the energy dependence of the monitor is straightforward to determine and thus the incident flux spectrum $\phi(E)$ can be found.

As previously stated the more usual manner to eliminate the detector efficiency and incident flux spectral dependence is to use the vanadium reference method. Here data is collected for scattering from both the sample and the vanadium reference. Since vanadium is primarily an incoherent scatterer, no structural information is imparted to the scattered beam. Thus, the cross section $\frac{\partial\sigma}{\partial\Omega}(Q) = \frac{\partial\sigma}{\partial\Omega}(Q)_{incoh}$ is independent of Q and equal to a constant. The count rate, $C(Q)_{vanadium}$, produced by scattering from a vanadium sample then is proportional to the product of $\phi(E)$ times $\eta(E)$. By dividing the data from the sample, $C(Q)_{sample}$, by the data from the reference it is a simple matter to extract the differential cross section $\frac{\partial\sigma}{\partial\Omega}(Q)$ for the sample:

(3.6)

$$\frac{\partial\sigma(Q)}{\partial\Omega_{sample}} = C_1 \frac{\frac{\partial\sigma}{\partial\Omega}(Q)_{sample}\,\eta(E)\phi(E)}{(\frac{\partial\sigma}{\partial\Omega}_{vanadium} = C_2)\eta(E)\phi(E)} = \frac{C_1}{C_2}\,\frac{C_{sample}(Q)}{C_{vanadium}(Q)}$$

Being able to determine the differential cross section independently of the efficiency and the incident spectrum is a tool of tremendous power and is used universally for diffraction measurements done by time of flight.

3.4 The CP-5 Time of Flight Diffractometer

The instrument used to perform the experiment was the High Pressure Time of Flight Diffractometer attached to the CP-5 reactor at Argonne National Laboratory. It is under the auspices of Dr. James Jorgensen. The continuous beam from the reactor is pulsed using a high strength steel alloy rotor with a slit shape such that the transmission function has a sharp high energy cutoff. The flight path from the rotor to the sample was 12" with the beam dimensions being 1.25" x .187" at the sample. An array of detectors was at a scattering angle of 90° and placed 135" from the sample. The detectors were 1" diameter Reuter Stokes BF_3 (96% enriched in B^{10}) counters with 167 cm pressure. The scattered beam traversed the diameter of the tubes and resulted in an efficiency which may be approximated by

$$\eta(E) = 1 - e^{-.0603/E^{1/2}} \qquad (E \text{ in eV}) . \tag{3.7}$$

Time focussing principles were used to position the detectors in the array to optimize resolution (Carpenter, 1967,; Holas, 1968).

The sample was similar to that used in the single lambda experiment. It consisted of 4.673 gm of powdered aAs in a vanadium tube container .250" ID x 2.00" long with .008" wall thickness. The axis of the tube was normal to the incident beam and in the same direction as the 1.25" dimension of the beam. Consequently 2.92 gm aAs and .762 gm vanadium container were in the beam. The vanadium reference used was a rod .25" OD x 6-1/2" long in a similar orientation as the sample with 6.25 gm in the incident beam.

Data from four different arrangements was acquired, each being for a fixed length of time. The assumption here is that reactor power is independfent of time and hence the number of counts collected is a linear function of time. The four arrangements were with 1) arsenic plus container, 2) container alone, 3) vanadium reference, 4) nothing in the sample position of the incident beam. If all four runs were for the same length of time and attenuation effects are neglected then the differential cross section is calculated easily.

$$\frac{\partial\sigma}{\partial\Omega}(Q) = \frac{N_V \bar{\sigma}_V^S}{4\pi} \cdot \frac{C_{aAs}(Q) - C_{cont}(Q)}{C_{Van}(Q) - C_{nothing}(Q)} \qquad (3.8)$$

where

$\overline{\sigma}_V^S$ = scattering cross section of vanadium

N_V = number of vanadium atoms in beam

and $C_{aAs}(Q)$, cont,Van,nothing refer to the counts from arrangements 1,2,3,4 above.

Data was accumulated for 24 hours for runs 1,3, and 4 above and 18 hours for vanadium.

The counts per time channel averaged over the total time range collected was 10,000 counts/channel for both the vanadium and the sample plus container, which would lead to 1% statistics. Similar averages for the container and nothing (background) were 2500 cts/ch and 1700 cts/ch respectively. These counts corresponded to 2% and 2.5% statistics but the shape of the functions that produce these counts is presumably quite smooth and thus after smoothing these effective counts should be known to better than 1%.

Calibration of the instrument to find the precise relationship between time of arrival and wave vector transfer was performed by scattering from a sample of known crystalline lattice spacing and making correlation between intensity peaks that correspond to particular lattice spacings and the time of arrival of these peaks.

The resolution of the instrument depends on the time uncertainty of the origin of neutrons from the chopper

and geometrical factors. The geometrical factors relevant are the uncertainty in path length and uncertainty in scattering angle. Because the chopper aperture and sample are small, and the detectors are time focussed, the geometrical contribution to the resolution is negligible in comparison to the pulse width of the source. Thus, the fractional resolution of the diffractometer may be characterized by $R = \Delta t/t$ where Δt is the pulse width and t is the time of arrival corresponding to the Q of interest. This expression may be reformulated by noting that

$$t \propto \frac{1}{v} \propto \frac{1}{\sqrt{E}} \propto \lambda = \frac{4\pi \sin(\theta_s/2)}{Q} \propto \frac{1}{Q} \quad .$$

It is then straightforward to derive that

$$R = \frac{\Delta t}{t} = \frac{\Delta Q}{Q} \tag{3.9}$$

Continuing we find the fractional resolution R to be

$$R = \frac{\Delta Q}{Q} = \frac{\Delta t \; hQ}{Lm4\pi \sin(\theta_s/2)} = CQ \tag{3.10}$$

where C is a constant whose value depends on the total flight path length L, the scattering angle θ_s, and the pulse width Δt. Using the given flight path and scattering angle, and taking the pulse width Δt = 15 μsec existing when the present data was being accumulated, we find the resolution of this instrument to be

$$R = \frac{\Delta Q}{Q} = 1.79 \times 10^{-3} Q \qquad (3.11)$$

The worst resolution occurs at the largest Q where Q = 14.75 Å^{-1}. Therefore the worst fractional resolution is $R=\Delta Q/Q= 2.64\%$. Any measurement of S(Q) would then be resolution limited if features in the diffraction pattern, whose widths we will call ΔQ_{MEAS}, have widths comparable to the resolution width, $\Delta Q = 1.79 \times 10^{-3} Q^2$. Again using Q = Q_{max} we find a worst resolution width of $\Delta Q = .389$ Å^{-1}. The features of aAs at this large Q as will be shown later, have a periodicity of 2.5 Å^{-1}, with a correspondingly implied $\Delta Q_{MEAS} = 1.25$ Å^{-1}. We see that the resolution is approaching one third the characteristic size of the features and thus is becoming a limiting factor in the precision of the measurement at large wave vector transfer.

3.5 The ZING-P Time of Flight Diffractometer

We now include a brief description of ZING-P time of flight diffractometer, even though data from this instrument was not extensively analyzed. First we should point out that the pulse width resolution and incident spectrum characteristics of a truly pulsed source are different from those of a chopper attached to a continuous source. The pulse widths of a pulsed source depends on the energy of the departing neutron in a

manner that is characteristic of neutron slowing down in the specific moderator used. The general trend is for the pulse width to be proportional to the inverse of the neutron velocity.

$$\Delta t \propto \frac{1}{v} \propto \frac{1}{\sqrt{E}} \tag{3.12}$$

Since the time of arrival is also proportional to the inverse of the velocity, the resolution tends to be a constant.

$$R = \frac{\Delta Q}{Q} = \frac{\Delta t}{t} = C \tag{3.13}$$

The ZING-P diffractometer had a fractional resolution of less than 1.5% throughout the range of the measurement.

$$R = \frac{\Delta Q}{Q} \leq .015 \tag{3.14}$$

In a manner identical to that done previously we find

$$\Delta Q = Q * .015 \tag{3.15}$$

and at $Q_{max} = 14.75$ Å^{-1}, $\Delta Q = .22$ Å^{-1}.

The intensity spectrum $\phi(E)$ of a pulsed source is similar to that of a reactor in that it is basically a Maxwellian with a characteristic temperature near to that of

the surroundings. However in the higher energy region ($E \geq 5\ k_B T$ the spectrum becomes 1/E for a pulsed source. This means that on the ZING-P diffractometer there is a large increase in the relative intensity of neutrons with energy $E \geq 5\ k_B T$ relative to that obtained from a reactor. The greater source intensity at large wave vector transfer combined with better resolution in this range than achieved on the CP-5 time of flight diffractometer, lead to the ability to discern structure to larger Q on the pulsed source than on the chopped continuous source.

The diffractometer (Carpenter et al., 1975) was attached to the ZING-P pulsed neutron source. Neutrons were produced by impinging 200 MeV neutrons onto a lead target. The resulting spallation neutron spectrum peaks around 2 MeV but has a tail that continues up to the energy of the incident proton, i.e., 200 MeV. The neutrons were then moderated by a combination of beryllium and polyethylene. The sample was 90 gm of powdered aAs placed in a pancake shaped container of 10 cm diameter and approximately 3mm thickness. The initial flight path from the source to the sample was 4.34 m, and the scattered flight path from the sample to the detectors was .45 m. The detector array was at scattering angle $\theta_s = 150^o$ and consisted of eleven 1.59 cm diameter x 25 cm long, 6 atmosphere He^3 detectors arranged in a time focussing configuration. The vanadium reference method was again used for data reduction.

CHAPTER IV

Analysis

4.1 Introduction

The final object of a diffraction measurement from an amorphous material is the structure factor S(Q) or its Fourier transform, the radial distribution function G(r). However, before one arrives at the correct S(Q) certain corrections must be made to the initially reduced data. Initial reduction of data obtained by time of flight diffraction using the vanadium reference method, and single wavelength diffraction was described previously and will not be repeated here.

The corrections that need to be considered are multiple scattering and attenuation, and inelastic scattering. Multiple scattering and attenuation corrections will be made using a computer code, MSCATD, developed by Mildner (1974), Copley (1974) and Bischoff (1970). Because of the need for input cross sections to this code, a description of the source and derivation of appropriate cross sections will be included before the multiple scattering corrections. Inelastic scattering corrections (commonly called Placzek corrections), (Placzek (1952)) will be developed using a combination of theories of Sjolander (1958), Carpenter and Pelizzari (1975), and Marshall and Lovesey (1971). Although

a rather extensive development of this theory will be made, the application of the corrections will not be carried out as the large atomic mass of the sample makes the corrections to be of minimal magnitude. Comparisons are made between the results derived from this theory and those produced by Sinclair and Wright's (1974) adaptation of Placzek's method for a pulsed electron linac. The agreement is quite reasonable over regions of appropriate validity. The description of this inelastic scattering correction is included because this is the first time that this particular development has been applied and it may prove more effective in the future for lower atomic mass materials. Also, further refinement may make the application of this method to materials of mass equivalent to arsenic more appropriate.

The results of the two measurements after application of the multiple scattering and attenuation correction factors are then displayed. Since both data sets span only limited ranges of Q, the data sets were joined to produce the extended Q range structure factor. A brief comparison with the results of the ZING-P measurement which extended to a Q of 25 $\AA^{-1}$ will be made.

Finally, the Fourier transformation from S(Q) to G(r) will be carried out. This transformation has some inherent difficulties, namely introduction of termination and normalization error. A method will be described that successfully minimizes the normalization error and removes the termination error.

4.2 Cross Sections

In order to perform the multiple scattering and attenuation corrections, thermal neutron cross sections for coherent and incoherent scattering and absorption must be known for the materials of interest. The only materials that are of concern are vanadium and the sample, arsenic. Vanadium is used as a comparison scatterer in the vanadium reference method. The thermal (E = .0253 eV) neutron cross sections as recommended by BNL 325 (1973) are tabulated below on the left with inferred values on the right.

$\sigma_a = 5.04 \pm .04$ b

$\sigma_s = 4.93 \pm .036$

$\sigma_t = 9.97 \pm .05$ b

$a_{coh} = -.48 \pm .1$ fm $\rightarrow$ $\sigma_{coh} = .0296 \pm .012$ b

$\sigma_{inc} = 4.90 \pm .03$ b

Since $\sigma_{inc} = \sigma_s - \sigma_{coh} = 4.93 - .029 = 4.90 \pm .03$ then clearly most of the scattering is incoherent. This is the usefulness of vanadium as a reference scatterer.

It is interesting to note that the only reference to measuring the total scattering cross section of vanadium in BNL 325 (1973) is from Brockhouse (1953), and this is not a very recent measurement. However, there is apparently enough consistency with total and absorption cross section measurements to permit the assignment of the small uncertainty. Also, since people doing neutron scattering

experiments often use vanadium, significant errors in these cross sections would probably have been detected.

Arsenic has not generated the neutronic interest that vanadium has. BNL-325 (1973) lists recommended thermal neutron (E = .0253 eV) cross sections for arsenic as found below. Tabulated values are on the left and inferred values are on the right.

$\sigma_a = 4.3 \pm .1$ b

$\sigma_s = 7 \pm 1$ b

$\sigma_t = 11.3 \pm 1$ b

$a_{coh} = 6.4 \pm .1$ fm $\rightarrow$ $\sigma_{coh} = 5.15 \pm .16$ b

$\sigma_{inc} = 1.85 \pm 1$ b

There is clearly a large uncertainty in the total and scattering cross section, which results in a large uncertainty in the incoherent cross section. This uncertainty in the incoherent cross section presents a problem because in order to extrapolate the diffraction data to small wave vector transfer one needs to know the ratio of incoherent to total scattering cross sections. Since the coherent cross section is well known, this uncertainty is primarily in the incoherent port.

Measurements by Pelizzari (1977) of the incoherent scattering cross section done by integration of the double differential cross section led to an estimate of $\sigma_{inc} = .75 \pm .3$ b. Another estimate of the incoherent cross

section was obtained from data by Walton et al. (1961) given in BNL-325 (1976).

Their total cross section values were plotted vs. $1/\sqrt{E}$. Since absorption cross sections are 1/v, a straight line fit of the data, as shown in Fig. IV.2-1, to the function than

$$\sigma_{tot}(1/\sqrt{E}) = a + b/\sqrt{E} \qquad (4.1)$$

will yield values for a and b where a is the total scattering cross section and b depends on the absorption. Results of this calculation give

$$\sigma_a\ (.0253\ eV) = 4.73\ b$$
$$\sigma_s = 6.10\ b$$

with unknown estimated error.

If we assume the BNL 325 (1973) coherent cross section of $\sigma_{coh} = 5.15$ b is correct we are left with $\sigma_{inc} = .95$ b. This agrees more favorably with the measurement of Pelizzari (1977) of $\sigma_{inc} = .75$ b than the BNL 325 (1973) recommended value of $\sigma_{inc} = 1.85 \pm 1$ b, although within allowed uncertainty. As a supplementary check it was thought worthwhile to obtain a printout from Encoded Nuclear Data File-BIV (ENDFB-IV). This code produced current values for the cross section of at E = .025 eV of

$$\sigma_{tot} = 6.10\ b$$
$$\sigma_s = 1.73\ b.$$

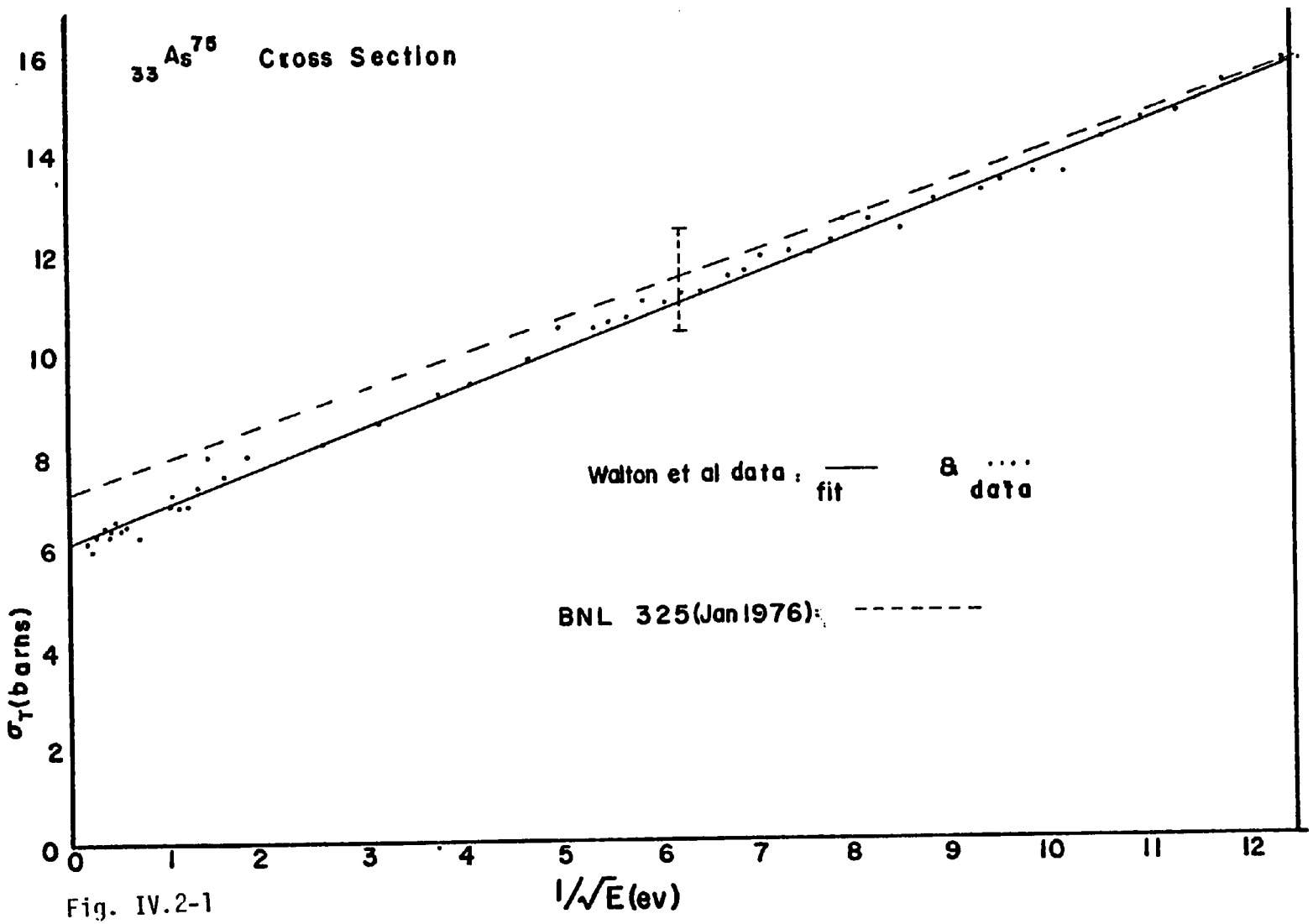

$_{33}As^{75}$ Cross Section
Walton et al data : —— fit & .... data
BNL 325(Jan 1976): - - - - - - -
σ_T(barns)
$1/\sqrt{E}$(ev)
0
2
4
6
8
10
12
14
16
0
1
2
3
4
5
6
7
8
9
10
11
12

Fig. IV.2-1

These values are clearly in major conflict with previously quoted values. Dr. Prael related (Prael, 1977) that significant errors in the low energy range for elements not commonly encountered in reactor design such as arsenic, are not unexpected. He states that this data file is designed to be used for calculations on fast reactors involving the higher energy region cross sections. This fact should be emphasized and is inserted as a word of warning to persons doing neutron scattering measurements and in need of low energy cross section values.

It was decided to ignore the values produced by ENDFB-IV.

Finally we list the values of the E = .025 eV neutron cross sections of arsenic that were decided upon.

$$\sigma_a = 4.30 \text{ b}$$
$$\sigma_s = 6.10 \text{ b}$$
$$\sigma_{coh} = 5.15 \text{ b}$$
$$\sigma_{inc} = .95 \text{ b}$$

4.3 Multiple Scattering and Attenuation Corrections

Initial analysis of neutron diffraction data assumes that the sample is an ideal scatterer whose properties are such that neutrons are scattered only once and that there is no attenuation of beam on the way into the sample or on the way

out to the detector. In reality, of course, this is not the case and the processes of multiple scattering and attenuation in the target degrade the quality of the data. The effects can be minimized experimentally by scattering from thin samples so the probability of multiple scatter is small and beam attenuation is minute. This approach to solving the problem conveys with it the added difficulty of low count rates and long counting times brought about by the dearth of scattering centers. Since available neutron intensities are quite weak (for example in comparison to x-ray sources) the thin sample approach leads to worsening statistics combined with decreasing signal to noise ratio. Thus, there is a limit beyond which this approach is no longer useful.

Given that it is sometimes impractical to reduce the multiple scattering and attenuation to negligible levels experimentally, numerical methods have been developed to compensate for these effects. The most straightforward correction to apply is what is commonly called an attenuation correction. The attenuation correction compensates for the fact that some neutrons are removed from the incident beam and other neutrons are removed from the scattered beam. This correction also assumes that the removed neutrons are not seen by the detectors. Correction factors of this form are commonly used in x-ray diffraction. Depending on the sample geometry, the solution to the equations describing this attenuation

may be analytic. The International Tables for X-ray Crystallography has compilations of correction factors using these analytic functions for several geometries (specifically cylindrical and slab samples) as a function of attenuation cross section. In the case of the time of flight experiment, a continuous range of neutron wavelengths is used which leads to an energy dependence of the cross section. This cross sectional variation results in attenuation corrections that vary with energy at a given scattering angle. Single incident wavelength diffractometers alter only the scattering angle, hence their variation of attenuation correction factor depends solely on geometric considerations. The magnitude of the attenuation correction factor is a smooth function of the neutron energy, in the case of the time of flight experiment, or the scattering angle in the case of the constant wavelength measurement. For the materials measured this correction depends only weakly on the structure of the material.

Another correction factor that should be considered is from neutrons that scatter more than once in the sample before they reach the detector. Events such as this are called multiple scattering events and give rise to multiple scattering corrections. We note here that these events have the capability to put events into the detector that we do not wish to see, in contrast to the attenuation process looked at previously that could only remove neutrons from the beam.

The effect of multiple scattering of neutrons from a slab sample was investigated by Vineyard (1954). One of the significant results that he found was the approximation of constant ratio of successive scatters. He found that provided $\frac{\sigma_s}{\sigma_{tot}} \frac{J_2}{J_1} < 1.$ and that the scattering is isotropic, then

$$\frac{J_2}{J_1} \simeq \frac{J_{n+1}}{J_N} = \frac{J_1}{J_o} \tag{4.2}$$

where

σ_s = scattering cross section

σ_{tot} = total cross section

J_n = intensity of neutrons scattered n times

and since

$$\begin{aligned} J_T &= J_1 + J_2 + J_3 + J_4 + \ldots J_\infty \\ &= J_1 + J_2 + J_2\frac{J_3}{J_2} + J_2 \frac{J_3}{J_2} \frac{J_4}{J_3} + \ldots \\ &= J_1 + J_2 \left(1 + \frac{J_2}{J_1} + \left(\frac{J_2}{J_1}\right)^2 + \ldots \right. \\ &= J_1 + J_2 \sum_{n=o}^{\infty} \left(\frac{J_2}{J_1}\right)^n \end{aligned}$$

(4.3)

then

$$J_T = J_1 + J_2\left(\frac{1}{1 - \frac{J_2}{J_1}}\right) \quad . \tag{4.4}$$

Now provided one can estimate the first and second order scattering one can correct the observed intensity J_T for multiple scattering.

This method works quite well for isotropic incoherent scatters such as vanadium and has been used successfully, for example, by Mildner (1974), and Pelizzari (1974) for the correction of the data from reference scatterers in time of flight measurements using slab geometry.

The correction for multiple scattering effects from the sample that is not an isotropic incoherent scatterer presents a more formidable problem. The method chosen here for compensation of multiple scattering and attenuation effects is a Monte Carlo neutron path simulation program that was developed by Mildner, Pelizzari and Carpenter (1978) following the work of Copley (1974) and Bischoff (1970). This program, MSCATD, was used in the present experiment to correct the data from both the arsenic sample and the reference vanadium scatterer without the necessity of the incoherent approximation since the operation of the computer code had been achieved. The reader is referred to papers by Mildner, Pelizzari and Carpenter (1977), Mildner and Carpenter (1977), and Mildner (1974) for a more complete discussion of the Monte Carlo program used. A brief description of the method by which the code works is included next.

Generalized Monte Carlo programs tend to be extremely inefficient because the number of events of interest is small compared to the total number of events that must be followed. If a manner can be found to determine distributions from which to make judicious choices of paths, the running time for Monte Carlo simulations can be drastically reduced. Making efficient choices of these paths is how MSCATD, the multiple scattering and attenuation correction code, is able to perform its calculations in a small amount of time.

For the geometry as shown in Figure IV.3-1, choose a neutron traveling in the x direction with y-z coordinates such that it will hit the target. The x-y-z coordinates of where this ray enters and leaves the target are found. The difference between these two coordinates, t_1, is the path length in the target if the neutron is not attenuated. A collision is forced to occur within this distance. Since the collision is forced, two questions arise. First, from what distribution of path lengths should one pick the path length to scattering, and second after the scattering position is found what weight should be attributed to this event.

The path length distribution will be approached first. Incident neutrons, have an escape probability $e^{-\Sigma_T t_1}$ and a collision probability of $1-e^{-\Sigma_T t_1}$ where Σ_T is the macroscopic total cross section. We thus pick a path length before scattering, ℓ_1, from the cumulative distri-

bution for path lengths

$$F(\ell_1) = \frac{\int_0^{\ell_1} e^{-\Sigma_T x} dx}{\int_0^{t_1} e^{-\Sigma_T x} dx} \tag{4.5}$$

The distribution function $F(\ell)$ is thus normalized to 1. A random number $R_{\ell 1}$, between 0 and 1, is then made equal to the cumulative distribution $F(\ell_1)$.

We may then solve for ℓ_1 explicitly.

$$R_{\ell 1} = F(\ell_1) = \frac{1 - \exp(-\Sigma_T \ell_1)}{1 - \exp(-\Sigma_T t_1)} \tag{4.6}$$

$$\ell_1 = -\frac{1}{\Sigma_T} \log(1 - R_{\ell 1}(1 - \exp(-\Sigma_T t_1)) \tag{4.7}$$

The distance to the first collision is thus properly chosen from a distribution that can be obtained through the generation of random numbers.

The statistical weight of the neutron, W, must next be accounted for. There is a probability of Σ_s/Σ_T that the collision is a scattering event and a probability $(1 - e^{-\Sigma_T t_1})$ that the collision actually takes place within the sample.

$$W_1 = \frac{\Sigma_s}{\Sigma_T}(1 - e^{-\Sigma_T t_1}) \tag{4.8}$$

The method outlined provides an efficient way to choose position of the first collision and the worth of the neutron after this collision. One can then generalize this

approach to the second and higher order collisions such that

$$\ell_n = \frac{-1}{\Sigma_T} \log (1 - R\ell_n(1 - \exp(-\Sigma_T t_n)) \tag{4.9}$$

where

ℓ_n = the distance between $(n-1)^{th}$ and n^{th} scatter

t_n = distance to surface of target after $(n-1)^{th}$ scatter

$R\ell_n$ = random number [0,1]

and the worth of the neutron after the nth scatter is

$$W_n = \prod_{j=1}^{N} [\frac{\Sigma_s}{\Sigma_T}(1 - \exp(-\Sigma_T t_j))] \tag{4.10}$$

In a somewhat similar fashion the scattering angle after each collision is chosen from a distribution

$$f(\theta) = \frac{\int_0^{\theta} \frac{\partial\sigma}{\partial\Omega}(\theta',\lambda) \sin\theta' \, d\theta'}{\int_0^{\pi} \frac{\partial\sigma}{\partial\Omega}(\theta',\lambda) \sin\theta' \, d\theta'} \tag{4.11}$$

that in terms of Q is

$$R_Q = f(Q) = \frac{\int_0^Q S(Q)QdQ}{\int_0^{Q_{max}} S(Q)QdQ} \qquad (4.12)$$

where $Q = \frac{4\pi\sin(\theta_s/2)}{\lambda}$

$S(Q)$ = static structure factor

In this case the equation cannot be solved explicitly for Q because $S(Q)$ is in general not an analytic function. Thus a search is made through the running integral of $\int_0^Q S(Q)QdQ$ until it is equal to $R_Q \int_0^{Q_{max}} S(Q)QdQ$.

When this equality is found, the associated Q is then determined.

The azimuthal angle distribution is uniform and can thus be easily generated from a distribution of random numbers R_ϕ

$$\phi = 2\pi R_\phi \qquad 0 < R_Q < 1 \qquad (4.13)$$

With the scattering positions and weight determined after each collision, one must next score the events. After each collision, n, the direction to the detector is found and a score given that is the product of the weight of the neutron after the nth collision times the probability that the neutron scatter into the detector, times the probability that the neutron arrive at the detector. The probability that the scatter be into the detector is simply

$$P_{Dn} = \frac{\Delta\Omega_D}{\sigma_s(k)} \frac{\partial\sigma}{\partial\Omega}(\theta_{Dn})$$

$$= \frac{\Delta\Omega_D}{\sigma_s(k)} b^2 S(Q_{Dn}) \qquad (4.14)$$

where P_{Dn} = probability that the nth scatter is in the direction of the detector D.

$\Delta\Omega_D$ = solid angle subtended by detector

$\sigma_s(k)$ = scattering cross section = $\frac{2\pi}{k^2}a^2\int_0^{2k} QS(Q)dQ$

$k = \frac{2\pi}{\lambda}$

θ_{Dn} = angle between direction of travel and direction to the detector, immediately preceding the nth scatter.

The probability that the neutron escape to the detector is

$$\exp(-\Sigma_T L_{Dn})$$

where

L_{Dn} = distance from n^{th} collision to the surface of the sample in the direction of the detector.

Thus, the score for the nth collision is

$$S_n = W_n P_{Dn} \exp(-\Sigma_T L_{Dn})$$

$$= \left\{ \prod_{j=1}^{n} \frac{\Sigma_s}{\Sigma_T} (1-\exp(-\Sigma_T t_j)) \right\} \frac{\Delta\Omega}{\sigma_s(k)} b^2 S(Q_{Dn}) \exp(-\Sigma_T L_{Dn}) \qquad (4.15)$$

We are interested in distinguishing only between n = 1 for one collision and n > 1 for multiple collisions. All scores for n = 1 are summed in a separate bin and the results kept for later use. The score for each event is then the probability of a neutron reaching the detector given that one neutron is incident upon the target. A number of histories would obviously have to be run, so the overall probability is

$$P_n = \frac{1}{K} \sum_{j=1}^{K} {}_jS_n \qquad (4.16)$$

where K is the number of histories followed and ${}_jS_n$ is the score for the nth collision of the jth history.

It follows that

$$P_1(\theta) = \frac{1}{K} \sum_{j=1}^{K} {}_jS_1(\theta) \qquad (4.17)$$

$$P_m(\theta) = \sum_{j=1}^{K} \sum_{n=2}^{\infty} {}_jS_n(\theta) \qquad (4.18)$$

where m designates multiple.

With the probability of the simulated events having been determined, it is now useful to compute what might be called the ideal scattering probability. This is the probability of a neutron arriving at the detector provided the sample has ideal scattering characteristics. An ideal scatterer is one that produces no attenuation of the incident or scattered

neutron beam and no multiple scattering. Clearly such samples do not exist, but this is the usual approximation by which initial data analysis is carried out. With no attenuation, the probability of scatter is clearly

$$\Sigma_s t_1$$

The probability of scattering into a detector at a specific angle θ_s from before is

$$P_{D1}(\theta) = \frac{\Delta\Omega_D}{\sigma_s(k)} \frac{\partial\sigma}{\partial\Omega} (\theta_s) \tag{4.19}$$

It follows then that ideal scattering probability is merely

$$P_I(\theta_s) = \Sigma_s t_1 P_{D1} = N \sigma_s(k) t_1 \frac{\Delta\Omega_D}{\sigma_s(k)} \frac{\partial\sigma}{\partial\Omega} (\theta_s) \tag{4.20}$$

$$P_I(\theta_s) = N t_1 \Delta\Omega_D \frac{\partial\sigma}{\partial\Omega} (\theta_s)$$

where N is the number density of the target.

With the calculated ideal scattering, single scattering, and multiple scattering probabilities completed, we are now in a position to use these to make corrections to the data that has been processed as if it were an ideal scatterer. To compensate for attenuation one divides the processed data by P_1/P_I. To compensate for multiple scattering, one divides the processed data by

$$(P_1 + P_m)/P_1 = P_T/P_1 \tag{4.21}$$

where P_T is the total scattering probability. The overall correction to the data is thus accomplished by dividing by

$$(P_1/P_I) * [(P_1 + P_m)/P_1) = P_T/P_I. \quad (4.22)$$

That this is the correct form of a correction can readily be shown by the following argument. If our input $S(Q)$ is a reasonable approximation to the material and the code properly simulates the experiment, then the probability of total scatter, P_T, should approximate the actual data as a function of wave vector transfer, i.e.,

$$\frac{\text{Actual Data (Q)}}{P_T(Q)} \sim 1 \quad . \quad (4.23)$$

Similarly, the ideal scattering probability should follow the idealized, or corrected, data.

$$\frac{\text{Corrected Data (Q)}}{P_I(Q)} \sim 1 \quad (4.24)$$

Thus, the corrected data is obtained by dividing the actual data by total scattering probability over the ideal scattering probability.

$$\text{Corrected data} = \frac{\text{Actual Data}}{P_T/P_I} \quad (4.25)$$

The actual code used is more involved than outlined here as it is optimized for time of flight measurements such that many different wavelength neutron histories may be followed efficiently. What have been portrayed are the essential physical features and processes involved in this

useful method of correcting diffraction data for multiple scattering and attenuation effects.

One final question presents itself, and that is what to use as the input S(Q) or $\frac{\partial\sigma}{\partial\Omega}(Q)$. Since S(Q) is the final result we wish to obtain, we clearly cannot have the end product before we start. An option would be to use the S(Q) generated from a model. This approach has the possible deficiency of biasing the result in the direction of the proposed model. Another alternative is to take the initially reduced data as a first approximation to the true S(Q). This method has been used and does not bias the data towards any model. If the approximation to S(Q) and the result after correction differ appreciably the cycle may be reiterated using the corrected S(Q) as a model to produce a new corrected S(Q). For thin samples, we assert this approach converges rapidly and a second iteration is usually not necessary. If multiple scatter and attenuation effects are severe enough such that they become a significant fraction of the initially reduced S(Q), then the wavelength dependent correction factors should be viewed with caution. This arises in part because attenuation correction factors depend on factors of the form $e^{-nx\sigma}$. Small errors in the number density can produce large errors in correction factors when σ is large such as occurs at low neutron energies.

The results of these correction factors are shown on figures IV.3-2, IV.3-3, and IV.3-4.

The result of a measurment is to be divided by the appropriate correction factor. In the case of the single wavelength diffractometer, where no reference sample is used, the initially reduced data is divided by the appropriate values to yield results corrected for multiple scattering. In the time of flight experiment, where data is also taken from a vanadium reference, the corrected vanadium data is obtained by dividing the vanadium data by its correction factor, and the corrected arsenic data is obtained by dividing the arsenic data by its correction factor. The arsenic structure factor is the result of dividing the corrected arsenic data by the corrected vanadium data.

It is interesting to note that the corrections have structure that is in some sense an inverse of the structure factor S(Q). Where the structure factor has peaks, the correction factor has dips, and vice versa. This is to be expected, as one of the effects of multiple scattering is to lower the peaks and fill in the valleys of the actual structure factor. Behavior such as this comes about because when an incident neutron scatters it is most likely to scatter at a Q where the cross section is large. This accounts for lowering of the peaks of the uncorrected structure factor. Neutrons that are detected

after they scatter more than once contribute roughly uniformly to the uncorrected structure factor throughout the range of Q. The combination of these two properties leads to the effect previously described.

The sharp decrease in magnitude of the correction factor at small Q for the time of flight experiment is also expected and is from the large attenuation of the beam at low neutron energies.

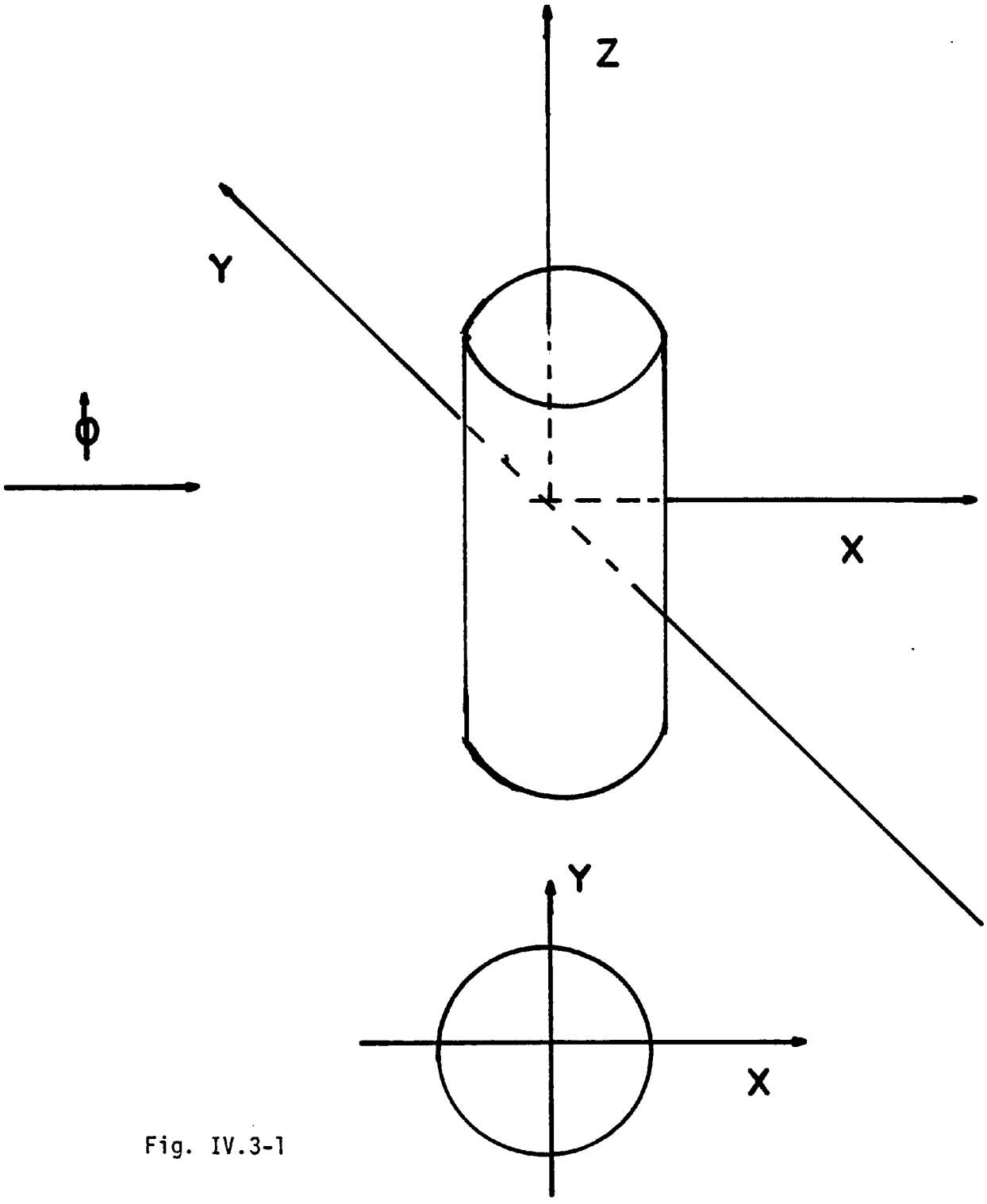

Fig. IV.3-1

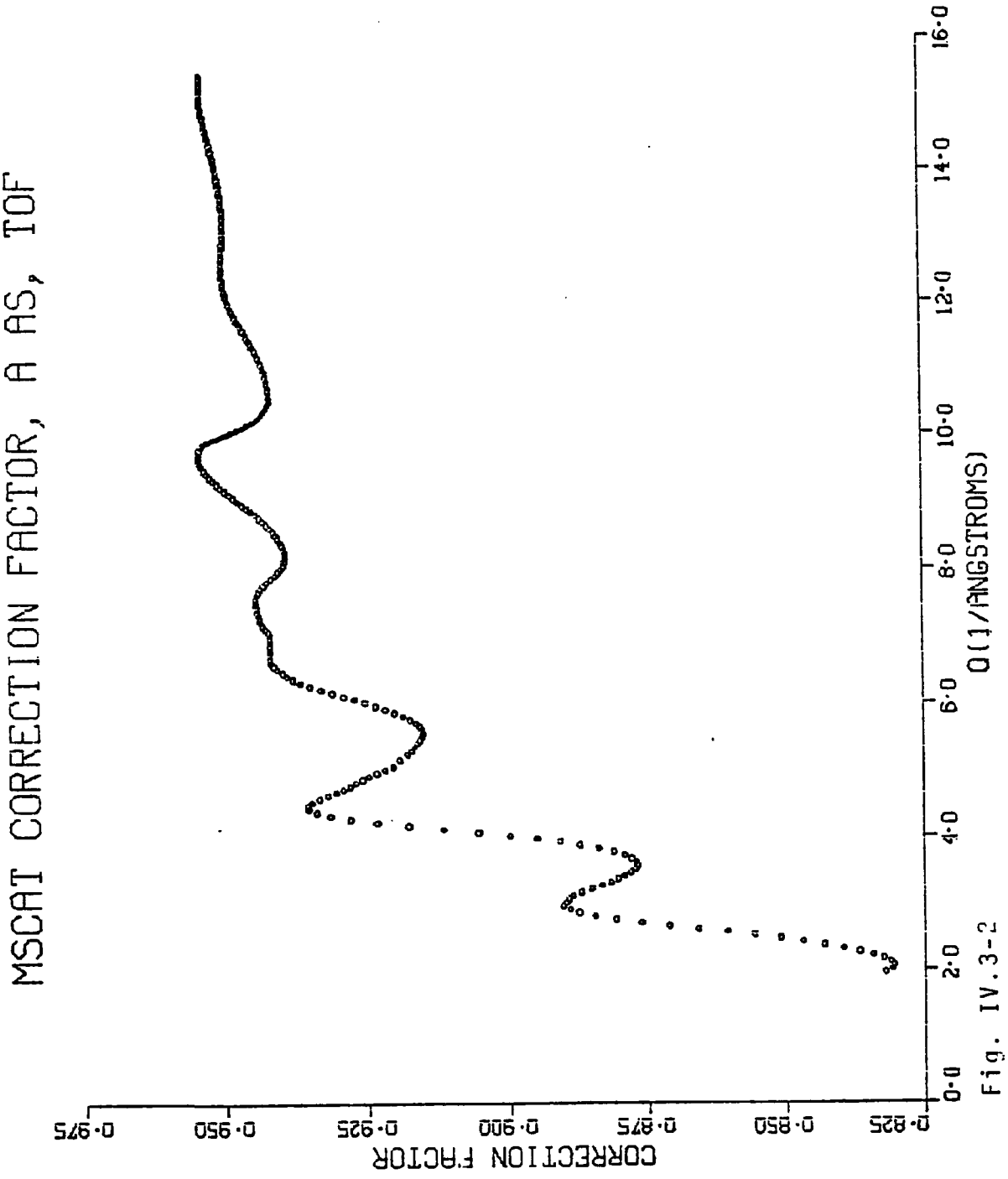
MSCAT CORRECTION FACTOR, A AS, TOF
CORRECTION FACTOR
0.825
0.850
0.875
0.900
0.925
0.950
0.975
0.0
2.0
4.0
6.0
8.0
10.0
12.0
14.0
16.0
Q(1/ANGSTROMS)

Fig. IV.3-2

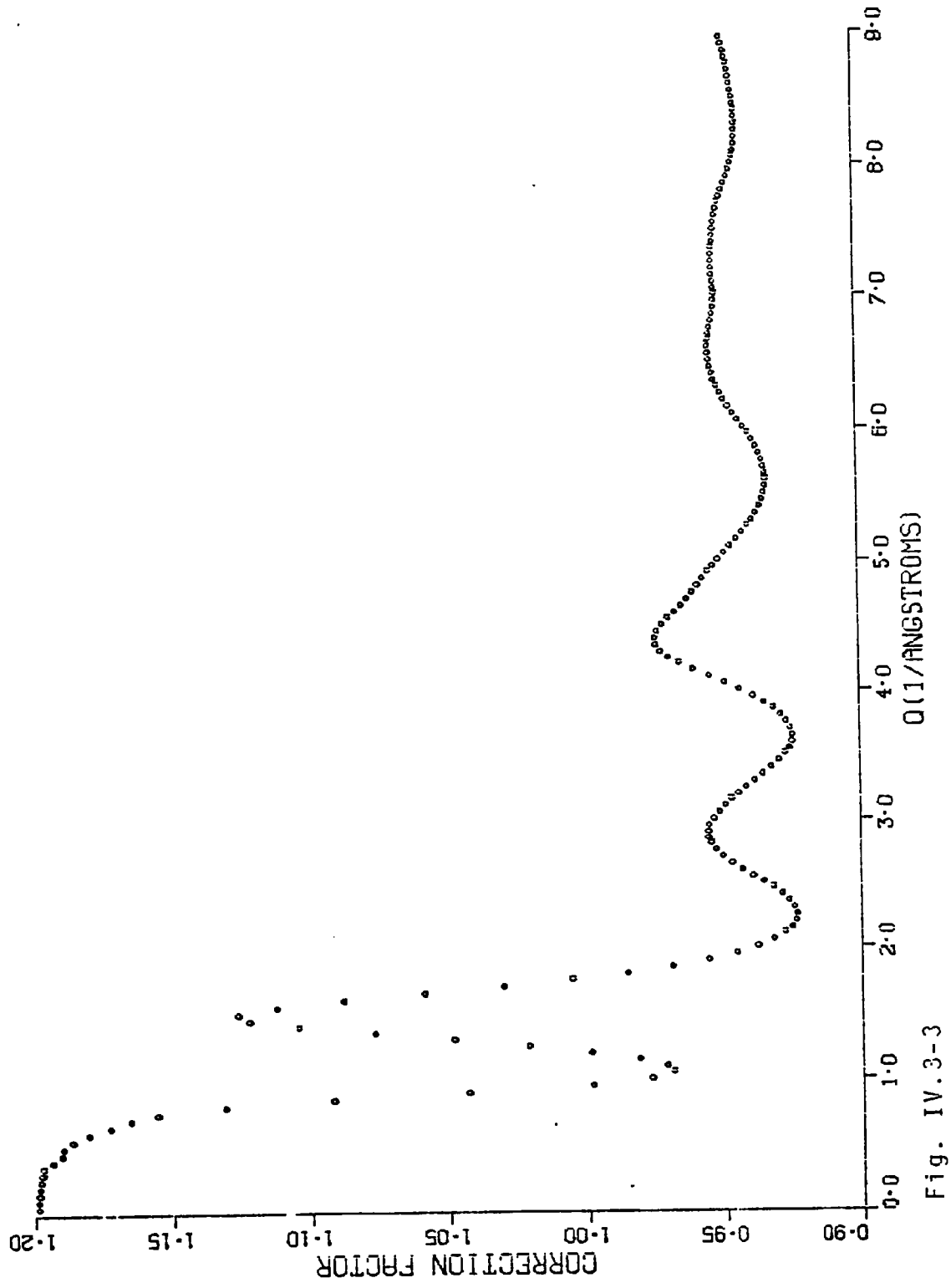
MSCAT CORRECTION FACTOR, A AS, 1 LAMDA
CORRECTION FACTOR
0.90
0.95
1.00
1.05
1.10
1.15
1.20
0.0
1.0
2.0
3.0
4.0
5.0
6.0
7.0
8.0
9.0
Q(1/ANGSTROMS)

Fig. IV.3-3

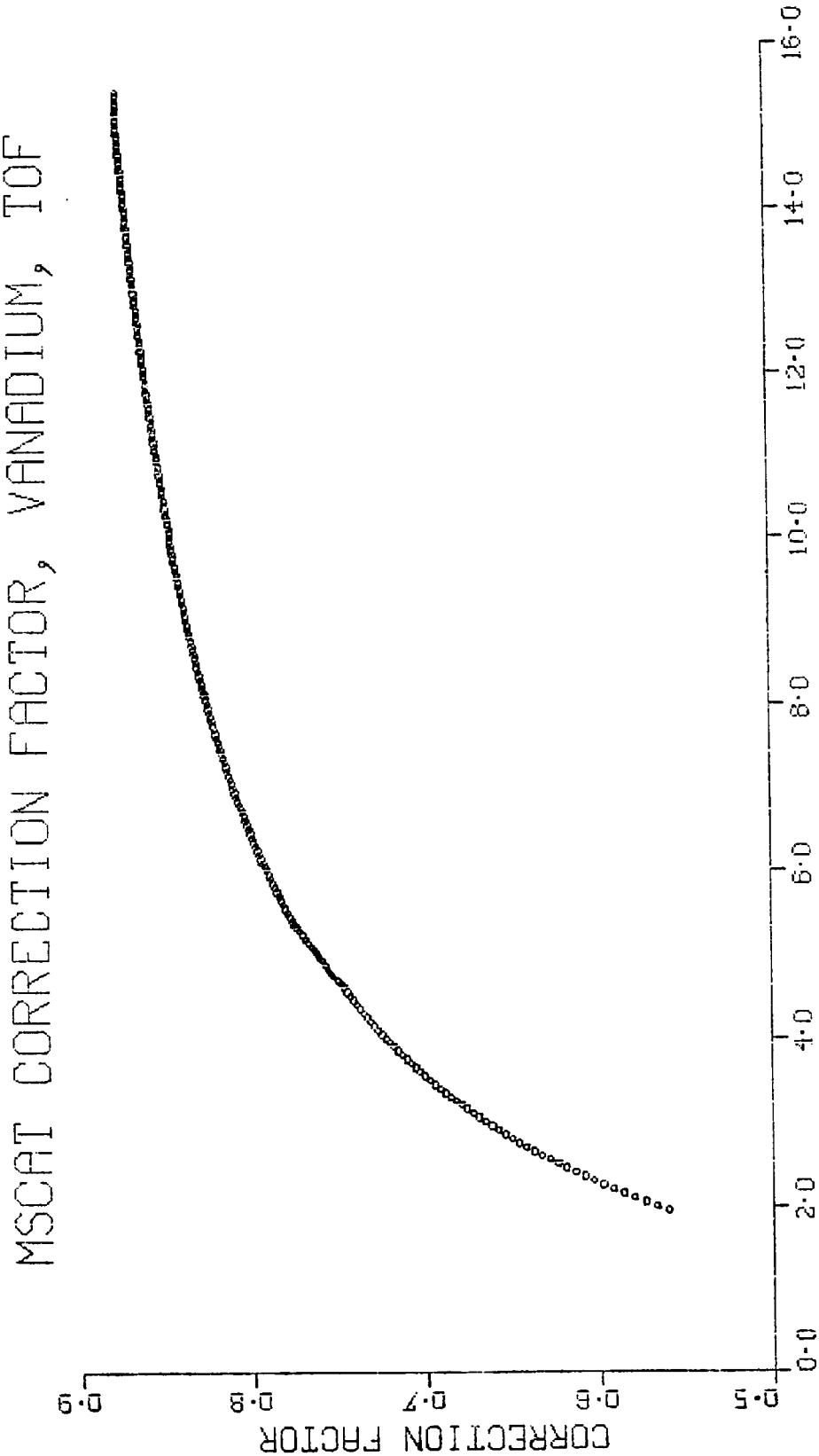
MSCAT CORRECTION FACTOR, VANADIUM, TOF
CORRECTION FACTOR
0·5
0·6
0·7
0·8
0·9
0·0
2·0
4·0
6·0
8·0
10·0
12·0
14·0
16·0
Q(1/ANGSTROMS)

Fig. IV.3-4

4.4 Inelastic Scattering Corrections

4.4.1 Introduction

In neutron diffraction measurements mention is often made of the need for 'Placzek' corrections to compensate for the inelastic scattering of neutrons from the sample. This correction is many times stated to be small and no further discussion of the problem is made. Recently, however, measurements of molecular liquids have been analyzed using extensive Placzek correction (Dore, 1977). The range and validity of Placzek corrections, especially when the corrections are large, has not been well established. We also note that these corrections tend to be largest, for the single incident wavelength diffractometer, in the region of large Q. In a time of flight experiment, these corrections are not necessarily largest at large Q, and therefore a sound method for treating the inelastic scatter must be developed for high accuracy diffraction measurements.

The approach taken follows from the path integral method touched on in Chapter II, Eqs. (2.38) and (2.39). We will model the (symmetrized) scattering law $S(Q,\varepsilon)$, and then integrate $S(Q,\varepsilon)$ along the integration path of the instrument and along a path of constant Q. The ratio of these two integrals will produce a correction factor that can be applied to the data to yield $S(Q)$.

$$S(Q) = \int_{\text{const } Q} S(Q,\varepsilon)d\varepsilon \quad . \tag{4.26}$$

Of course the question now arises as to what does one use as the model of $S(Q,\varepsilon)$. Clearly a measurement of $S(Q,\varepsilon)$ would serve as the best model, but then if the scattering law were known for all (Q,ε), there would be little point in correcting a diffraction measurement. All of the information necessary to compute the results of a diffraction measurement is contained within the complete mapping of $S(Q,\varepsilon)$ and therefore the diffraction measurement itself becomes redundant. Large region mappings of the scattering law are quite time consuming and are not frequently done.

We therefore propose, to approximate the scattering law utilizing the model set forth in Marshall & Lovesey (1971). Using this model for $S(Q,\varepsilon)$ we can numerically integrate through any path we need in (Q,ε) space to obtain corrections to the data. It is then claimed that the inelastic scattering corrections we make are only weakly dependent on the details of the model, and therefore even though the model is quite approximate, the corrections can be reasonably accurate.

4.4.2 Form of Correction Factors

The only static structural information that may be derived from an amorphous system is $S(Q)$, the static structure factor, or the correlation function $G(r)$ which are related by the standard Zernike-Prins (1927) relationship

$$G(r) = 4\pi r\rho(\rho(r) - \rho_0) = \frac{2}{\pi}\int_0^\infty Q(S(Q) - 1)\sin QrdQ \quad (4.27)$$

We will assume that G(r) is the object of the measurement and follow the functional relationship back toward the measurement to find an accurate method of determining G(r). Presently we ignore the effects of normalization and termination of the Fourier transform and see that the accuracy of G(r) depends only upon the correctness of S(Q). We remove the effects of multiple scattering processes from this function by the procedure described in the previous section. What is still left to consider is the effect of inelastic scattering. The static approximation is often justifiably made which assumes that all atoms in the target are fixed and no recoil is permitted. This is clearly not the exact case, and compensation for this may be made. Let us determine in what manner the S(Q) that we measure depends on the details of the measurement.

The accurate S(Q) that we wish to determine is the integral of $S(Q,\varepsilon)$ over a range of ε from $-\infty$ to $+\infty$ along a path of constant Q.

$$S(Q)_{exact} = \int_{\substack{-\infty \\ \text{Path of const. } Q}}^{+\infty} S(Q,\varepsilon)d\varepsilon \quad (4.28)$$

One can relate the double differential cross section to the scattering law $S(Q,\varepsilon)$ by Eq. (2.35). The scattering law, $S(Q,\varepsilon)$ is a function only of the sample structure and dynamics. The conventional interpretation of diffraction measurements is to identify $\frac{\partial\sigma}{\partial\Omega}(Q)_{meas}$ with $S(Q)$. However, this is not exactly what we obtain from a measurement. The result of a measurement yields

$$\frac{\partial\sigma}{\partial\Omega}(Q) = \int_{\substack{\text{Instrumental}\\ \text{Integration}\\ \text{Path}}} W(Q,\varepsilon)\,\frac{\partial^2\sigma}{\partial\Omega\partial\varepsilon}\,d\varepsilon \tag{4.29}$$

where $W(Q_\varepsilon,\varepsilon)$ is a weighting function that depends on the detector efficiency, and the incident flux. The integration path is also not necessarily coincident with the path of constant Q. Thus, in order to compensate for the inappropriate weighting and an integration path of nonconstant Q, a correction to the data of the following form is proposed.

$$S(Q)_{corrected} = \left[\frac{\int_{-\infty}^{+\infty} S(Q,\varepsilon)_{model}\,d\varepsilon}{\int_{\substack{\text{Instrumental}\\ \text{Integ Path}}} W(Q,\varepsilon)\frac{\partial^2\sigma}{\partial\Omega\partial\varepsilon}(Q,\varepsilon)_{model}\,d\varepsilon}\right]\int_{\substack{\text{Inst}\\ \text{Integ}\\ \text{Path}}} W(Q,\varepsilon)\frac{\partial^2\sigma}{\partial\Omega\partial\varepsilon}(Q,\varepsilon)\,d\varepsilon \tag{4.30}$$

The $S(Q)_{corrected}$ may then more accurately be interpreted as $S(Q)$ than the result of an uncorrected measurement.

The integral along the instrumental integration path in the numerator is taken to be the measured $\frac{\partial\sigma}{\partial\Omega}(Q)_{meas}$. The ratio of integrals preceding the $\frac{\partial\sigma}{\partial\Omega}(Q)_{meas}$ is the correction factor to the measured data and can be calculated numerically provided $S(Q,\varepsilon)$ is known. Clearly this is not known accurately or there would be no point in carrying out a diffraction measurement. The single differential cross section could be determined precisely from the double differential cross section. However, double differential cross sections are not known accurately over extensive (Q,ε) range particularly for amorphous materials. Nevertheless, the scattering law for isotropic samples may be modeled from the static structure factor, and the sound speeds of the material (Carpenter & Pelizzari, 1975). We then use a model for $S(Q,\varepsilon)$, the known weighting function $W(Q,\varepsilon)$ and integrate numerically along the appropriate paths to determine the correction to the data. It is then claimed that the correction factor thus obtained is only weakly dependent on the shape of the modeled $S(Q,\varepsilon)$. Provided $S(Q,\varepsilon)_{model}$ is a reasonable approximation to $S(Q,\varepsilon)_{real}$ then this correction factor should compensate reasonably accurately for the effects of inelastic scatter. This approach may seem naive, but it should be compared to the usual method of the Placzek expansion. Placzek assumes the scattering law to be an expansion about the elastic scattering value of Q.

$$S(Q,\varepsilon) = S(Q_e,\varepsilon) + S'(Q_e,\varepsilon)(Q^2-Q_e^2) + \frac{1}{2!}[S''(Q_e,\varepsilon)(Q^2-Q_e^2)^2] + \ldots \quad (4.31)$$

where the prime indicates differentiation with respect to Q^2. This form of the scattering law is often used with productive results, but its utility might seem in doubt as the corrections increase in magnitude. This form assumes no information about the material other than the values of the elastic scattering law. It seems that a model of the scattering law that is more descriptive and material dependent than that assumed by Placzek would be useful for comparing to the results of inelastic scattering data. If the descriptive model holds up for describing the double differential cross section, then one might infer that corrections to diffraction data for other isotropic systems using this model will be correct. Our next task is therefore to derive a model for the scattering law, $S(Q,\varepsilon)$.

4.4.3 Model of the Scattering Law

4.4.3.1 General

For a harmonically oscillating systems, the scattering law may be developed in a "phonon expansion"

$$S(Q,\varepsilon) = S_0(Q,\varepsilon) + S_1(Q,\varepsilon) + S_2(Q,\varepsilon) + S_3(Q,\varepsilon) + \ldots \quad (4.32)$$

in which $S_0(Q,\varepsilon)$ is the elastic contribution, $S_1(Q,\varepsilon)$ is the contribution from one phonon processes, $S_2(Q,\varepsilon)$ the two phonon contribution, and so on to higher order processes.

The model we propose separates this scattering law into three parts. They are 1) elastic scattering, 2) one phonon scattering, and 3) multiphonon scattering. The multiphonon scattering term includes two phonon and all higher order processes. Our modeled scattering law can then be represented as

$$S(Q,\varepsilon) = S(Q,\varepsilon)_{\text{elastic}} + S(Q,\varepsilon)_{\text{1 phonon}} + S(Q,\varepsilon)_{\text{multiphonon}} . \tag{4.33}$$

For a general description of this breakdown, see Marshall and Lovesey (1971) or Sjolander (1958).Methods chosen to calculate the one phonon and multiphonon scattering require a knowledge of the density of states of vibration of the

material. This density of states will be calculated using a modified Debye model (Brillouin, 1946). Integration of the density of states is then performed to obtain the Debye-Waller factor for the material. The elastic scattering, one phonon, and multiple scattering can then be calculated. In the following sections the model density of states is first derived. This is followed by the calculation of the Debye-Waller factor. The three parts of the scattering law are then each individually set forth, making appropriate use of the necessary density of state and Debye-Waller calculations.

4.4.3.2 Model Density of States

The density of states (which will be defined later) is represented by a modified Debye model. One aspect of this model is the specification of the dispersion relationship between ω and k. Other contributions to this model are the choice of appropriate unit cell volumes and cutoff frequencies. Once these quantities are known the calculation of the density of states may be completed.

We will assume that all modes are acoustic and have a linear, isotropic dispersion relationship. From this it follows that

$$\omega = vk \tag{4.34}$$

where ω = frequency of vibration

v = sound velocity in material

k = magnitude of propagating wave vector.

We will also concern ourselves with only one atom per spherical unit cell. It should be noted that if one is using the simplistic $\omega = vk$ dispersion relationship and the material contains only one equivalent molecular unit, then picking the basis to have one atom per unit cell and only acoustic modes is similar in the sense of a rough approximation, to choosing a larger unit cell and including the optic modes.

Since there is N = 1 atom per unit cell, and there are 3 modes of vibration per atom, there are clearly 3 modes per unit cell. These consist of one longitudinal and two transverse modes with their corresponding dispersion relationships.

$$\omega_L = v_L k \tag{4.35}$$

$$\omega_T = v_T k$$

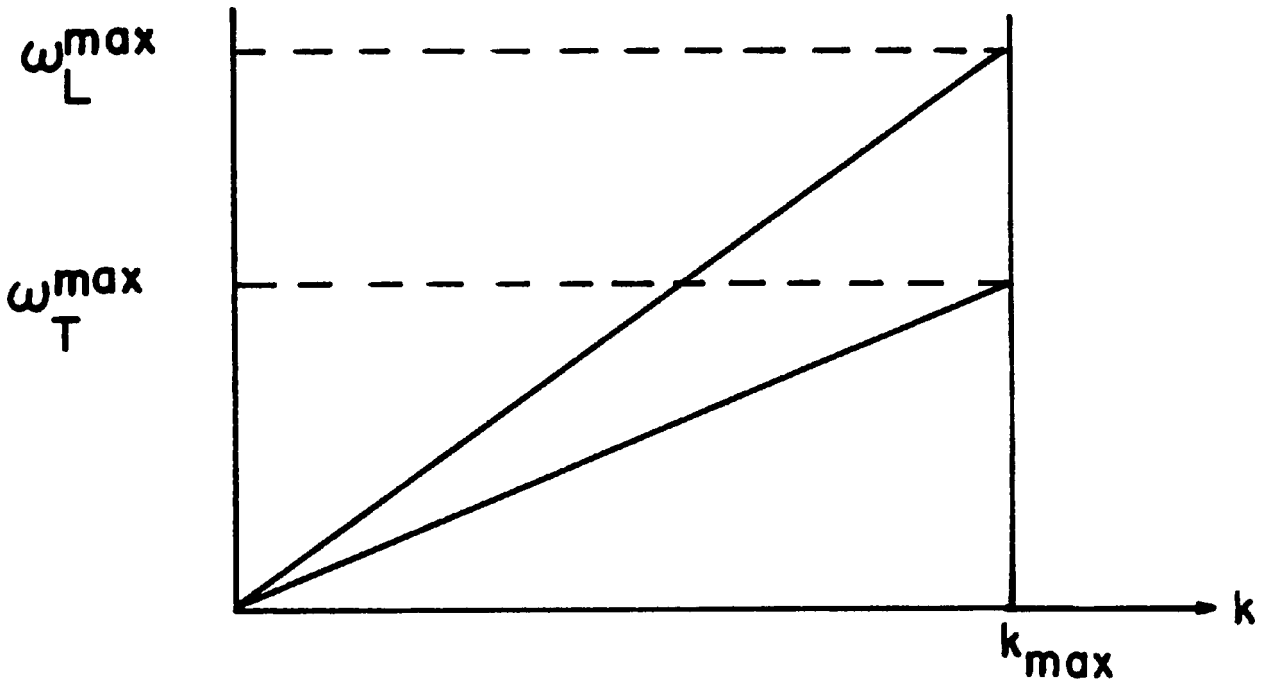

Dispersion relationship for isotropic crystalline solid with one atom/unit cell according to Brillouin (1953).

We have thus specified the dispersion relationship. We must now determine what these cutoff frequencies are in terms of the appropriate parameters which are the two sound velocities and a tabulated parameter of the material, the Debye temperature. The following procedure amounts to an internally self consistent method for normalizing the cutoff frequencies and the density of states. The normalization will be expressed as an effective 'volume' of the primitive unit cell.

If we assume the first Brillouin zone to be a sphere of radius k it then follows that

$$\frac{4}{3}\pi k^3 = V_r = \frac{(2\pi)^3}{V} = (2\pi)^3 \frac{N}{V_o} \qquad (4.36)$$

where V_r = volume in reciprocal space of the first Brillouin zone

V = volume in direct space of the primitive unit cell

N = number of atoms in the sample

V_o = volume of the sample

and $k \rightarrow k_{max}$.

The volume in direct space of the primitive unit cell is then

$$V = \frac{3 \cdot (2\pi)^3}{4\pi k_{max}^3} \tag{4.37}$$

Using the dispersion relation for the transverse and acoustic modes combined with the solution of the above expression for k_{max}, we find the two separate cutoff frequencies that are required for both dispersion relations to terminate at the same Brillouin zone boundary.

The values of the cutoff frequencies are

$$\omega_L^{max} = v_L \{\frac{3}{4\pi V}\}^{1/3} \qquad \omega_T^{max} = v_T \{\frac{3}{4\pi V}\}^{1/3} \tag{4.38}$$

If we use standard Debye theory with only one cutoff frequency, then

$$k_B \theta_D = \hbar \omega_D \tag{4.39}$$

where k_B = Boltzmann's constant

θ_D = Debye temperature

ω_D = Debye cutoff frequency

and one can obtain θ_D from published values of the Debye temperature. Using expressions equivalent to the standard Debye relationship but for specifically the longitudinal and transverse modes we obtain

$$\theta_L = \frac{\hbar\omega_L^{max}}{k_B} \qquad \theta_T = \frac{\hbar\omega_L^{max}}{k_B} \quad . \tag{4.40}$$

Using Eqs. (4.35), (4.40) and the relationship between the three temperatures

$$\frac{1}{\theta_L^3} + \frac{2}{\theta_T^3} = \frac{3}{\theta_D^3} \tag{4.41}$$

one arrives at a normalizing condition expressed as the volume of the primitive unit cell.

$$V = \frac{3}{4\pi} \left(\frac{h}{k_B \theta_D}\right)^3 \left[\frac{3}{\frac{1}{v_L^3} + \frac{2}{v_T^3}}\right] \tag{4.42}$$

This equation and (4.35) yield the cutoff frequencies uniquely provided v_L, v_T, and θ_D are known.

The Debye temperature of many materials are readily measured and often published. The transverse and longitudinal sound velocities can be measured without difficulty, although there is a shortage of published data on these values. To obtain rough estimates for isotropic or polycrystalline materials, the relationship to the bulk and shear moduli of the material may be used.

$$v_\ell = \sqrt{E/\rho} \qquad v_T = \sqrt{\mu/\rho} \tag{4.43}$$

E = Young's (bulk) modulus of a material

μ = shear modulus

ρ = density

For polycrystalline vanadium Reynolds (1952) gives E = 1.27×10^{12} dynes/cm^2 and $\mu = .466 \times 10^{12}$ dynes/cm^2. These values correspond to

v_ℓ = 4581 m/sec

v_T = 2775 m/sec

No equivalent values were found for amorphous arsenic. One might attempt to infer the sound speeds of aAs from those

determined for the single crystal. Pace et al. (1970) give elastic constants and sound velocities for eight combinations of symmetry directions and polarizations. However, in the first place it is not obvious how to average the values from the different symmetry and polarization directions. Secondly the electronic properties of aAs differ significantly from those of polycrystalline As, and thus there is reason to believe that the elastic constants, and hence sound velocities, would also differ.

The actual values of the two sound velocities for aAs were inferred from neutron inelastic scattering data of Leadbetter (1976) and the microscopic density (Stohr 1939). These calculations, carried out in Appendix I, give for aAs

$$v_L = 3479 \text{ m/sec}$$
$$v_T = 1624 \text{ m/sec}$$
$$\theta_D = 183^{\circ}K$$

These are reasonable values and we also find the Debye temperature in fair agreement with that calculated by Wu (1973/74) of $\theta_D = 169^{\circ}K$ at $20^{\circ}K$.

This completes the specification of the dispersion relationship. Now, knowing this dispersion it is a simple matter to determine the density of states for any k or ω. Here we briefly derive the density of states for a material

with one atom per unit cell and show how the acoustic velocities and Debye temperatures are related to this quantity.

The number of modes, N, in a spherical volume of reciprocal space of radius k is a constant times the volume of the sphere.

$$N = C\int_0^k d^3k' \qquad (4.44)$$

$$= C\frac{4}{3}\pi k^3 \quad .$$

We change variables to ω by using (4.31) and obtain

$$N = C\ \frac{4\pi}{3}\ \frac{\omega^3}{v^3} \qquad (4.45)$$

The density of modes (density of states) is merely the number of modes per unit frequency range. This quantity can be found by differentiating the above expression.

$$\frac{dN}{d\omega} = C\ \frac{4\pi\omega^2}{v^3} \qquad (4.46)$$

Normalization of this expression is done by observation of (4.44). One knows that the product of the volume of the first Brillouin zone times the volume of the primitive unit cell is $(2\pi)^3$. The integral on the right hand side of (4.44)is the volume of the first Brillouin zone. The number of modes in the first Brillouin zone is three. The constant C can then be reformulated in terms of the volume of the primitive cell as defined by (4.42) to be

$$C = \frac{3V}{(2\pi)^3} \quad . \tag{4.47}$$

The normalized density of states is then

$$D(\omega) = \frac{dN}{d\omega} = \frac{3V}{(2\pi)^3} \cdot \frac{4\pi\omega^2}{v^3} \tag{4.48}$$

Since we have two types of vibrations in the three modes with two different acoustic velocities the detailed expression becomes

$$D(\omega) = \frac{3V}{(2\pi)^3} \cdot 4\pi \left\{ \sum_{|\omega|<\omega_L^{max}} \frac{\omega^2}{v_L^3} + \sum_{|\omega|<\omega_T^{max}} \frac{2\omega^2}{v_T^3} \right\} \tag{4.49}$$

The density of states has been treated as a frequency distribution. It can just as easily be defined to be an energy distribution by using the Jacobian 1/h.

$$D(\varepsilon) = \frac{1}{h} D(\omega)$$

Future references to the density of states will be to $D(\varepsilon)$.

4.4.3.3 Debye-Waller Factor

The Debye-Waller factor, e^{-2W}, is a function that describes the average thermal motion of atoms in a solid. We take $2W = AQ^2$ where A is proportional to the mean square displacement of the nucleus from its equilibrium position.

If the elastic scattering law has a functional form similar to that of the Debye-Waller factor, then the Q

dependence of elastic scattering from an incoherent scatterer is reasonably well represented. Similarly, this functional form should appear in the one phonon and multiphonon structure factors.

The quantity A can be obtained by integration of the density of states function $D(\varepsilon)$, that was previously derived, in the following manner (Marshall and Lovesey, 1971).

$$A = \frac{h^2}{2M} \int_0^{\varepsilon_{max}} \frac{D(\varepsilon) \coth(\frac{\varepsilon}{2kT})}{\varepsilon} \, d\varepsilon \qquad (4.50)$$

where M = mass of target atom

ε = energy of photon

The value for A is found to be A = .0108[$\mathring{A}^2$].

The Debye-Waller factor will be found in the three contributions to the scattering law and thus it has been presented before the separate parts of the scattering law.

4.4.3.4 Elastic Scattering

The zero phonon scattering is the elastic scattering which we represent as

$$S(Q,0) = S_{e\ell}(Q)\,\delta(\varepsilon) \qquad (4.51)$$

where $S_{e\ell}(Q) = S(Q)e^{-2W}$

and 2W was previously determined.

4.4.3.5 One Phonon Scattering

A model for the one phonon scattering law in terms of the structure and the acoustic-wave modes of vibration of the material has been derived by Carpenter (1975). When this model is combined with other assumptions presumed to be valid for an isotropic material and acoustic wave modes, he arrives at a result of

$$S^1(Q,\varepsilon) = e^{-2W} \frac{\hbar Q^2}{2m} \frac{V}{(2\pi)^2} \frac{1}{2\varepsilon \sinh(\frac{\varepsilon}{2kT})} (\frac{q_L^2}{v_L} f_L(Q,\varepsilon) + \frac{q_T^2}{v_T} f_T(Q,\varepsilon)) \quad (4.52)$$

with

$$f_L(Q,\varepsilon) \equiv \int_{-1}^{1} \mu^2 \, S((Q^2+q_L^2-2Qq_L\mu)^{1/2}) d\mu \quad (4.53)$$

$$f_T(Q,\varepsilon) \equiv \int_{-1}^{1} (1-\mu^2) \, S((Q^2+q_T^2 - 2Qq_T\mu)^{1/2}) d\mu \quad (4.54)$$

$$\mu = (Q^2 + q^2 - K^2)/2Qq \quad (4.55)$$

$$q_{L,T} = \frac{\varepsilon}{\hbar v_{L,T}} \quad (4.56)$$

The point of this formulation is that the only quantities necessary to formulate the scattering law according to this model are the two acoustic velocities and the structure factor, S(Q).

4.4.3.6 Multiphonon Scattering

In evaluating the contribution of multiphonon events to the scattering we use the Sjolander incoherent approximation. This says that the multiphonon cross section is rather insensitive to the details of the vibrational properties of the material and the interference terms in the coherent cross section make a no contribution to the scattering. For an isotropic system, we find from Sjölander (1958) that in the incoherent approximation, the scattering law can be written as

$$S(Q,\varepsilon) = \exp(-2W-\varepsilon/2kT)* \frac{1}{2\pi\hbar}\int_{-\infty}^{\infty}\exp[\frac{i(\varepsilon\ )}{\hbar}]t\exp(\frac{\hbar Q^2}{2m}[\gamma(t)-\gamma(0)])\ dt \qquad (4.57)$$

where

$$\gamma(t) = \int_{o}^{\varepsilon_{max}}[\coth(^{\beta\varepsilon})\cos(\frac{\varepsilon t}{\hbar})+i\sin\ (\frac{\varepsilon t}{\hbar})]\ \frac{D(\varepsilon)}{\varepsilon}\ d\varepsilon \qquad (4.58)$$

m = mass of nucleus

$\beta = \frac{1}{2k_BT}$

$D(\varepsilon)$ = density of states of sample .

The problem is how to choose some representation of $\gamma(t)$ such that the $\int dt$ may be carried out. In actuality, it may be best to carry out all of both integrals numerically after one has chosen a representative distribution function. The total numerical approach was not followed, but rather Sjölander's approximation was used.

He arrives at a final result for the multiphonon scattering law of

$$S(Q,\varepsilon)\Big|_{\substack{\text{multiphonon}\\(n \geq 2)}} = \exp(-2W-\frac{\varepsilon}{2k_BT})\{\frac{1}{\sqrt{\bar{\alpha}_2}} F(Z_1,X_1)+\frac{\bar{\gamma}_2}{\sqrt{\bar{\alpha}_2}} F_1(Z_1,X_1)\} \tag{4.59}$$

with the quantities contained within this expression defined below.

$$2W = \frac{\hbar Q^2}{2m}\bar{\gamma}(0) \qquad \text{(the Debye Waller factor)}$$

$$\bar{\gamma}(0) = \int_0^{\varepsilon_{max}} \frac{\varepsilon D(\varepsilon)}{\sinh(\frac{\varepsilon}{2kT})}\, d\varepsilon$$

$$\bar{\alpha}_2 = \frac{1}{\bar{\gamma}(0)} \int_0^{\varepsilon_{max}} \frac{\varepsilon D(\varepsilon)}{\sinh(\frac{\varepsilon}{2kT})}\, d\varepsilon$$

$$\bar{\alpha}_4 = \frac{1}{\bar{\gamma}(0)} \int_0^{\varepsilon_{max}} \frac{\varepsilon^3 D(\varepsilon)}{\sinh(\frac{\varepsilon}{2kT})}\, d\varepsilon$$

$$F(Z,x) = \sum_{n=2}^{\infty} \frac{Z^n}{n!} \frac{\exp(-x^2/2n)}{(2\pi n)^{1/2}}$$

$$F_1(Z,x) = \sum_{n=2}^{\infty} \frac{Z^n}{n!n} \frac{\exp(-x^2/2n)}{(2\pi n)^{1/2}} H_4(x/\sqrt{n})$$

$$\bar{\gamma}_2 = \frac{\bar{\alpha}_4 - 3\bar{\alpha}_2^2}{4!\bar{\alpha}_2^2}$$

$$Z_1 = \frac{\hbar^2 Q^2}{2m} \bar{\gamma}(0) \qquad X_1 = \varepsilon/\sqrt{\bar{\alpha}_2}$$

$$H_4(x) = x^4 - 6x^2 + 3$$

The manner in which this expression for the multiphonon scattering law is obtained is rather detailed and not delineated here.

4.4.4 Results of the Model

The inelastic scattering corrections are carried out by two computer codes, MULTPHON and PATHINTG. MULTPHON, standing for multiphonons, models the total symmetrized scattering law given the parameters of Debye temperature, longitudinal and transverse sound velocities, atomic weight, density and uncorrected diffraction pattern. The generated scattering law is stored in a file to be used by PATHINTG. PATHNTG, for path integral, is an adaptation of a code developed by C. A. Pelizzari that integrates through the scattering law along a specified path and properly weights the various contributions to the integral. The integration path of constant Q is simple to find. However, the path that an instrument follows is not so straightforward. For the time of flight instrument, the path is one of constant time of arrival of the neutrons, and constant scattering angle. The equations to solve are

constant time of arrival

$$\frac{L_1}{v_0} + \frac{L_2}{v'} = \tau_0 \qquad (4.60)$$

τ_0 = time of arrival

L_1 = initial flight path length

L_2 = final flight path length

v_0 = initial neutron velocity

v' = scattered neutron velocity

conservation of neutron energy

E_0 = initial neutron energy

E' = scattered neutron energy

$$E_0 + \varepsilon = E' \tag{4.61}$$

One chooses a time of arrival, τ_0 (which corresponds to elastic scattering for some wave vector transfer), and an energy transfer, ε, and then solves the equations for their roots v_0, v' by Newton's method. The velocities v_0, v' and the scattering angle θ_s, are used to determine the wave vector transfer, Q.

$$Q = \frac{m}{\hbar}\sqrt{v_0^2 + v'^2 - 2v_0 v' \cos\theta_s} \tag{4.62}$$

For a given time of arrival, this procedure is carried out for numerous energy transfers to find the complete path.

The path is easier to locate for the constant wavelength diffractometer. Here E_0 (and thus also v_0) is set by the monochromating crystal. Then an energy transfer, ε, is chosen and the following equations are solved.

$$E' = E_0 + \varepsilon \tag{4.63}$$

$$v'^2 = 2E'/m \tag{4.64}$$

$$Q = \frac{m}{\hbar}\sqrt{v_0^2 + v'^2 - 2v_0 v' \cos\theta_s} \tag{4.65}$$

where again θ_s is the scattering angle. The scattering angle here will vary in contrast to the time of flight diffractometer. The result from the integration along the instrumental path is divided by the result from integration along the path of constant Q to produce the correction factors on the accompanying Figures IV.4-1, IV.4-2. The instrumental paths of integration are also displayed on Figures IV.4-3, IV.4-4.

We see that the maximum correction is $\sim$ 7% at $Q = 15\ \text{Å}^{-1}$. From the similarity of results by the two methods, one might then infer that the results from the path integration method will be correct for materials other than vanadium. A comparison of the correction factors indeed shows a correspondence in shape.

In Appendix II a comparison is made between correction factors produced by integrating the scattering law through the path of the instrument and the path of constant Q, and the correction factors produced by Placzek methods as adapted to a pulsed source by Sinclair and Wright (1974). This comparison is done on vanadium. From the similarity of results by the two methods, one might then infer that the results from the path integration method will be correct for materials other than vanadium. A comparison of

the correction factors indeed shows a correspondence in shape. This similarity might be expected as both vanadium and arsenic are heavy elements such that the energy taken away by recoil of the target atom from the neutron is small. Also, the scattering law model tends to be rather insensitive to the details of the structure factor S(Q). We note that the correction factor for vanadium varies from more unity than for arsenic, as it should. This is because vanadium has the smaller mass and is subject to more recoil.

Finally, in the vanadium reference method the appropriate correction factors need to be applied both for the vanadium and the arsenic. The net correction to the initially reduced data is the ratio of these two corrections. It is apparent that these factors vary by at most 3% throughout the range of the simulation and thus corrections to the diffraction pattern will be not greater than 3%. It is interesting to see that inelastic scattering contributions are minimized using the vanadium reference method by a similar inelastic scattering contribution in the sample and the reference.

For the case of the single wavelength diffractometer, there is no reference scatterer to be concerned with. The graph of the correction factor for this instrument is shown in Figure IV.4-2. The variation of this factor from one unity is seen to be less than 1% over the range in which this data was used, but no comparison is made with other methods of calculation.

The conclusion of this analysis of the error introduced to the diffraction pattern from inelastic scattering events is less than 1% from the single wavelength diffractometer, and less than 3% from the time of flight diffractometer. In light of their small contribution and relative uncertainties, it was concluded that the data could best be analyzed by ignoring the effects of inelastic scattering.

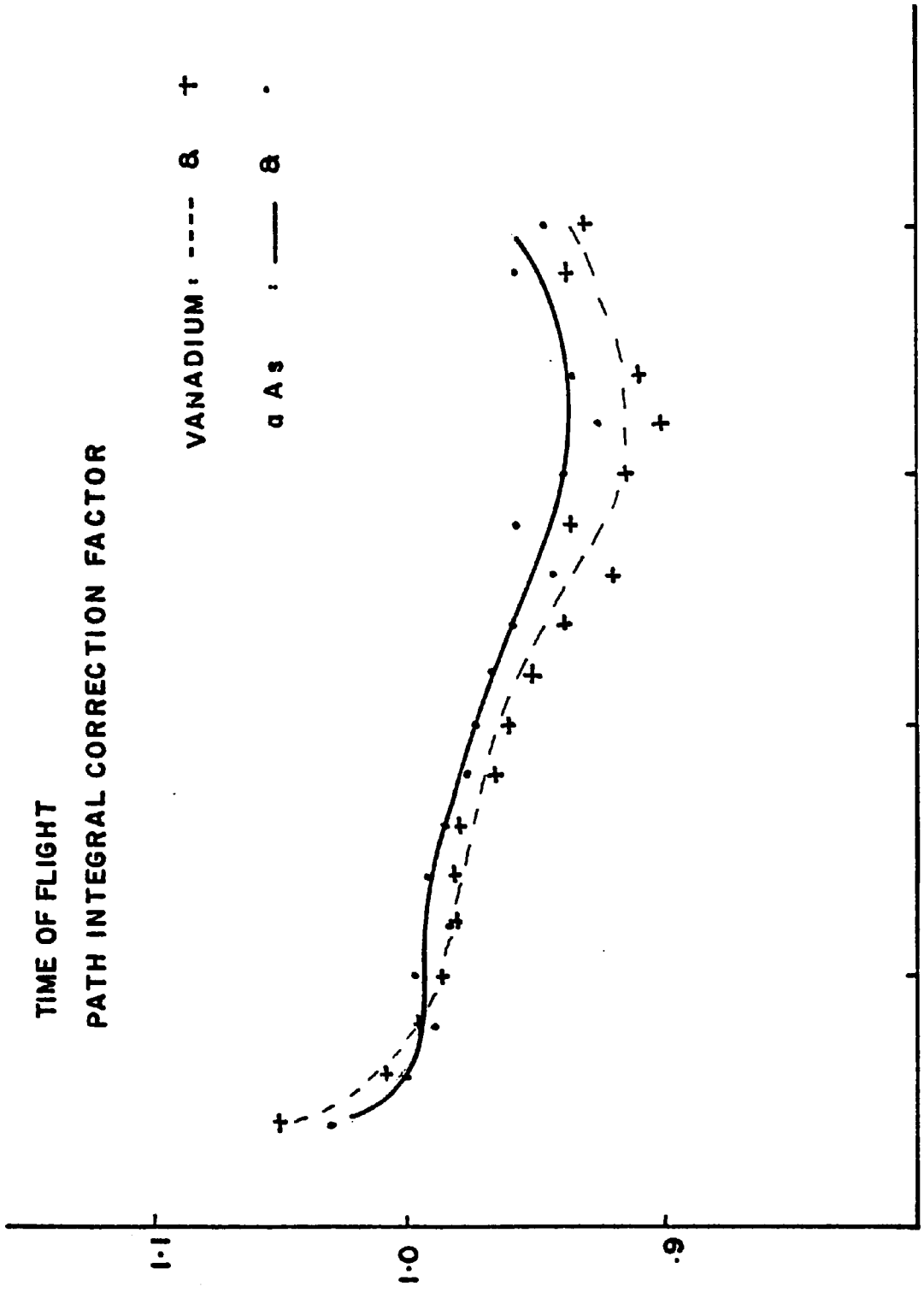
TIME OF FLIGHT
PATH INTEGRAL CORRECTION FACTOR
VANADIUM : ---- &
a As : —— &
1·1
1·0
·9
0 1 2 3 4 5 10 15 20
Q(Å⁻¹)

Fig. IV.4-1

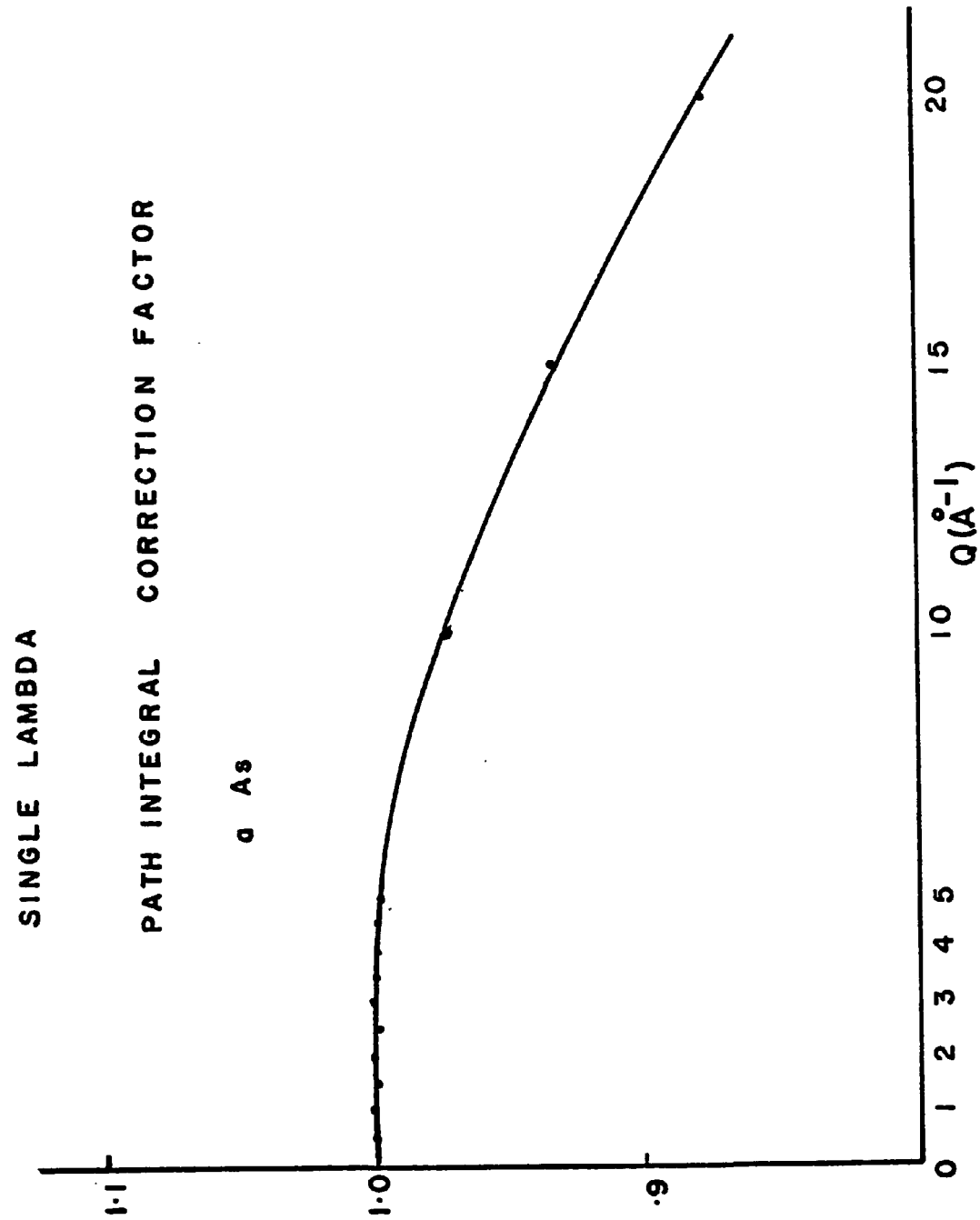
SINGLE LAMBDA
PATH INTEGRAL CORRECTION FACTOR
a As
1·1
1·0
·9
0 1 2 3 4 5 10 15 20
Q(Å⁻¹)

Fig. IV.4-2

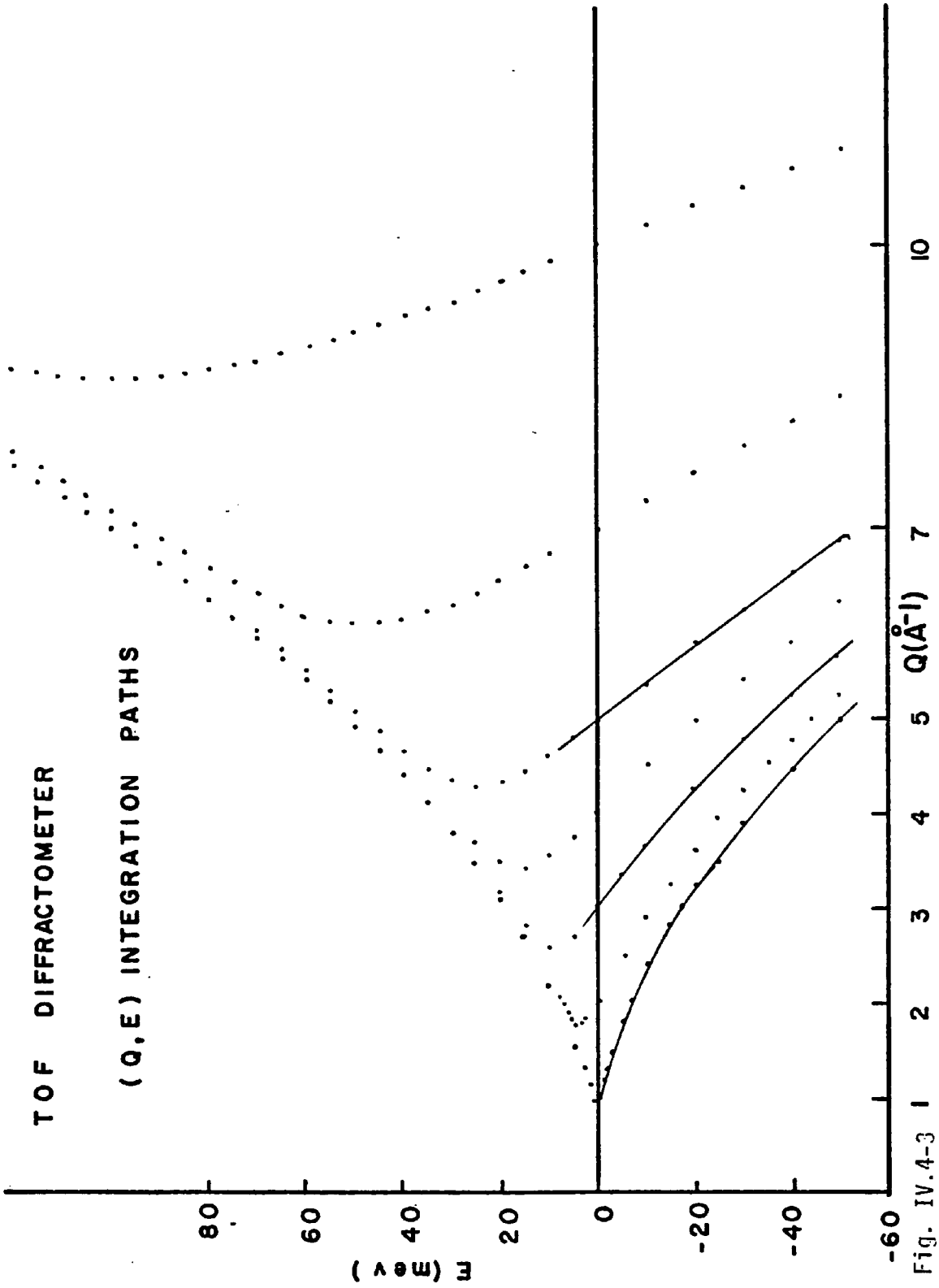
TOF DIFFRACTOMETER
(Q,E) INTEGRATION PATHS
E (meV)
80
60
40
20
0
-20
-40
-60
1
2
3
4
5
Q(Å⁻¹)
7
10

Fig. IV.4-3

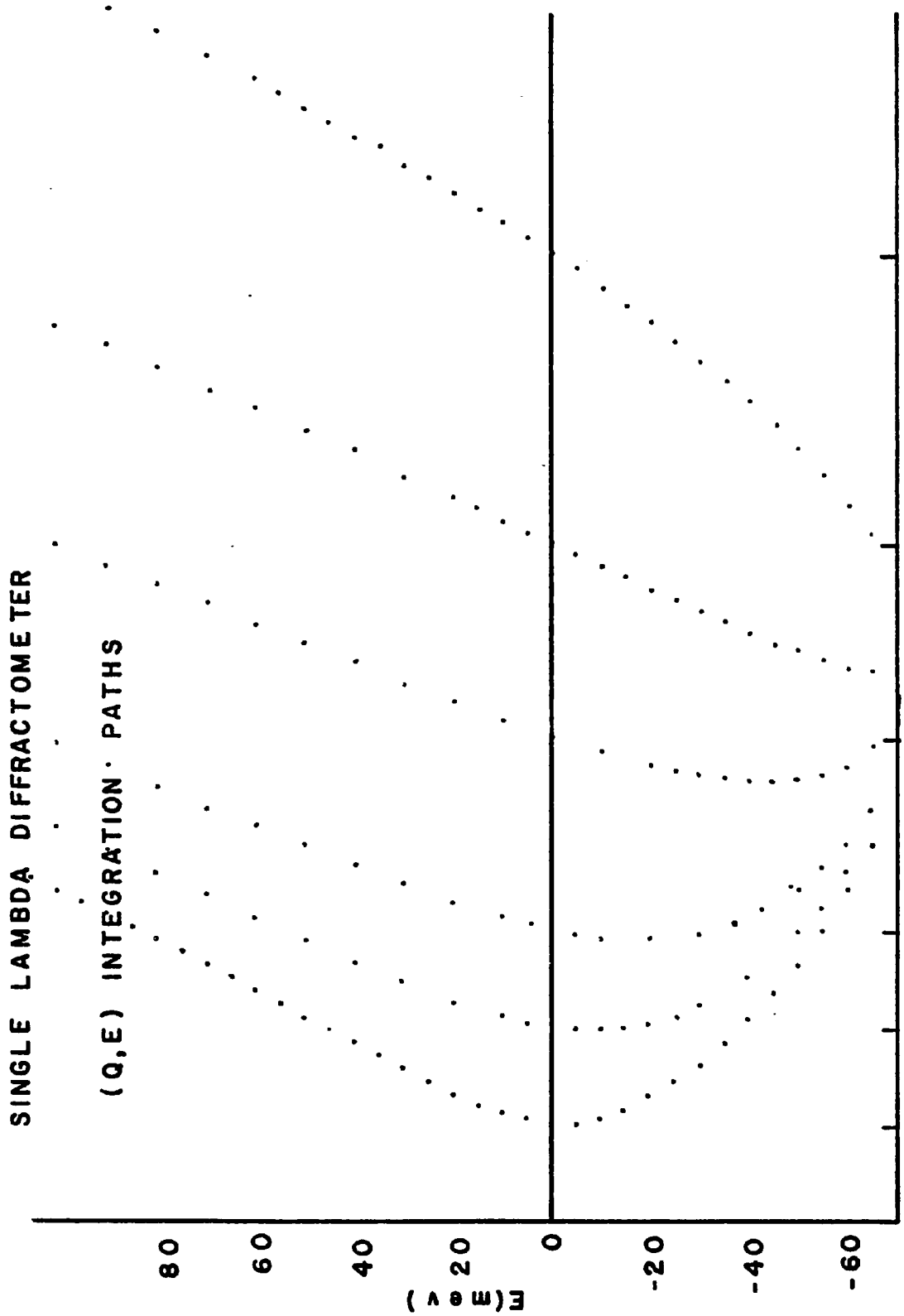
SINGLE LAMBDA DIFFRACTOMETER
(Q,E) INTEGRATION PATHS
E(meV)
80
60
40
20
0
-20
-40
-60
1
2
3
5
7
10
Q(Å⁻¹)

Fig. IV.4-4

CHAPTER V

Results

5.1 General

In this section we will display uncorrected and corrected diffraction data. As previously stated, use will not be made of any inelastic scattering corrections, and therefore the only corrections to be applied are those of attenuation and multiple scattering. The single wavelength diffractometer diffraction pattern is handled first, next comes that of the time of flight diffractometer, and then the two results are joined to form a single extended Q range diffraction pattern. Comparisons of this diffraction pattern are made with other experiments. The results from the ZING-P diffractometer are also included for reference, although no corrections are applied to this data. Finally, a comparison of the results with existing models is made.

5.2 Single Wavelength Diffraction

The diffraction pattern from the single wavelength diffractometer was accumulated over a scattering angle range of $5^{o} \leq \theta_{s} \leq 110^{o}$ which corresponds to a Q range of $\sim .52$ $\text{Å}^{-1} \leq Q \leq 9.8$ Å^{-1}. The pattern, shown in Fig. V.3-1, was smoothly extrapolated from .75 Å^{-1} to a limiting

value at Q = 0 that is dependent on the magnitude of the incoherent scattering cross section for arsenic. The slight ripple at 4.3 $\AA^{-1}$ is an artifact of the splining program used to smooth the data. This ripple does not affect the final result as the two results are joined at 4.1 $\AA^{-1}$. The limitations on the Q range of the data are made in the low Q region by the increasing background. As the detector moves to smaller angles it eventually enters the primary beam, thereby producing large background signal. A limitation on the maximum Q is created by the largest scattering angle that can be obtained. The detectors could move to a maximum scattering angle of 110°.

The diffraction pattern corrected for multiple scattering and attenuation is shown superimposed on the uncorrected data in Fig. V.3-2. It can be seen that the corrections are not very large, but they in fact do raise the peaks and lower the valleys of the pattern as is to be expected.

5.3 Time of Flight Diffraction

The diffraction pattern from the time of flight diffractometer on CP-5 gave results from Q = 1.9 $\AA^{-1}$ to Q = 20 $\AA^{-1}$ and is found in fig. V.3-3. The limitations are that of the neutron spectrum from the reactor which falls off at energies that correspond to both minimum and maximum wave vector transfer. Also, the

neutron chopper that was used to pulse the beam has a low energy cutoff that is related to the frequency of rotation. This also decreases the intensity in the low Q range. It should be pointed out that a wave vector transfer of 1.9 $\AA^{-1}$ on this machine corresponds to a neutron energy of 3.7 meV. Neutrons of this energy are lower in energy than those normally used in variable wavelength diffraction experiments and severe attenuation of the beam will be present because of the high absorption cross sections of the material at this energy.

The attenuation takes place in both the sample and the vanadium reference, and the ratio of these corrections produces the net result. However, the error in the net correction can rapidly increase as the neutron energy decreases if there is a small error in the density of the sample or the reference. Since the sample is a powder, accurate determination of the bulk density is difficult. Also, attenuation and multiple scattering in the vanadium wall of the sample container has not been considered. At these very low energies this is not a valid procedure. Because the energy of the neutrons goes as Q^2, this problem with attenuation that occurs at very low energy rapidly disappears with increasing wave vector transfer.

The corrections to the data are dominated by compensation for 1/v absorption, and thus the raising of the peaks and filling of the valleys is not as evident in this corrected diffraction pattern as was in the case of the single

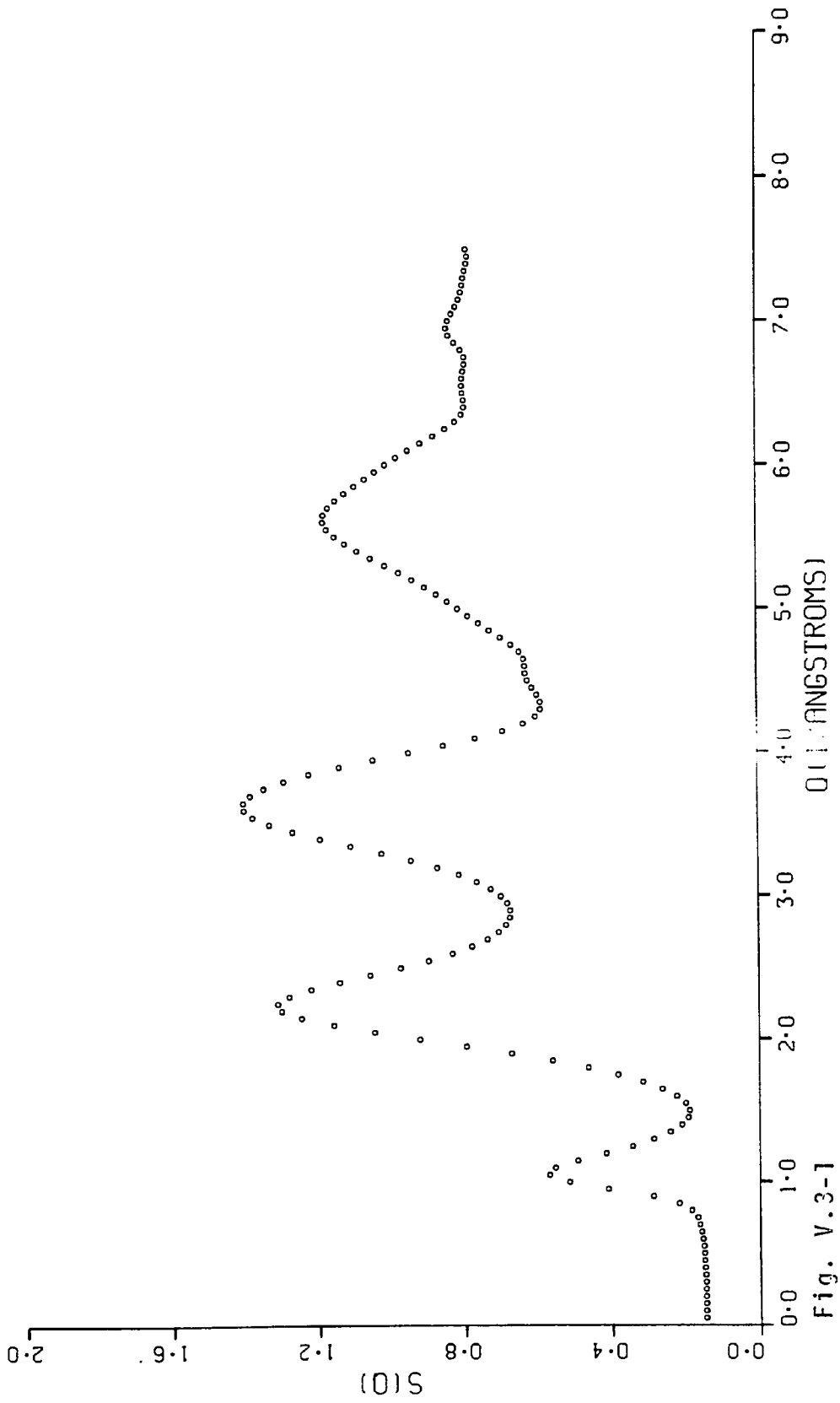
S(O),A AS, 1 LAMDA, UNCORRECTED
S(O)
0·0
0·4
0·8
1·2
1·6
2·0
0·0
1·0
2·0
3·0
4·0
5·0
6·0
7·0
8·0
9·0
O (ANGSTROMS)

Fig. V.3-1

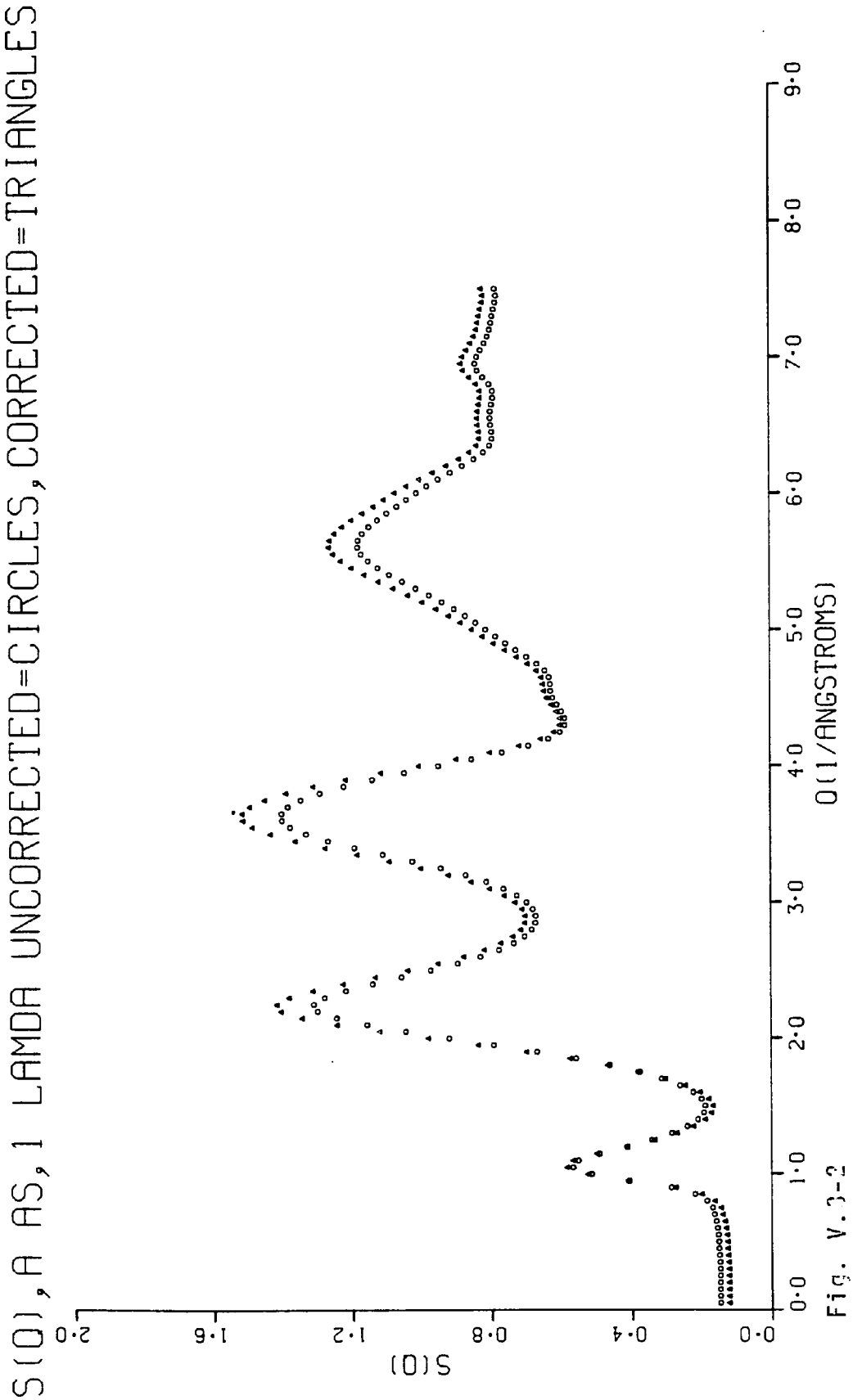
S(Q),A AS,1 LAMDA UNCORRECTED=CIRCLES,CORRECTED=TRIANGLES
S(Q)
0·0
0·4
0·8
1·2
1·6
2·0
0·0
1·0
2·0
3·0
4·0
5·0
6·0
7·0
8·0
9·0
Q(1/ANGSTROMS)

Fig. V.3-2

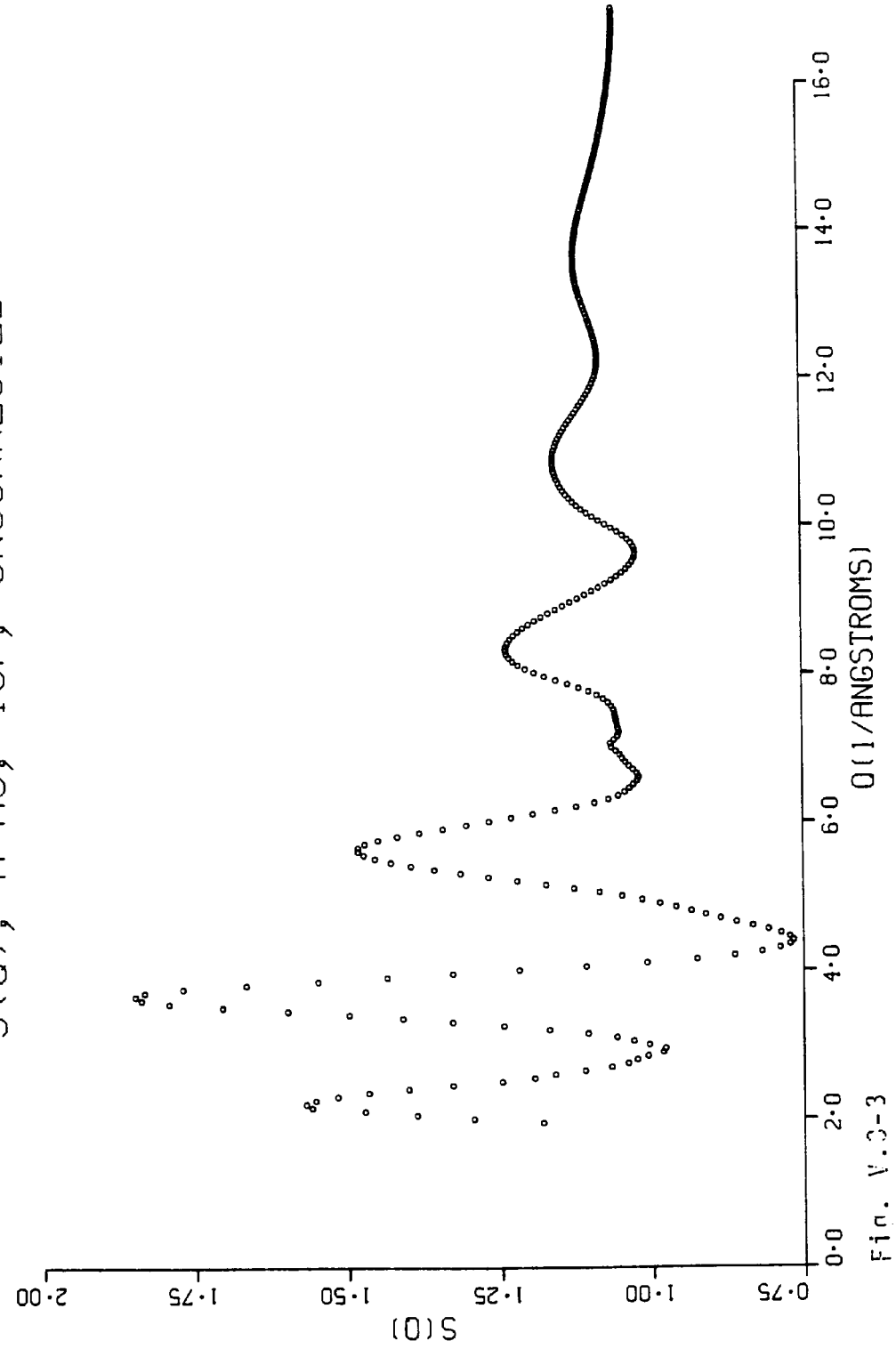
S(Q), A AS, TOF, UNCORRECTED
S(Q)
2·00
1·75
1·50
1·25
1·00
0·75
0·0
2·0
4·0
6·0
8·0
10·0
12·0
14·0
16·0
Q(1/ANGSTROMS)

Fig. V.3-3

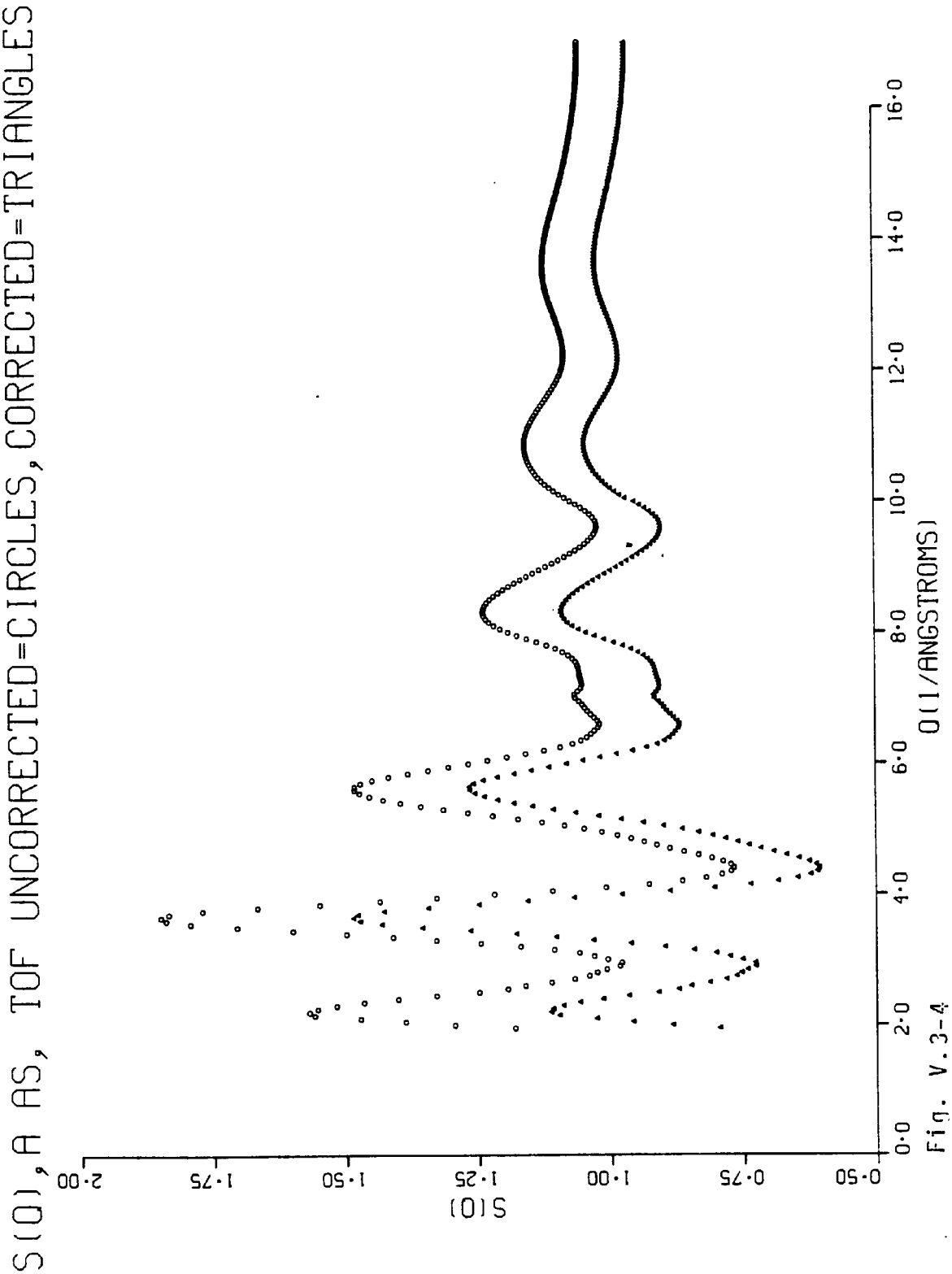
S(Q), A AS, TOF UNCORRECTED=CIRCLES, CORRECTED=TRIANGLES
S(Q)
0·50
0·75
1·00
1·25
1·50
1·75
2·00
0·0
2·0
4·0
6·0
8·0
10·0
12·0
14·0
16·0
Q(1/ANGSTROMS)

Fig. V.3-4

wavelength experiment. The corrected data is shown with the uncorrected results superimposed on them in Fig. V.3-4.

5.4 The Joined Results: Total Diffraction Pattern

The corrected sets of data were joined within a region where good overlap of the two was found to occur. In the region from 3 $\AA^{-1}$ to 7 $\AA^{-1}$ the correspondence between the corrected diffraction pattern from the different instruments is excellent. This agreement can be readily observed by comparing the corrected one wavelength S(Q) with the corrected S(Q) from the time of flight machine plotted on the expanded scale as plotted in Fig. V.4-1. The peaks at 2.2 $\AA^{-1}$ and 3.6 $\AA^{-1}$ overlap particularly well, and in fact better than the data from the uncorrected patterns. This is encouraging and gives us some faith in the multiple scatter and attenuation corrections.

The position of 4.1 $\AA^{-1}$ was chosen as the particular point to join the data sets. This position is within the region of excellent matchup and the slopes of the curves are in good agreement. The generally excellent quality of the transform reassures us that the joining of the data sets has been properly done and that a reliable extended Q range diffraction pattern has been obtained.

It is observed that there is a significant discrepancy in the magnitude of the peak at 2.2 $\AA^{-1}$ obtained from the different instruments. This has been a problem of some concern and the source of this variation is not fully

resolved. It was initially postulated (Carpenter, 1977) to be caused by the difference in integration paths of the two instruments. If this were the case, the inelastic scattering corrections in this region would be quite severe, on the order of 30%. It was partly due to discrepancy in the low Q region that the rather extensive project of attempting to determine inelastic scattering corrections was undertaken. The outcome of the inelastic scattering analysis tends to imply that the differing instrumental integration paths is not the cause of the difference. The present thought is that the cause is from attenuation in the sample and reference scatterer used in the time of flight experiment. As previously stated, the attenuation in these low Q regions in the time of flight experiment, which correspond to 4 meV neutrons, is severe. Use should be made of data that requires the least correction, and in the low Q region this is data from the single wavelength diffractometer. The lower regions of Q space could be measured better on the time of flight machine by using neutrons of higher energy to measure an equivalent wave vector transfer.

$$Q = \frac{4\pi \sin(\theta_s/2)}{\lambda}$$

$$= \frac{4\pi \sqrt{2mE}}{h} \sin(\theta_s/2) \qquad (5.1)$$

Clearly one can maintain the same Q but use higher energy neutrons by decreasing θ_S appropriately. Unfortunately, there existed only one detector at $\theta_S = 90^o$ on the instrument that was used.

Finally, the fully corrected diffraction pattern is displayed in Fig. V.4-2. A few comments on some features of this pattern are in order here. The first peak at 1. $\mathring{A}^{-1}$, although seen before, is quite unusual for glassy material in that it is at a Q smaller than the location of the first peak in the diffraction pattern at the crystal. In most isotropic materials the first peak in the structure factor will be the one that corresponds to the nearest neighbor distance. In amorphous arsenic the first peak corresponds to a crystal plane distance of $d = 2\pi/Q = 6.3$ $\mathring{A}$. This is clearly too large to be the nearest neighbor distance, but implies some order on distances at this dimension. In fact this is a rather large distance to notice such visible ordering.

The second peak which corresponds roughly to that produced from nearest neighbor distances, occurs at 2.25 $\mathring{A}^{-1}$ and has a related distance of 2.79 $\mathring{A}$. By actually doing the Fourier transform we find the nearest neighbor distance of 2.44 $\mathring{A}$.

Beyond about 10 $\mathring{A}^{-1}$ it has been shown by Dore (1977) that the structure factor is sensitive only to nearest neighbors. An interesting example of this can be seen by noting that $d = \frac{2\pi}{\Delta Q}$ where ΔQ wavelength of the

ripple in the pattern. The ripple between 10 Å^{-1} and 15 Å^{-1} has a wavelength of approximately 2.5 Å^{-1}. Thus, the nearest neighbor distance from this analysis would be $d = \frac{2\pi}{\Delta Q} \sim 2.50$ Å .

The plotted data continues to 20 Å^{-1}, but use was made of it only to 14.75 Å^{-1}. The precise method of determining the cutoff position will be described in the analysis of the Fourier transform of the data. The reliability of the data at large Q falls off because of decrease in the incident neutron flux at higher energies as pointed out earlier. One is always striving to obtain accurate data out to larger and larger wave vector transfer as the resolution in r space of the Fourier transform is limited by the maximum Q of the data that is measured. The relationship is $\Delta r \sim \frac{2\pi}{Q_{max}}$ where r is the resolution of the radial density function g(r). Thus, the resolution that results from terminating the data at $Q_{max} = 14.75$ is $\Delta r = .43$ Å.

At this stage it is useful to make a comparison to other neutron measurements taken on amorphous arsenic. The results of Bellissent and Tourand (1976) are displayed in Fig. V.4-3. The results of an x-ray measurement by Krebs and Stephen (1964) are superimposed on the result of the present experiment in Fig. V.4-4. It is sufficient to say that the agreement with both other experiments is quite reasonable.

In a separate experiment carried out by the author of this thesis, the diffraction pattern of aAs was measured on

a pulsed neutron source, ZING-P. This result is shown in Fig. V.4-5. Since this was a truely pulsed source (as opposed to a chopped reactor beam) the source energy spectrum was different from that observed in a reactor. The Maxwellian part of the spectrum is similar, but the magnitude of the 1/E portion of the spectrum is much larger than in a steady state source. This increase in intensity at higher energies means more neutrons are available for diffraction at large energies and hence measurements to greater Q's are possible. The ZING-P instrument used also had detectors at $\theta_S = 150^o$ which again made access to large Q easier. However, the lack of detectors at smaller scattering angles prohibited reliable measurements below approximately 5 $\AA^{-1}$. We note the similar problem of dropoff of structure factor at small Q. The feature that is particularly interesting is the persistence of structure to Q's of 25 $\AA^{-1}$. The ripple has a characteristic wavelength of 2.5 $\AA^{-1}$ which implies a nearest neighbor distance of $\sim$ 2.5 $\AA$. The persistence of this ripple implies that the width of the nearest neighbor peak in the radial distribution function is narrower than is currently thought. Other existing measurements usually terminate the S(Q) data at $Q < 15\AA^{-1}$ that gives a G(r) resolution of $r = .4$ $\AA$. With this S(Q) data to $Q = 25$ $\AA^{-1}$, the resolution is .25 $\AA$ and the large Q ripples are in effect Fourier components that all add at one distance in real space. Thus one may be able to determine

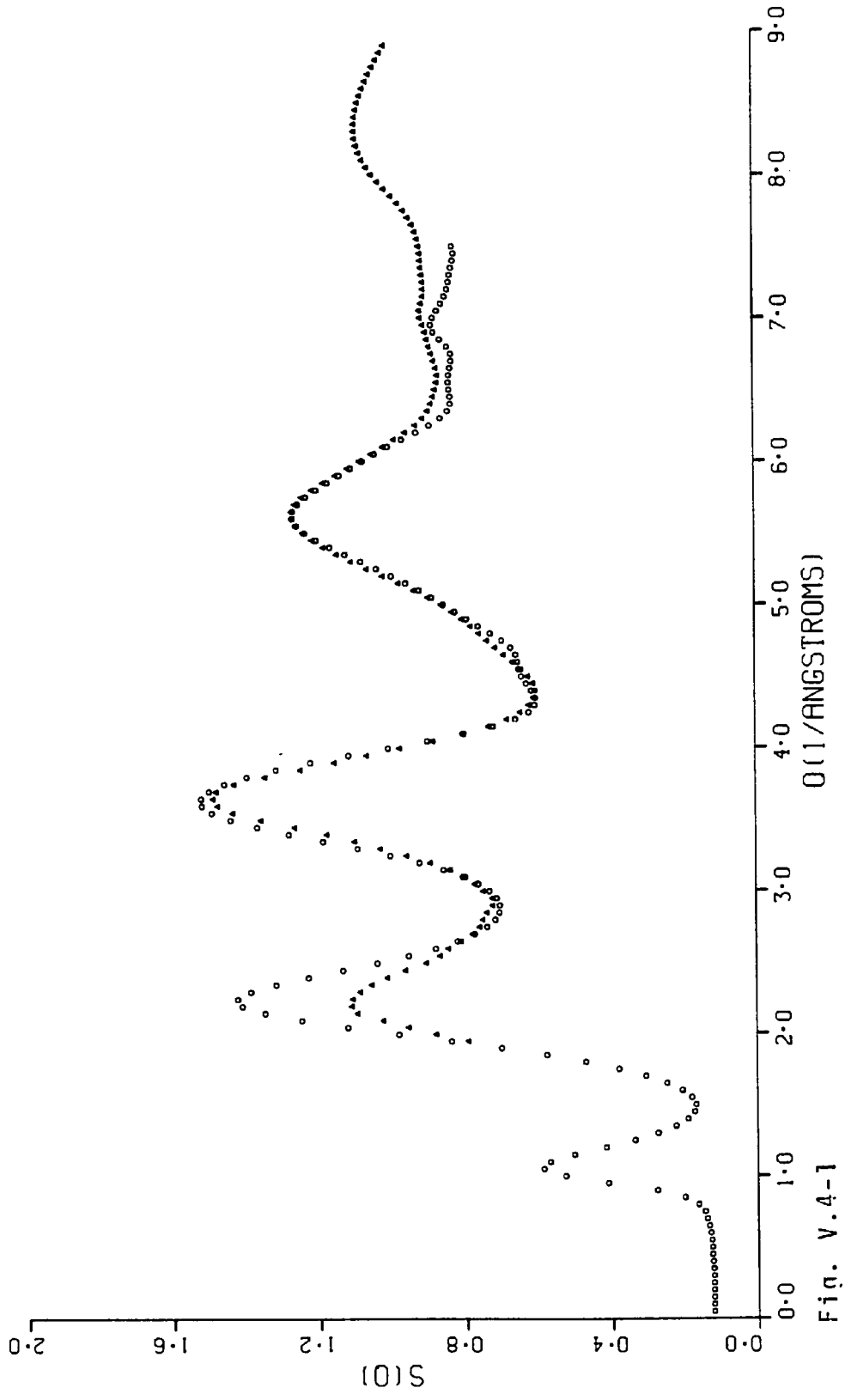
JOINING OF S(Q) 1 LAMDA=CIRCLES, TOF=TRIANGLES
S(Q)
0·0
0·4
0·8
1·2
1·6
2·0
0·0
1·0
2·0
3·0
4·0
5·0
6·0
7·0
8·0
9·0
Q(1/ANGSTROMS)

Fig. V.4-1

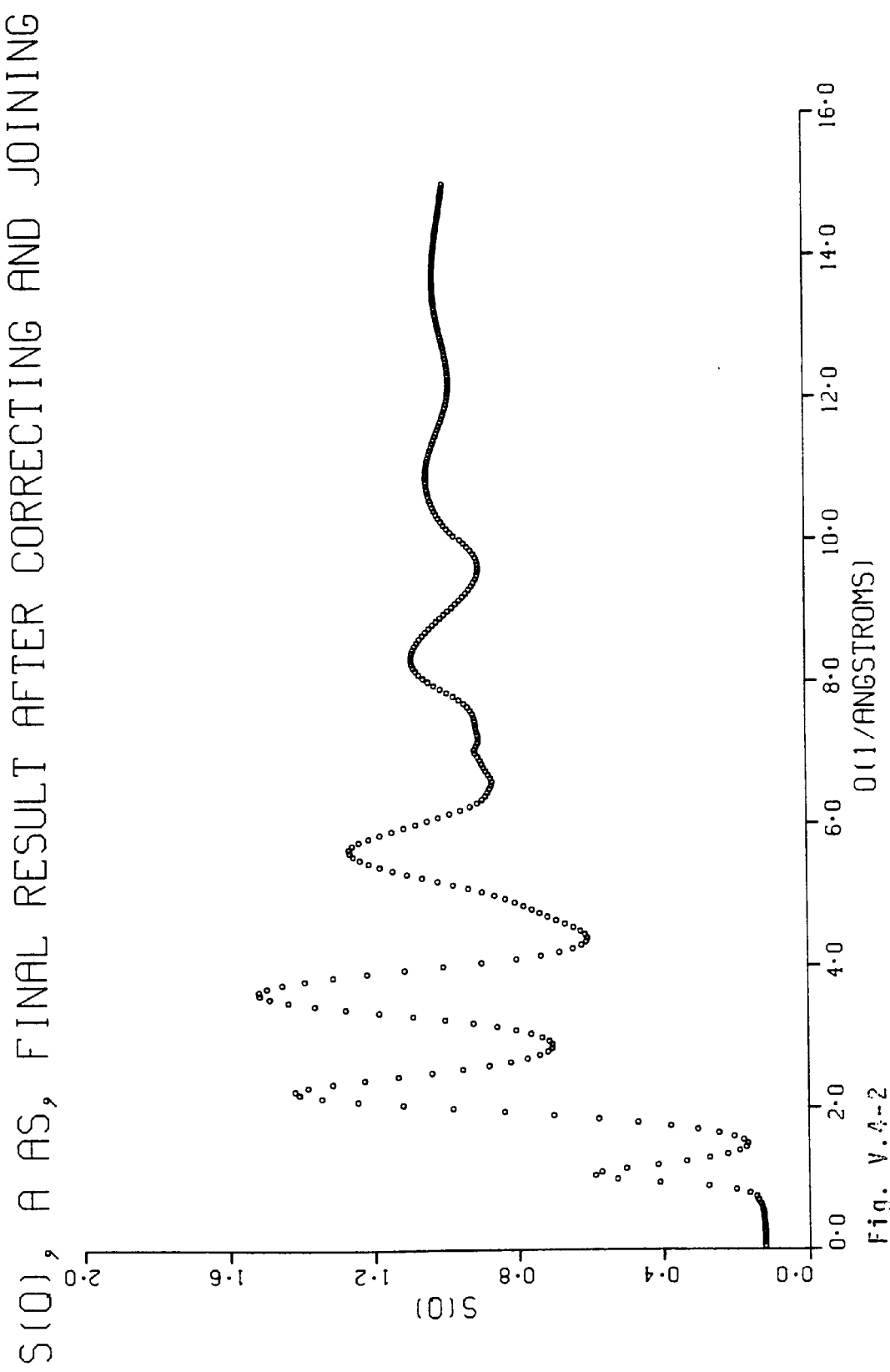
S(Q), A AS, FINAL RESULT AFTER CORRECTING AND JOINING
S(Q)
0·0
0·4
0·8
1·2
1·6
2·0
0·0
2·0
4·0
6·0
8·0
10·0
12·0
14·0
16·0
Q(1/ANGSTROMS)

Fig. V.4-2

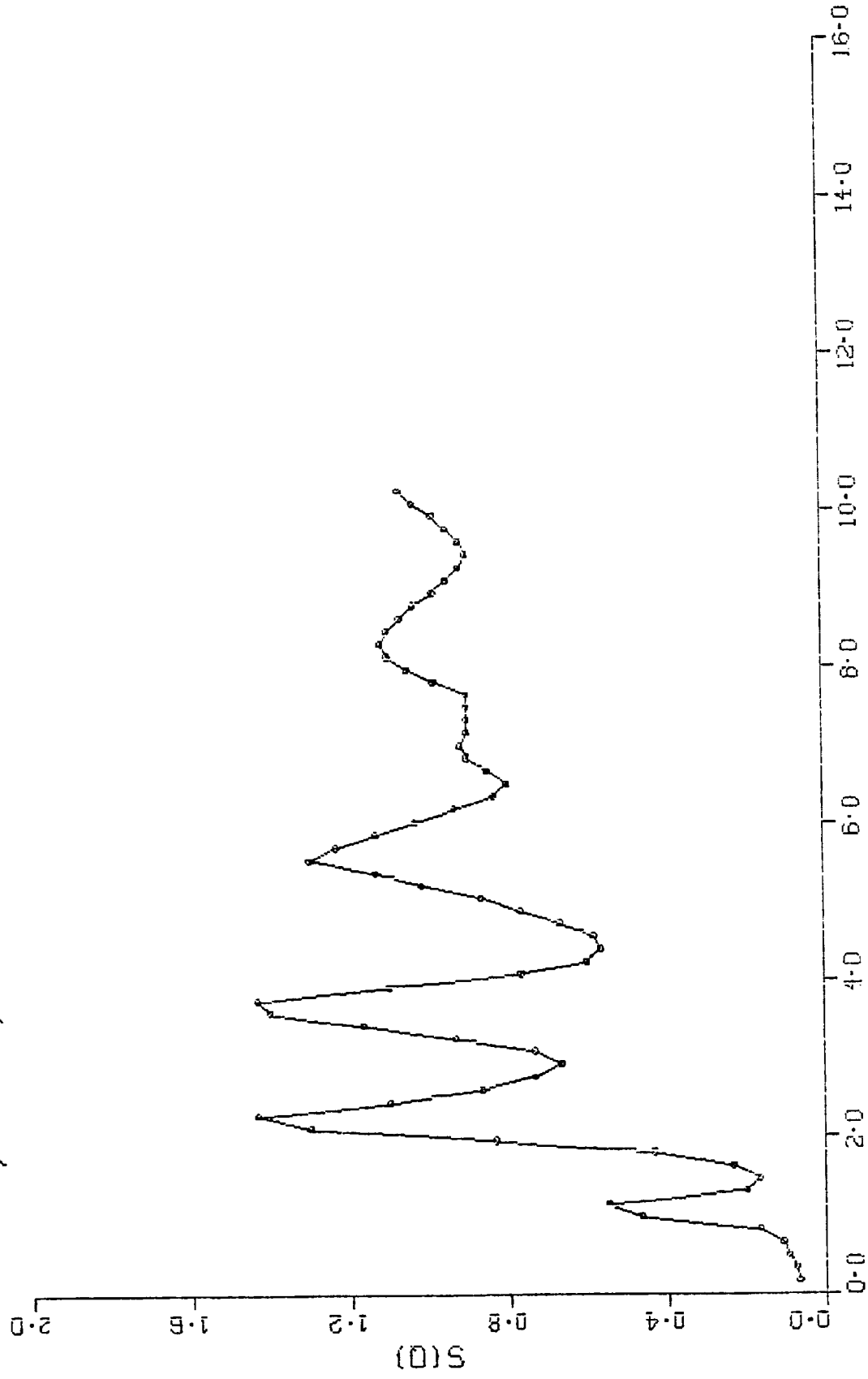
S(Q), A AS, NEUTRONS(BELLISSENT AND TOURAND)
S(Q)
0·0
0·4
0·8
1·2
1·6
2·0
0·0
2·0
4·0
6·0
8·0
10·0
12·0
14·0
16·0
Q(1/ANGSTROMS)

Fig. V.4-3

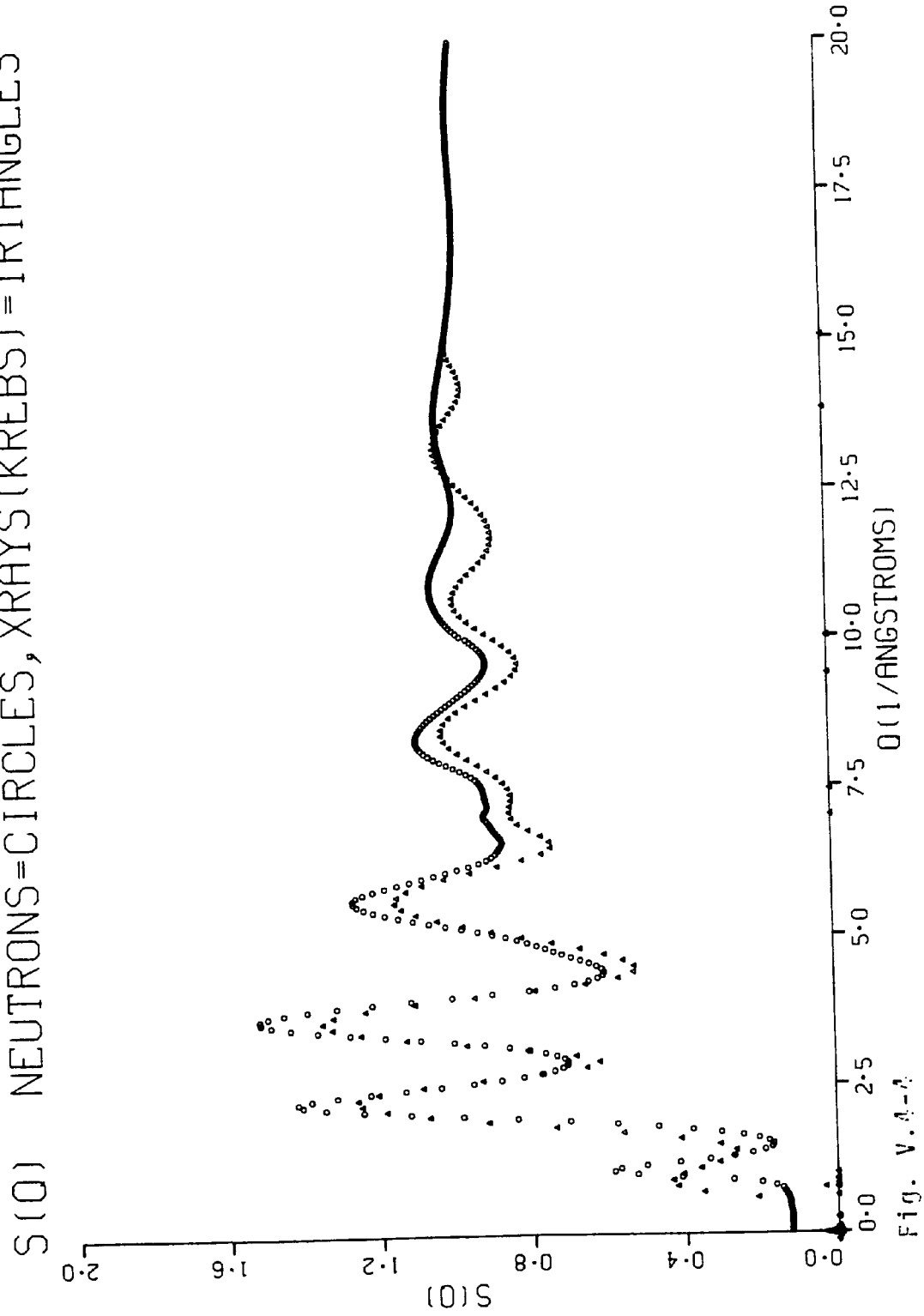
S(Q) NEUTRONS=CIRCLES, XRAYS(KREBS)=TRIANGLES
S(Q)
0·0
0·4
0·8
1·2
1·6
2·0
0·0
2·5
5·0
7·5
10·0
12·5
15·0
17·5
20·0
Q(1/ANGSTROMS)

Fig. V.4-4

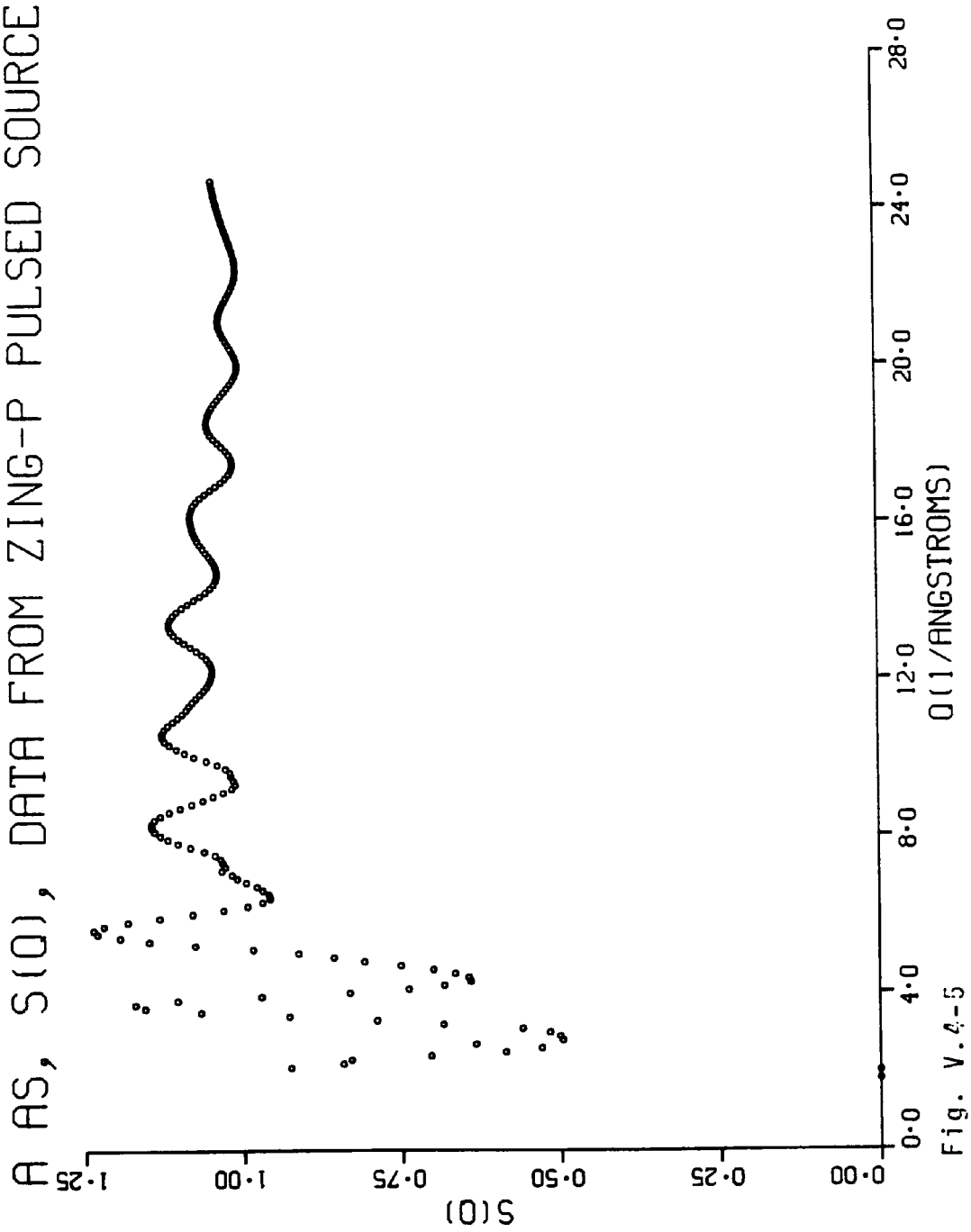
A AS, S(Q), DATA FROM ZING-P PULSED SOURCE
S(Q)
0.00
0.25
0.50
0.75
1.00
1.25
0.0
4.0
8.0
12.0
16.0
20.0
24.0
28.0
Q(1/ANGSTROMS)

Fig. V.4-5

what the distribution of near neighbors actually is with data such as this rather than being resolution limited.

Unfortunately this data presented some problems that were incommensurate with the objective of obtaining a very reliable diffraction pattern such that multiple and inelastic scattering corrections of order 10% could be made to obtain a very accurate S(Q). The average level of the pattern decreases above 15 $\AA^{-1}$ and then increases again. Behaior such as this is unphysical as the mean value should approach a limit asymptotically. This behavior seems to be linked to discrepancies between two different data runs taken on the vanadium reference scatterer. The two runs produce results that differ by more than a constant ratio, as clearly should not be the case. Spurious background seems to have occurred at some time during the acquisition of data, but resolution of the problem was prohibited by termination of the neutron source operation.

5.5 Fourier Transformation of the Structure Factor

Diffraction data from amorphous materials may be analyzed either in the reciprocal space in which the structure factor is obtained, or by taking the Fourier transform and observing the information in real space. It is more usual to do the analysis in real space because the physical meaning of the information is more transparent. Observing the results in real space means we are looking at the radial

density function in one of its various forms.

For a monoisotopic material the standard Fourier transform relationships between real and reciprocal space are

$$G(r) = 4\pi r\,(\rho(r) - \rho_0) = \frac{2}{\pi}\int_0^\infty (S(Q)-1)Q\,\sin(Qr)dQ \qquad (5.2)$$

$$Q\,(S(Q)-1) = 4\pi\int_0^\infty r(\rho(r)-\rho_0)\sin Qr\,dr \qquad (5.3)$$

where $\rho(r)$ = static pair density

$$\lim_{r\to\infty}\rho(r) = \rho_0 = \frac{N}{V}\ . \qquad (5.4)$$

The static pair density is the number of pairs of atoms within some small volume d^3r about the pair spacing distance r averaged over all directions $\hat{r}$. As r becomes large the static pair density goes to the average density, N/V, where N is the number of atoms within volume V.

Since the relationship between the reciprocal and real space is straightforward transformation of the data should also be straightforward. However, there are three problems that quickly present themselves. The first is that a continuous integral must be approximated by a numerical sum with some finite mesh size. In reciprocal space the mesh width was chosen to be $Q = .05\ \text{Å}^{-1}$ while in real space it is $r_{mesh} = .05$ Å. Some checks were made on the accuracy of the numerical approximation using

the above mesh sizes to the integrals and no significant discrepancies could be found. This mesh size in r space is considered more than adequate because of the Q_{max} resolution limit. The resolution is limited at least by $\Delta r_{resol} = \frac{2\pi}{Q_{max}} = .42$ Å. Since $r_{mesh} = .05 << r_{resol} = .42$ no trouble should be encountered by the mesh size in discerning features in the radial density function. Similarly features in the structure factor S(Q) are in general large compared to $\Delta Q_{mesh} = .05$ $Å^{-1}$ and so the spacing in reciprocal space is also sufficient. Since the numerical approximation to the integral has been tested to be adequate, no further mention of numerical integration will be made.

The second is that the S(Q) data does not go to $Q = \infty$. The data can only be taken out to some limit in Q_{max}. Thus the limits of the integral are not from $0 \leq Q \leq \infty$ but rather $0 \leq Q \leq Q_{max}$. The error that this finite integral introduces into the transform is called termination error. It produced spurious ripples with the largest magnitude at smallest r. We will return to this subject shortly.

The third problem is that of properly normalizing the structure factor. Absolute normalization is done by a comparison of the scattering from the sample to the scattering from vanadium. We recall (3.8) the description of the vanadium reference method, and can rearrange to the following.

$$\frac{I^S(Q)}{I^V(Q)} = \frac{N^S \bar{\sigma}_s{}^S \quad S^S(Q)}{N^V \bar{\sigma}_s{}^V \quad S^V(Q)} \tag{5.5}$$

$I^{S,V}(Q)$ = observed intensity scattering from the sample or vanadium

$N^{S,V}$ = number density per unit area of beam for sample or vanadium

$\bar{\sigma}_s{}^{S,V}$ = average scattering cross section of sample or vanadium

$S^{S,V}(Q)$ = structure factor for sample or vanadium

The structure factor for an incoherent scatter is defined to be one, $S_V(Q) \equiv 1$, independent of Q. Thus an absolute normalization of $S^S(Q)$ is obtained by knowing the ratio of the intensities, N^S, N^V, $\sigma_S{}^S$, and $\sigma_S{}^V$. These numbers are difficult to determine to accuracies of 1% and thus absolute normalization of $S^S(Q)$ is limited to an accuracy of not less than 1%. However, errors introduced into the transform by discrepancies in S(Q) from a proper normalization by even this small an amount are severe, with the main contribution again appearing about r = 0. This arises because the Fourier transform of a step function at Q = Q_{max} is a Bessel function $\frac{\sin Q_{max} r}{r}$. This normalization error is minimized by fine tuning of the choice of Q_{max} at which to terminate the data in conjunction with using $S(Q_{max})$, the last data point, as $S(Q = \infty)$. The meaning of this last sentence is more easily perceived by

defining a new structure factor S'(Q) such that

$$S'(Q) - 1 = \frac{S(Q) - S(Q = \infty)}{S(Q = \infty)} \tag{5.6}$$

If S(Q) is very accurate and correctly normalized, then S'(Q) = S(Q) since S(Q = ∞) = 1. As is more usually the case, however, the S(Q) obtained is not correctly normalized. Then normalization adjustments are readily carried out by the choice of S(Q = ∞). A most convenient method of picking S(Q = ∞) is to set it equal to $S(Q_{max})$. Then by varying the Q_{max} at which to terminate the data precise regulation of the normalization is easily achieved.

The question that obviously presents itself is how to choose the appropriate Q_{max}. One solution is to use the Krogh-Moe normalization (Krogh-Moe, 1956). Recall the fundamental relationship between S(Q) and $\rho(r)$ in Eq. (5.2). At small r, $\rho(r)$ must be zero since it is physically impossible for atoms to be closer together than a few Angstroms. We can then approximate sin(Qr) by Qr because r is small. Thus

$$-4\pi r\rho_o = \frac{2}{\pi}\int_o^\infty Q[S(Q)-1]QrdQ \qquad (5.7)$$

or

$$\rho_o = \frac{-1}{2\pi^2}\int_o^\infty Q^2[S(Q)-1]\,dQ \qquad (5.8)$$

We can clearly not perform this integral over the infinite range, and we therefore terminate it at some value of $Q = Q_{max}$. If we then evaluate the integral for termination at various chosen values of Q_{max}, we have a relationship between the running integral of the function $Q^2(S(Q) - 1)$ and the microscopic density ρ_o which is presumably known.

Let us now grant the possibility that S(Q) is not correctly normalized, substituting S'(Q) for S(Q) and taking the limit of the integral to Q_{max}.

$$\rho_o = \frac{-1}{2\pi^2}\int_o^{Q_{max}} Q^2\left[\frac{S(Q) - S(Q_{max})}{S(Q_{max})}\right] dQ \qquad (5.9)$$

By carrying out the above integral to various Q_{max}'s one can conveniently determine the Q_{max} and the corresponding $S(Q_{max})$ to be used to minimize normalization errors. Even finer adjustment of this normalization can be done once the appropriate Q_{max} is determined by holding Q_{max} fixed but altering the value of $S(Q_{max})$ by small amounts.

For amorphous arsenic at 4.73 gm/cm^3 mass density, the number density is ρ_o = .038 at/Å^3 and this led to a Q_{max} = 14.75 Å^{-1} using this normalizing procedure. The degree of success of Krogh-Moe normalization can qualitatively be seen by noting the Fourier transform of S(Q) in Figure V.5-1. For r less than the nearest neighbor distance, we should have

$$G(r) = -4\pi r\rho_o \quad . \tag{5.10}$$

The small magnitude of the ripples and the tendency to oscillate about a $-4\pi r\rho_o$ line reinforces our faith in this normalization method. At this point these ripples will be hopefully only from the termination error. Initial transformation of S(Q) often produces oscillations of much larger magnitude as noted in Pelizzari (1974). This very useful normalization condition was observed by Krogh-Moe (1956), used with some success by Pelizzari (1974), and further delineated by Rahman (1977).

We are now in a position to compare the normalization produced for Fourier transform optimization to an absolute normalization with respect to the vanadium reference. This comparison could be portrayed in any of a number of ways, but one is to assume that the vanadium scattering cross section is known, along with the number of atoms of arsenic and vanadium atoms in the beam. Differences can then be expressed by the variation of the effective arsenic cross section from the actual cross section. The $S(Q = \infty)$ produced from the Krogh-Moe normalization gave an effective scattering cross section for arsenic of 6.32 b while the actual cross section is 6.04 b, a discrepancy of only 4.4%. Agreement of this magnitude between the Krogh-Moe and absolute normalization is considered excellent.

We now return to the problem of errors introduced into the transform by terminating the integral at a finite limit. These termination errors can be minimized by a number of methods. Researchers who have previously looked into the problem include Kaplow, Strong and Averbach (1965), Konner and Karl (1972), Narten (1969), Yarnell et al. (1973), and Pelizzari (1974). The procedure used here for the removal of termination errors is similar to that of Kaplow, Strong and Averbach (1965) and Yarnell et al. (1973). It works amazingly well, at least in comparison with many observed attempts at such removal.

Initially, the corrected S(Q) is transformed to large r (in this case, to $r \rightarrow 20$ Å) using the appropriate normalization condition as previously shown. Termination ripples now make themselves apparent at small r as is seen in Fig. V.5-1. Because $\rho(r) = 0$ for distances smaller than the nearest neighbor distance any structure at values of r below this distance must be spurious.

The correlation function that we are using is $G(r) = 4\pi r(\rho(r) - \rho_0)$, and thus if $\rho(r) = 0$ for small r, this function should go as $-4\pi r\rho_0$ where ρ_0 is already known. It is then an easy operation to replace G(r) for any values of r below the nearest neighbor distance by the appropriate $-4\pi r\rho_0$ value. We also replace G(r) by $-4\pi r\rho_0$ for r greater than the nearest neighbor distance if $G(r) < (-4\pi r\rho_0)$, which would imply $\rho(r) < 0$. The result of these operations is seen in Fig. V.5-2. At this point it is useful to look for spurious ripples in G(r) and remove them appropriately as advocated by Kaplow, Strong and Averbach. However, the removal of the other spurious ripples seems to be very subjective and this additional removal is not advocated. In contrast, the other alterations recommended here are straightforward, unique, and physically justified. The corrected G(r) is then transformed back to S(Q) and carried out to an extended Q limit that is greater than Q_{max}. A comparison between the original S(Q) and the altered $S_A(Q)$, as seen in Fig. V.5-3, is indicative of the success with

which removal of normalization and termination error has been done. The lack of unphysical high frequency ripples that are at variance with the original S(Q) is particularly noteworthy. The only place where one can detect any spurious features at all is for $0 < Q \leq .75$. These discrepancies are reassuringly small in magnitude. A variation in the $S(Q = \infty)$ of 1% from that finally used in the normalization alters the shape of the first peak at 1 Å^{-1} in such a way as to make it smaller in magnitude and twice as wide. This variation also raises the $S(Q = 0)$ intercept by a factor of two. Thus we see that the error removal procedures are quite sensitive to small variations in input parameters and we should be quite pleased with such fine agreement. The extended $S_A(Q)$ is at variance with the original S(Q) for $Q > 14.75$ as we might expect. The original S(Q) was used only up to this limiting value of Q because of unreliability of the data beyond this point. The generated oscillations in $S_A(Q)$ arise from the removal of the termination error and have a frequency characteristic of the nearest neighbor distance. We are encouraged by the similarity between the generated $S_A(Q)$ at large Q and the characteristics of the experimentally determined features of S(Q) as determined on the ZING-P diffractometer. These normalization and termination error procedures complement each other in minimizing spurious features provided the identical ρ_o is used for determining the $S(Q = \infty)$ and altering the small G(r) data.

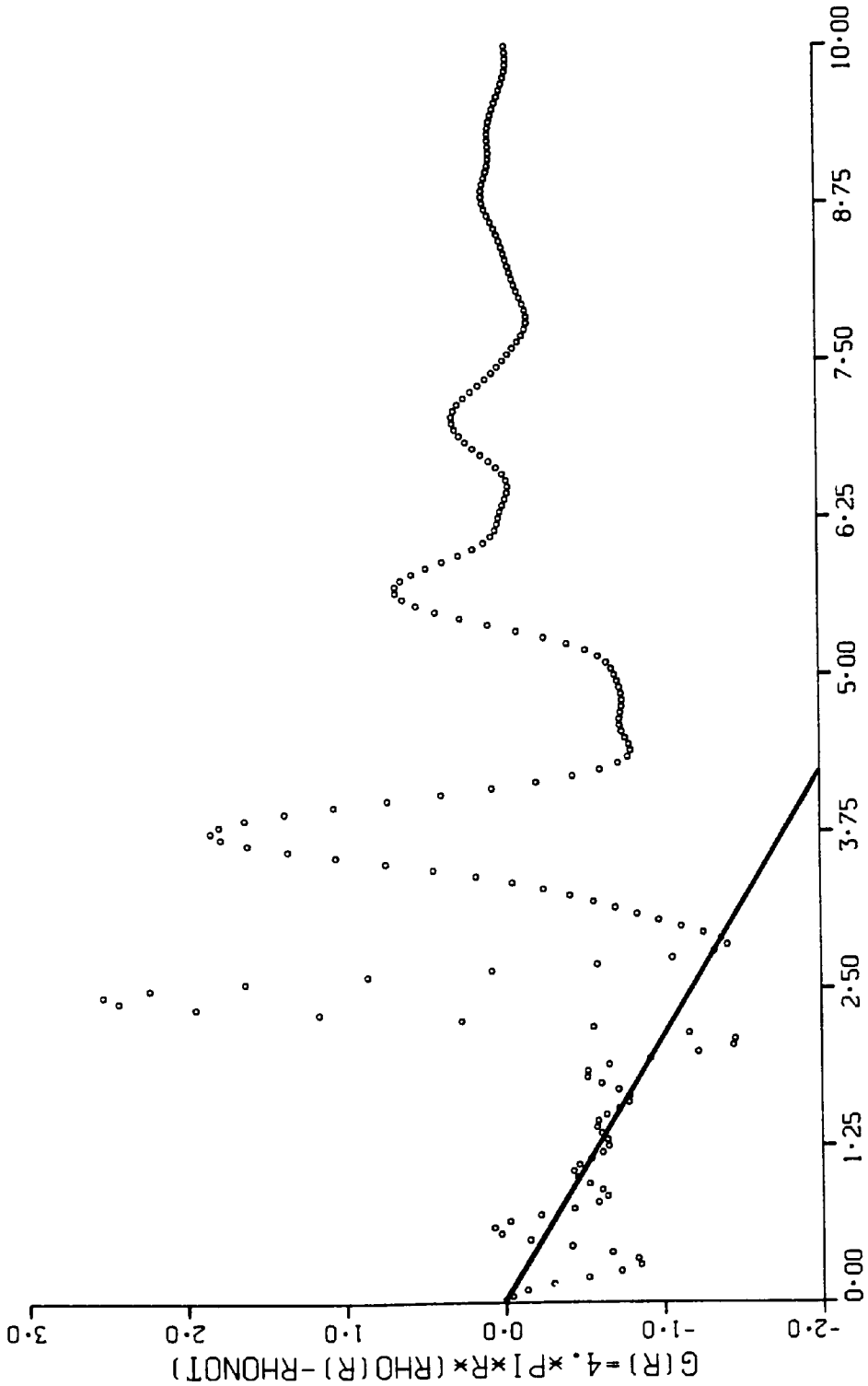
G(R), A AS, F.T. OF S(Q)
G(R)=4.*PI*R*(RHO(R)-RHONOT)
3·0
2·0
1·0
0·0
-1·0
-2·
0·00
1·25
2·50
3·75
5·00
6·25
7·50
8·75
10·00
R(ANGSTROMS)

Fig. V.5-1

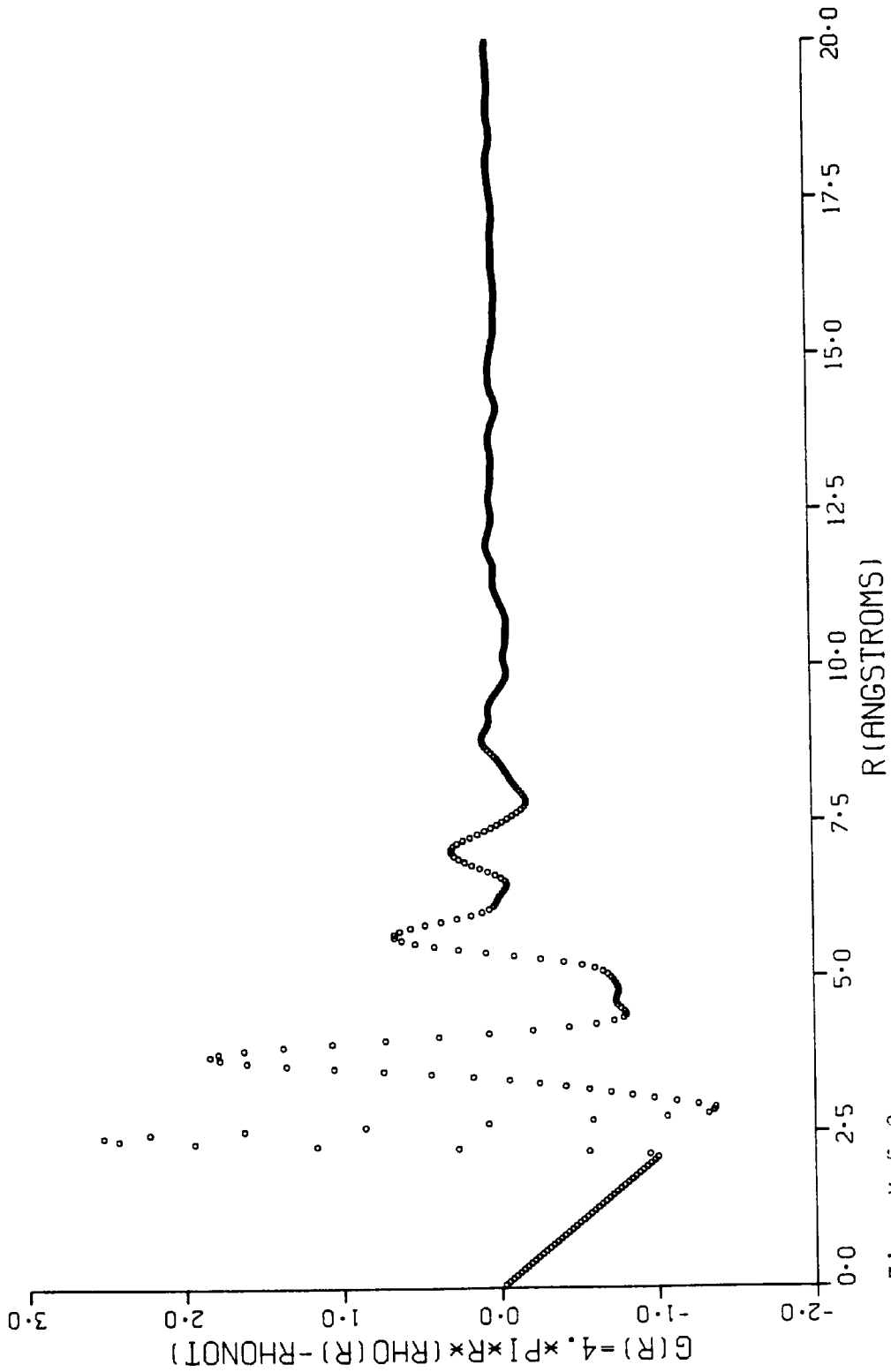
G(R), A AS, LOW R VALUES OF G(R) ALTERED
G(R)=4.*PI*R*(RHO(R)-RHONOT)
3·0
2·0
1·0
0·0
-1·0
-2·0
0·0
2·5
5·0
7·5
10·0
12·5
15·0
17·5
20·0
R(ANGSTROMS)

Fig. V.5-2

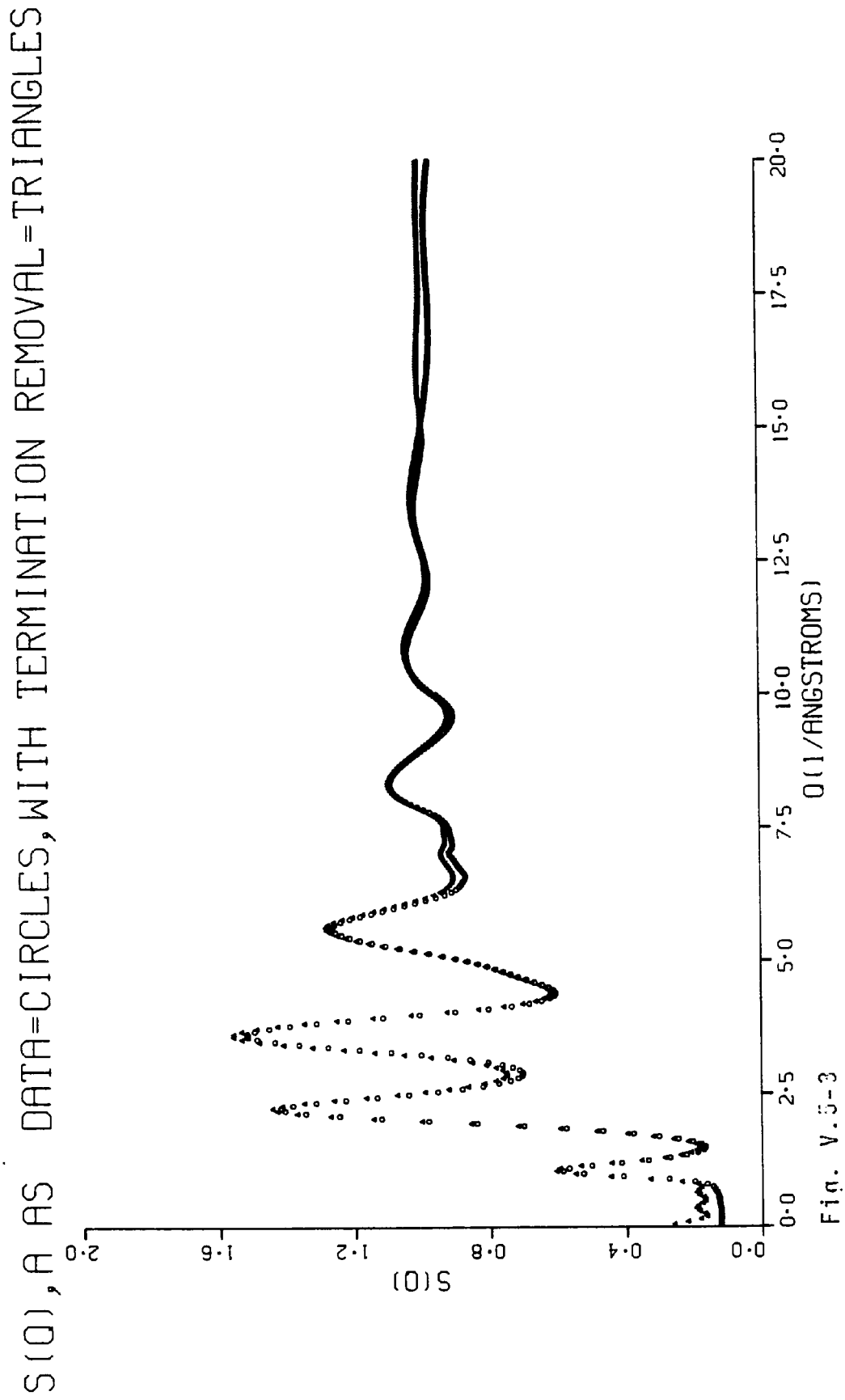
S(Q), A AS DATA=CIRCLES, WITH TERMINATION REMOVAL=TRIANGLES
S(Q)
0·0
0·4
0·8
1·2
1·6
2·0
0·0
2·5
5·0
7·5
10·0
12·5
15·0
17·5
20·0
Q(1/ANGSTROMS)

Fig. V.3-3

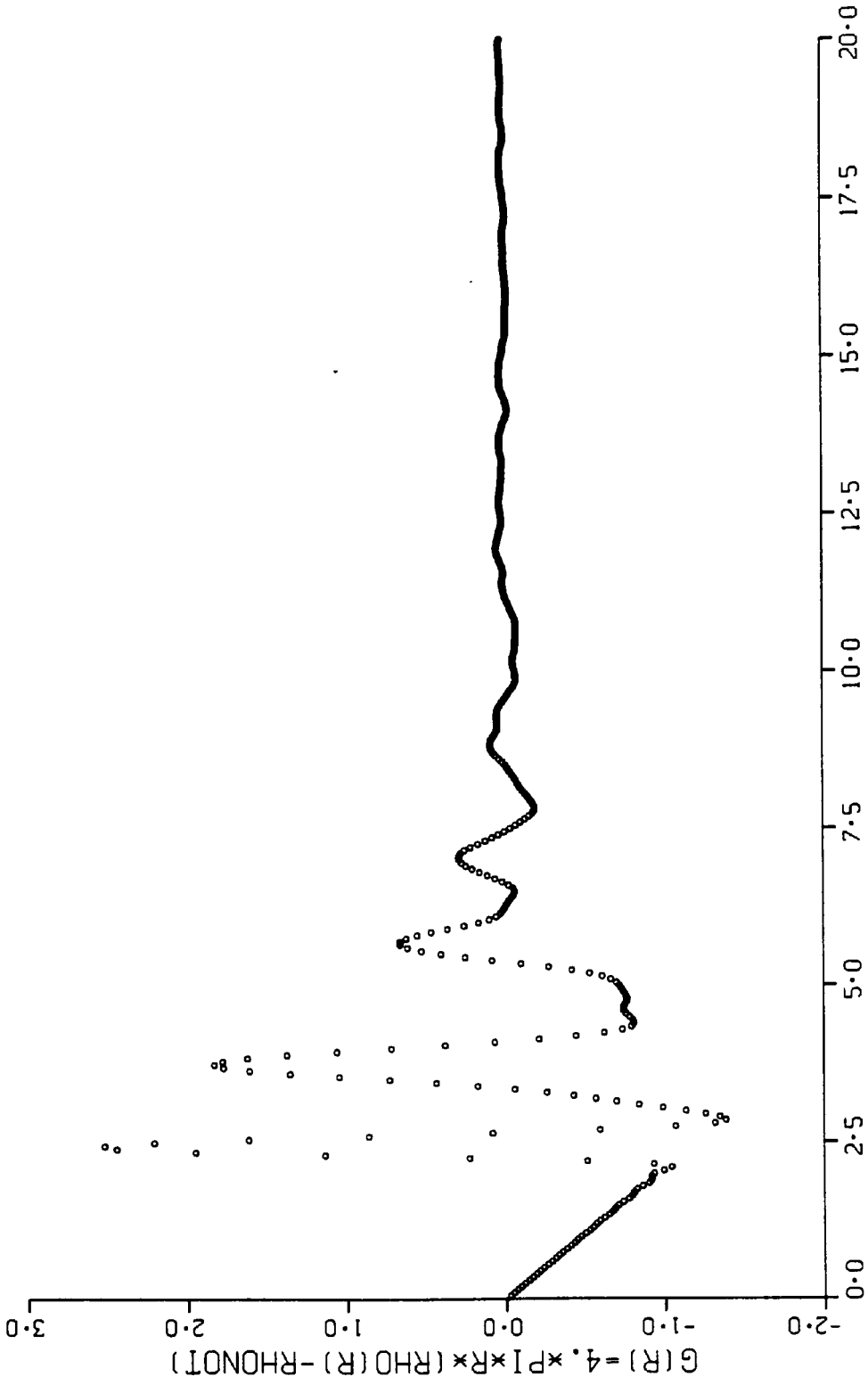
G(R),A AS, DOUBLE TRANSFORM
G(R)=4.*PI*R*(RHO(R)-RHONOT)
-2·0
-1·0
0·0
1·0
2·0
3·0
0·0
2·5
5·0
7·5
10·0
12·5
15·0
17·5
20·0
R(ANGSTROMS)

Fig. V.5-4

Finally, we may retransform the altered $S_A(Q)$ back to G(r) space to obtain $G'_A(r)$. A comparison of $G_A(r)$ (where $G_A(r)$ is the original G(r) with appropriate alterations at small r)with G'(r) is again an indication that the operations have been done successively. Figure V.5-4 illustrates this result and we find total agreement as far as can be easily discerned by comparison with Fig. V.5-2. The two results were not superimposed as distinction between the two would be difficult to resolve. Similarity of this degree can be viewed as giving confidence in the analysis.

Since the $G_A(r)$ and $G'_A(r)$ are so similar it makes little difference which we use for additinal analysis of the radial density function. We have rather arbitrarily chosen the $G_A(r)$ and henceforth all references to the radial density function will refer to the function $G_A(r)$, and symbolic reference will be to G(r) where we have chosen to drop the subscript A.

5.6 Comparison to Existing Models

Continuous random network models of the structure of amorphous arsenic have been developed by at least two different groups. Guttman (1977) has determined the coordinates of a triply coordinated structure using a computer to minimize the potential energy of a material whose atoms each have three nearest neighbors. More will be said about this model later and a comparison with the present experiment will be made.

Greaves and Davis (1974) report a handbuilt model of 533 atoms constructed from copper wires and junctions present at an angle of 97°. The 97° is that angle between bonds within the double layer structure of the rhombohedral R $\bar{3}$m(D_{3d}^5) structure. The wires and junctions were connected to make a continuous random network. Elliot and Davis (1976) report a modification of this structure by computer relaxing the original coordinates. However, our comparison is to the original model. Figure V.6-1 shows this comparison. We see the agreement of the model with the data is quite good for the first two peaks with some general characteristics being evident in the third and fourth peaks also. The model gives a narrower and larger result for distribution of nearest neighbors as represented by the first peak. This behavior is not unexpected and the model may more accurately portray the actual structure better than the experiment in this region. This is because, as pointed out earlier, the resolution in r space is limited by the Q_{max} of the experiment. If the data is taken to larger Q, the first peak in the RDF may in fact become more narrow as represented by the model. However, the width of this feature may be limited at room temperature by the thermal vibrations of the material. Amorphous arsenic is reported to have a Debye temperature of 169°K (Wu, 1973) in contrast to the accepted value of rhombohedral arsenic of 278° K (Wu, 1973). The low Debye temperature of the material would imply a rather wide spread in the

distribution of the nearest neighbors at room temperature. However, rudimentary examination of the data from the ZING-P experimental facility leads one to believe that the nearest neighbor distribution is in fact quite narrow, which in turn implies a large Debye temperature. This apparent conflict may be resolved by the Debye temperature of aAs at room temperature being significantly different from that of material at 20° K, where it was measured by Wu (1973).

A useful quantity to analyze is the number of atoms within a sphere of given radius r from the origin atom. When this quantity is determined as a function of r it is called the running coordination number and is defined as

$$N(r) = 4\pi \int_{o}^{r} r'^{2} \rho(r') dr' \quad . \tag{5.11}$$

The running coordination as determined from the data is plotted in Fig. V.6-2. The form of this curve is quite characteristic of an amorphous material in that it rises from zero to a plateau that represents number of the nearest neighbors, and then no more distinct plateaus are present. At a value of r = 2.90 Å, N(r) is clearly on the plateau, but the specific value was chosen because this is where a minimum in the function G(r) occurs. The N(r) = 3.08 for the number of near neighbors is reassuring as arsenic is triply coordinated in its crystalline forms.

After the initial plateau, the coordination number rises sharply as one approaches a distance representative of second near neighbors distance and then tends to level off again when thisdistance is passed. However, by this point overlap of the second and third nearest neighbors has begun to occur, and thus a real plateau is never generated again. If one determines the point where the slope of N(r) is a minimum after the first plateau, one finds that this occurs at r = 4.30 Å and an N(r) = 13.6. Although there is no real plateau here, the magnitude of this coordination number minus the number of first nearest neighbors is an indication of the number of second nearest neighbors. We thus find 10.6 second near neighbors occurring at an average distance of 3.95 Å as determined by the position of the second peak in G(r). We note that in rhombohedral arsenic, there are three second near neighbors occurring at 3.15 Å (Breitling and Richter, 1949)and this corresponds to the mesomeric bond between atoms in adjacent double layers of the crystal. In the amorphous material this short second neighbor distance is no longer present. It is probably the absence of this mesomeric bonding of second near neighbors that leads to the decrease in density in going from the crystalline to amorphous material. This same lack of bonding is also responsible for the major decrease in conductivity of the amorphous material. Greaves and Davis (1974) report the conductivity of rhombohedral arsenic at room temperature

to be $\sim 10^4$ ohm^{-1}cm^{-1}, while that of amorphous arsenic is 10^{-7} ohm^{-1}cm^{-1}, a difference of 11 orders of magnitude. In the rhombohedral crystalline material there are six third nearest neighbors occurring at r = 3.77 Å. This distance is that between atoms that have two bonds between them and occurs for atoms within the double layer of the crystal. There should clearly be six atoms satisfying this condition. If we use rhombohedral arsenic as a prototypical structure of the amorphous material, we find that atoms that would be at the 3.15 Å near neighbor distance in the crystal are now found in the amorphous material at a distance that is similar to the distance between atoms separated by two bonds. The result is a broad distribution of second near neighbors of the amorphous material with a coordination number of 10.6 as compared to the idealized case of 6 + 3 = 9 obtained from elementary analysis of rhombohedral arsenic. We note that the shape of the second peak of G(r) is not symmetric as one might expect, and thus would be made up of a sum of two distributions. Nevertheless, a peak at the rhombohedral value of 3.15 Å is clearly absent.

One can next determine the bond angle between the second near neighbors from geometric considerations. With the first and second peaks of G(r) at 2.45 Å and 3.75 Å respectively, we find the angle to be $\theta = 99.8^{o}$.

This angle is computed by representing the near neighbor distance by the equal sides, a, of an isosceles triangle, and the second near neighbor as the base, b. The angle between the equal sides is then

$$\theta = 2 \sin^{-1} \left(\frac{b}{2a}\right) \quad . \tag{5.12}$$

Greaves and Davis (1974) arrived at a similar angle of 98.2° in their model. The distribution of angles about this angle can be determined by the half width at half maximum of the second peak in G(r) and the same geometric considerations. Differentiating the above expression with respect to b we arrive at

$$d\theta = \frac{db}{a \cos\left(\frac{\theta}{2}\right)} \quad . \tag{5.13}$$

The value of the half width at half maximum of G(r) at the second peak is determined to be $\Delta G(r) = db = .312$ Å. Letting $\theta = 99.8°$, and $a = 2.45°$ as before, we find $\Delta\theta = \pm 7.3°$. Thus the bonding angle distribution may be represented as $\theta = 99.8° \pm 7.3°$.

We see that beyond ~ 5 Å the Greaves and Davis model begins to break down, but the rough features of the data can be seen in it. The model might naturally have difficulty in predicting G(r) at large r value as the model is only ~ 14 Å on a side. If one took an atom in the middle of the model, it is only 7 Å to each edge.

We now observe the comparison with the Guttman model (Wilde, 1977)) as seen in Fig. V.6-3. This model is essentially an adaptation to a triply coordinated system of the method described by Guttman (1974) in "Simulation of Continuous Random Network Models with Periodic Boundary Conditions" that was developed for four-coordinated materials. Here a body-centered array of atoms with periodic boundary conditions is taken as the starting point.

Bonds are then connected until each atom is bonded to three other atoms. This structure is then relaxed to its minimum energy using a Keating potential that is a combination of a harmonic force term in the nearest neighbor separation and one that contains a bond angle harmonic force term. The model is then further relaxed by reconnecting bonds and relaxing until no more energy can be extracted from the material. Models of this type are clearly highly adaptable to computer generation. The particular model used here contained 54 atoms.

We note the remarkable agreement of this model with the data through the first two peaks and a reasonable following of the experiment to even larger r. The model size used here was quite modest and clearly statistics are affecting the results severely, particularly at the large distances. Significant promise is shown for this modeling method if it can be extended to larger size. However, we must be aware that the number of atoms needed in the model goes up as the cube of the increase in r dimension.

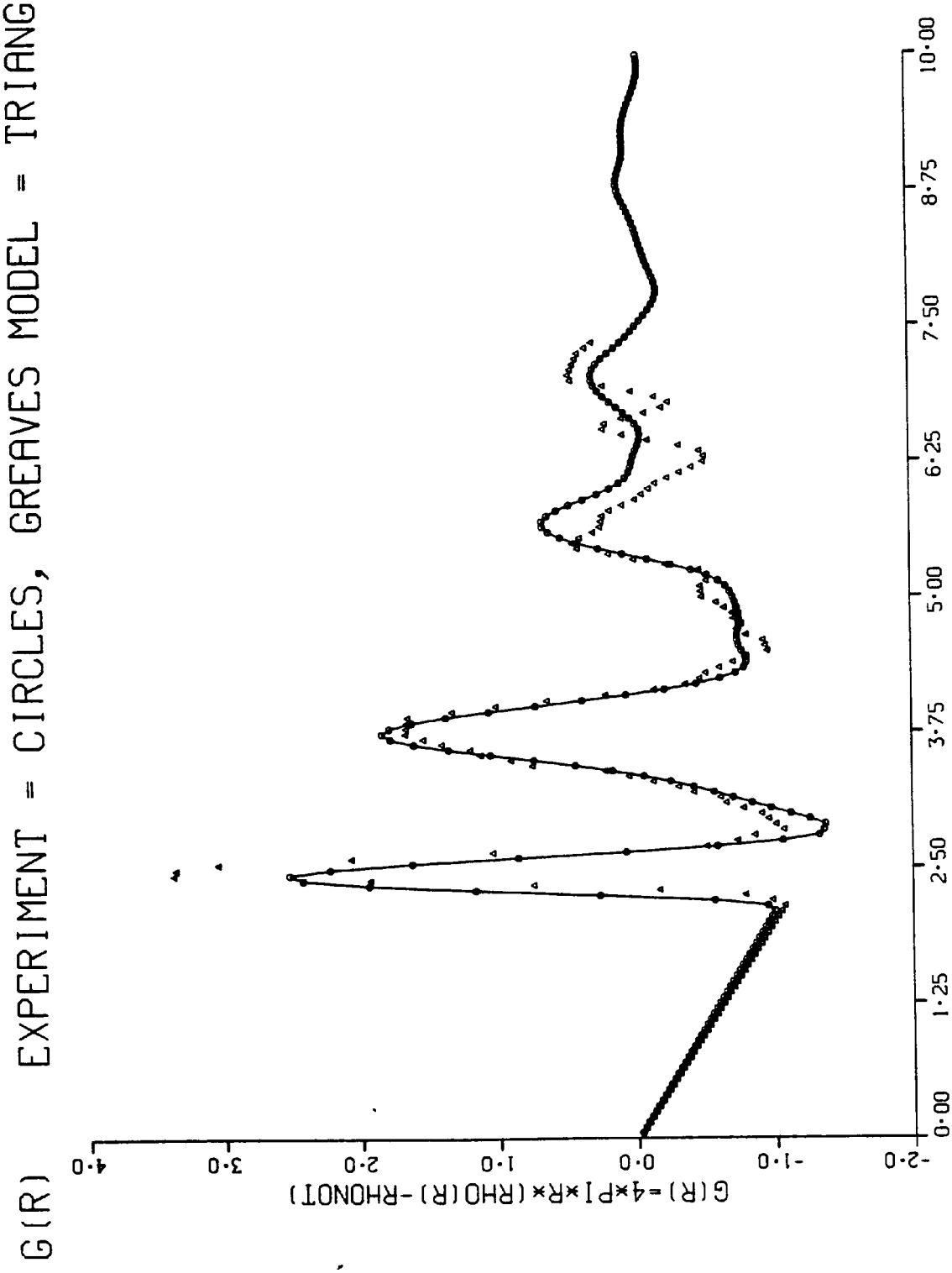
G(R) EXPERIMENT = CIRCLES, GREAVES MODEL = TRIANGLES
G(R)=4*PI*R*(RHO(R)-RHONOT)
4·0
3·0
2·0
1·0
0·0
-1·0
-2·0
0·00
1·25
2·50
3·75
5·00
6·25
7·50
8·75
10·00
R(ANGSTROMS)

Fig. V.6-1

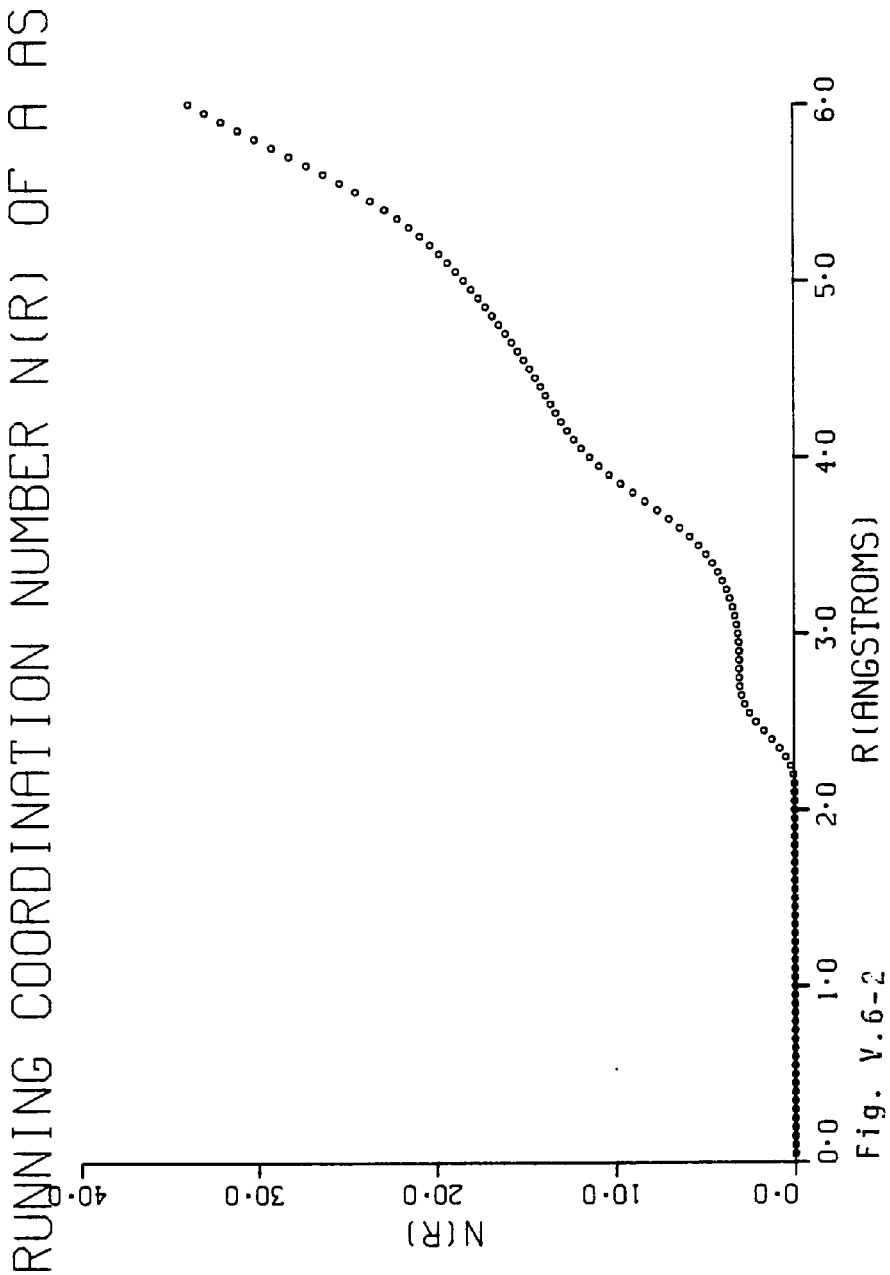
RUNNING COORDINATION NUMBER N(R) OF A AS
N(R)
0·0
10·0
20·0
30·0
40·0
0·0
1·0
2·0
3·0
4·0
5·0
6·0
R(ANGSTROMS)

Fig. V.6-2

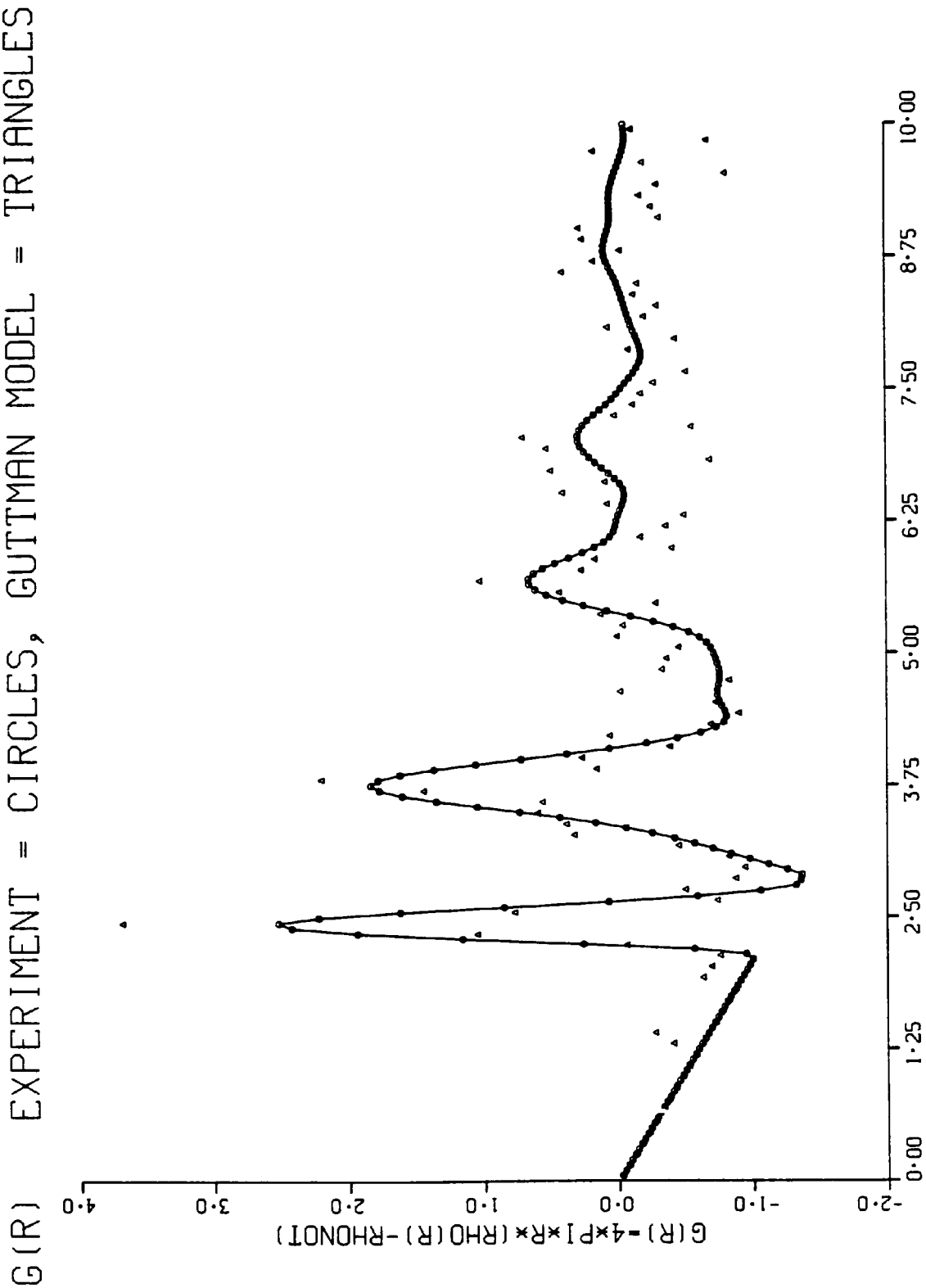
G(R) EXPERIMENT = CIRCLES, GUTTMAN MODEL = TRIANGLES
G(R)=4*PI*R*(RHO(R)-RHONOT)
4·0
3·0
2·0
1·0
0·0
-1·0
-2·0
0·00
1·25
2·50
3·75
5·00
6·25
7·50
8·75
10·00
R(ANGSTROMS)

Fig. V.6-3

CHAPTER VI

Conclusions

The structure factor S(Q) and differential pair correlation function G(r) of aAs obtained in this measurement are in reasonable agreement with those previously obtained by neutron and x-ray diffraction. A synopsis of the structural features obtained from this experiment is included in Table VI.1-1. An adaptation of the method of Kaplow, Strong and Averbach for removal of termination and normalization errors is developed and found to be excellent in its ability to carry out its desired function.

Originally the object of this thesis was to measure a monoatomic glass to very large momentum transfer. The data from the prototype source had excellent characteristics for doing these large Q diffraction measurements but unfortunately also had discrepancies with respect to reproducibility of the data that were deemed too large to make inelastic and multiple scattering. The instrument also had no small angle detector with which to measure the small Q structure factor. Consequently, the data from the pulsed source which extended to $\sim$ 25 Å^{-1} was not extensively analyzed. However, the data did show significant structure at large Q and initial analysis ignoring any multiple and inelastic scattering showed that G(r) had a

very narrow nearest neighbor distribution (figure VI.1-1).

The effect of multiple scattering and attenuation can be reasonably well accounted for, but the proper method is to use thin samples to minimize the need for this correction. General sample size attenuation corrections seem to work well, but the validity of the form of structure dependent multiple scattering corrections is not well established.

Inelastic scattering corrections appear to be minimal for materials with $Z \geq 50$ and would appear to be best ignored for the present. A method to determine the effect of inelastic scattering on time of flight diffraction data is to do a map of $S(Q,\varepsilon)$ and then do the integration of $S(Q,\varepsilon)$ along the path followed by the instrument. A comparison could then be made with the experimental diffraction data, but the data should not be taken by the vanadium reference method. If the vanadium reference method is used the scattering law $S(Q,\varepsilon)$ of vanadium undesirably enters into the experiment.

For molecular liquids of small atomic mass where measurements to large Q are needed, the inelastic scattering, correction can be significant (Dore, 1977). A method of parameterizing this effect is to use small samples on a pulsed source with detectors at various angles. In this case the attenuation is presumably small and can be properly accounted for. Any variation between the structure factor measured at the same Q but different

scattering angles (and hence different incident neutron energies and integration paths) is then dependent only on the inelastic scattering. Although this method will not unambiguously map the scattering law, realistic measures of the magnitude of the effect of inelastic scattering can be obtained.

We now conclude with a few recommendations for further measurements. First, the measurement should actually be carried out to a large Q of 30 to 40 $\AA^{-1}$, which should be easily possible with the new generation of pulsed sources. On the same instrument, data should be taken to optimally measure the structure factor to as low a Q as possible in order to obtain an accurate extended Q range pattern. The method of termination and normalization error removal developed here should be applied. It would then be useful to do this experiment at room temperature and low temperature, for example at that of liquid nitrogen. There currently exists an uncertainty as to the amount that thermal motion contributes to the width of the first peak in G(r) and hence the magnitude of the Debye temperature. These measurements should clarify this situation.

Another useful measurement on this material would be the diffraction pattern and conductivity as a function of pressure. Since the density of the amorphous material is 80% that of normal rhombohedral arsenic there is reason to believe that upon compression the amorphous phase may take

on properties displayed by the crystal. Since the conductivity of the crystalline form is much greater than that of the amorphous form, this material may provide an excellent system for observing structural changes leading to crystallization (Greaves et al. 1973).

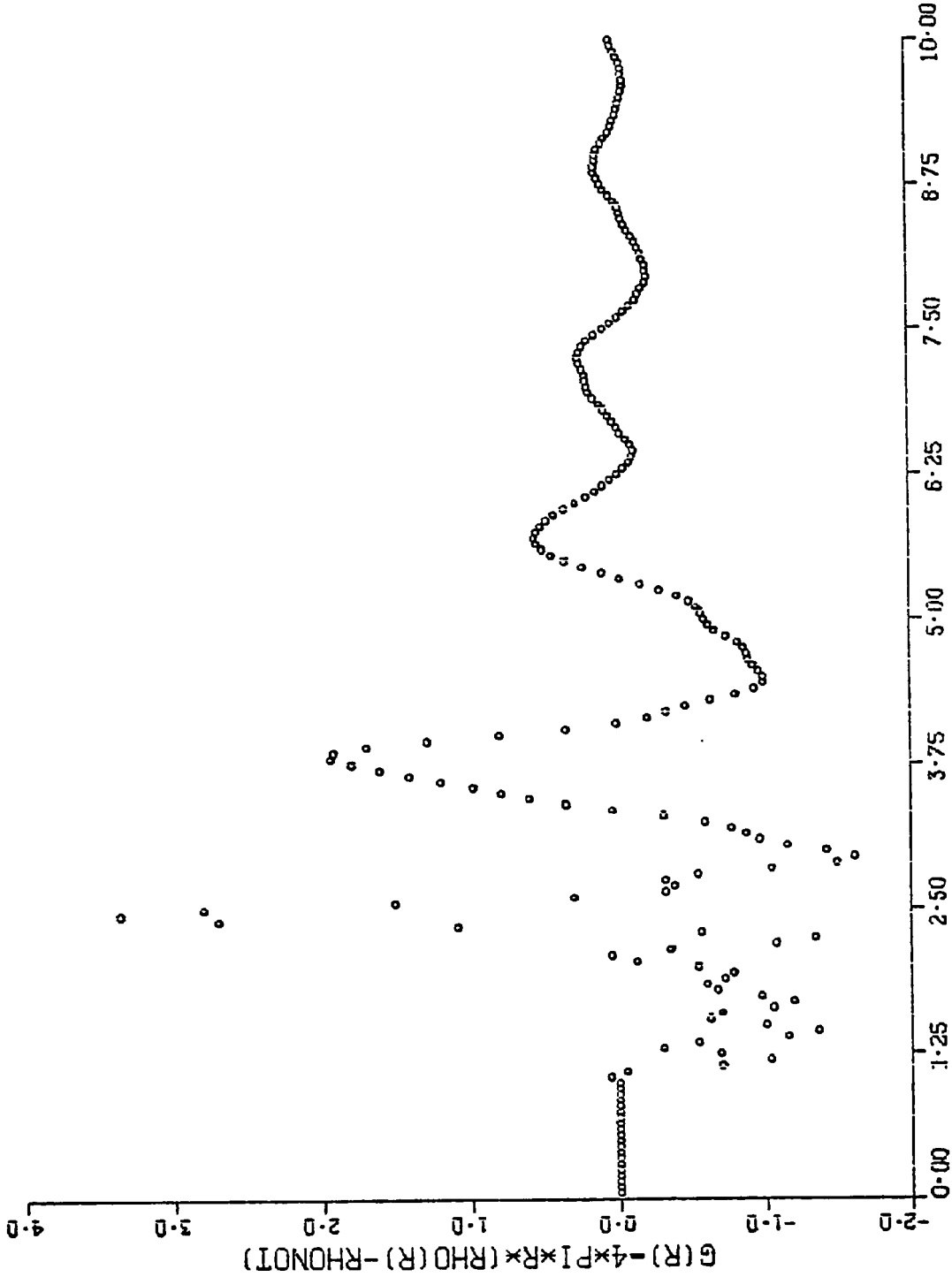
G(R), AMORPHOUS ARSENIC, ZING
G(R)=4*PI*R*(RHO(R)-RHONOT)
-2·0
-1·0
0·0
1·0
2·0
3·0
4·0
0·00
1·25
2·50
3·75
5·00
6·25
7·50
8·75
10·00
R(ANGSTROMS)

Fig. VI.1-1

Characteristics of Amorphous Arsenic

(as obtained from experiments using the CP-S reactor)

nearest neighbor distance	2.45 Å
numbered nearest neighbors	3.08
second nearest neighbors distance	3.75 Å
number of second nearest neighbors	10.6
mean bond angle	99.8°
mean bond angle distribution (half width at half max)	±7.3°
Debye-Waller factor (from density of states model)	$2\omega = AQ^2$ $A = .0108$ Å^2

Table VI.1-1

APPENDIX I

From Leadbetter (1976) we determine $\varepsilon_L^{max} = 30$ meV and $\varepsilon_T^{max} = 1.4$ meV. Using the relationship for characteristic temperature $\theta_{L,T} = \frac{\hbar\omega_{L,T}}{k_B}$ and the equation relating θ_L, θ_T, and θ_D, we obtain the following values.

$$\varepsilon_L^{max} = 30 \text{ meV}$$

$$\varepsilon_T^{max} = 14 \text{ meV}$$

$$\theta_L = 349^o \text{ K}$$

$$\theta_T = 163^o \text{ K}$$

$$\theta_D = 183^o \text{ K}$$

The volume of the primitive unit cell in the spherical approximation can be obtained from macroscopic considerations.

$$\rho = 4.73 \text{ gm/cm}^3$$

$$A = 75$$

$$V = \frac{\rho N_A}{A} = 2.63 \times 10^{-23} \text{ cm}^3$$

Recall the expression for the volume of the primitive unit cell in terms of the radius of the first Brillouin zone.

$$V = \frac{3(2\pi)^3}{4\, k_{max}^3}$$

Using this formula together with the value obtained for this volume, we find the radius of the first Brillouin zone.

$$k_{max} = 1.31 \text{ Å}^{-1}$$

Recall the dispersion relation

$$\omega = vk$$

and the equivalent formulation at its limiting values

$$v_{L,T} = \frac{\omega_{max}}{k_{max}} = \frac{\varepsilon_{L,T}^{max}}{\hbar\, k_{max}} \quad .$$

The above formula used with the radius of the first Brillouin zone and the earlier tabulated values for $\varepsilon_{L,T}^{max}$ yields the required velocities

$$v_L = 3479 \text{ m/sec}$$

$$v_T = 1624 \text{ m/sec}$$

APPENDIX II

Comparison of the Path Integral Method of Inelastic Scattering Correction to a Formulation by Sinclair and Wright

In order to have some confirmation of our inelastic scattering correction factors, it is useful to make a comparison to the results achieved using conventional Placzek corrections.

As originally derived, Placzek (1952) derived corrections to compensate for the variation the instrumental integration path from that of constant Q, which is desired for a total scattering measurement. The results of his derivation were written in a form useful for the single incident wavelength experiment. Sinclair and Wright (1974) have adapted his derivation to the time of flight experiment. Their particular adaptation is to a pulsed source, but over certain regions of interest, the analysis is quite adequate for a chopped reactor beam. Some initial points should be made concerning Placzek's original expansion. It is reasonably valid provided that the neutron energy is large in comparison to the level ($E_0 >> \Delta$) spacing of modes to be excited in the system. In aAs and vanadium, the $\Delta \approx \varepsilon_{max}$ of the system is $\sim$ 30 meV. We thus might expect Placzek's expansion to break down for neutron energies $E_0 < \sim$ 100 meV, therefore we should use E_0 = 100 meV as the minimum of any comparison

between the two results. Sinclair and Wright (1974) (henceforth denoted as S&W)made a number of assumptions with respect to the source and detectors that must be kept in mind. Their derivation was for a pulsed linac neutron source. Their pulsed source spectrum has the energy shape of a Maxwellian combined with a 1/E tail on the high energy region. The source we used was a steady state reactor neutron beam chopped by a rotor. In general the reactor will have a Maxwellian distribution with approximately the same characteristic energy but without the 1/E tail. The chopper alters the distribution so that it is different from a Maxwellian.

Another approximation used by Sinclair and Wright is that the detector efficiencies are 1/v, ($\eta(E) \propto 1/\sqrt{E}$). The detectors used and simulated in our experiment are 30% efficient at 25 meV. At E = 100 meV, $\eta \sim 17\%$. Thus although not completely valid for $E \geq 100$ meV, the 1/v detector is not a bad approximation.

Using these assumptions and the expressions of S&W,calculations have been carried out for the incoherent scatterer, vanadium. Results of the calculations are compared with those obtained from vanadium using the path integration technique.

Formulation of Sinclair and Wright

Sinclair and Wright evalute the total scattered intensity $I(Q_e)$ at a wave vector transfer equal to its elastic value Q_e.

$$I(Q_e) = \frac{1}{N}\frac{\partial\sigma}{\partial\Omega} \tag{A2.1}$$

N = number of atoms in sample

$\frac{\partial\sigma}{\partial\Omega}$ = differential cross section

The formulation (S&W Eq. 29) for this quantity produced by a pulsed source with incident spectrum of the form $\phi(E) = 1/E^n$ is presented below.

$$I(Q_E)=\overline{b^2}\{1-\frac{2\sin^2\theta}{\mu}[1-f(1-2n)]+\frac{2\sin^2\theta}{\mu^2}*[1-f(1-2n)(1+2nf)\sin^2\theta]+$$
$$\frac{\overline{K}}{3\mu E_o}(\cos2\theta-2f(1+2n)[1-2f(1+n)]\sin^2\theta)+\overline{b}^2\int_o^\infty G^D(\overline{r},0)e^{i\overline{Q}_e\cdot\overline{r}}d\overline{r} \tag{A2.2}$$

where

$$\overline{b^2} = \frac{\sigma_{inc}}{4\pi}$$
$$\overline{b}^2 = \frac{\sigma_{coh}}{4\pi}$$
$\theta = \theta_s/2$ $\quad\theta_s$ = scattering angle

$\mu = M/m$ $\quad$ M = target atom mass $\quad$ m = neutron mass (A2.3)

$f = L_2/(L_1 + L_2)$ $\quad L_1$ = source to target flight path

L_2 = target to detector flight path

n: the energy dependence of the incident spectrum

$$n = \frac{1}{E\phi(E)} \frac{\partial\phi(E)}{\partial E} \qquad \text{(A2.4)}$$

$\overline{K}$: average kinetic energy of the sample atoms

E_o: energy of elastically scattered neutrons at the Q of interest

Q_e: elastic wavevector transfer.

$G^D(r,0)$: the distinct atom Van Hove correlation function. Its value and structure are unnecessary for making comparisons for vanadium, which has a coherent scattering cross section equal to zero.

Characteristic of TOFD Unit of CP-5

$L_1 = 12"$

$L_3 = 135"$

$f = .918$ (assume $f = 1$)

$f = 1$

$\theta_s = 90^o \rightarrow \theta = 45^o$

$$E_o = \frac{h^2}{2m} \frac{Q^2}{(2\sin\theta)} \rightarrow \quad E_o[\text{meV}] = 1.0359\ Q^2[\text{Å}^{-1}]^2 \qquad \text{(A2.5)}$$

Characteristics of Vanadium

$\mu = \frac{M}{m} = 51$

$\overline{b}^2 = 0$ (coherent x sec $\sim$ 0)

$\overline{K} = 39.7$ meV (from Vanadium model, $\overline{K} \sim 3/2$ kT)

Characteristics of Source Spectrum

Sinclair and Wright characterized their linac pulsed source spectrum by the functional form of $\phi(E) \propto 1/E^n$ where n varies with energy. If the actual source spectrum is known n can be evaluated for any energy.

$$n = \frac{1}{E\phi(E)} \frac{d\phi(E)}{dE}$$

This method of characterizing a source is convenient for pulsed sources with thin moderators, because above a certain energy n becomes a constant. They determined that for their source at E > 300 meV, n = .83. In the lower energy region, the spectrum of a pulsed source is Maxwellian and thus should be similar to the spectrum of a reactor. Therefore as long as the energy is in the thermal region a rough characterization of the reactor spectrum, may be made from the graph (S&W Fig. 3) of n(E). At E = 103 meV we determine from S&W Fig. 3 that n = 1.8.

Evaluation of (A2.2) and Comparison to Path Integration Method

We will first evaluate S&W Eq. 29 (A2.2) at a wave vector transfer of 10Å^{-1} using the previously determined parameters and relations.

$$Q = 10\text{Å}^{-1} \rightarrow E_o = 103.6 \text{ meV} \quad \text{(from A2.5)}$$

$$I(Q_e)' = \frac{I(Q_e)}{\bar{b}^2} = \{1 - \frac{1}{51}[3.6] + 0 + \frac{(21.16)\bar{K}}{3*51E_o} = .983 \qquad (A2.6)$$

It should be pointed out that the dependence on n tends to cancel out for this particular arrangement. This can be observed by carrying out the same calculation as above except with n = 1, and then comparing the result with (A2.6). We find for n = 1, $I(Q_e)' = .986$.

The result obtained from the path integration method that is the equivalent of $I'(Q_e)$ is

$$\frac{\int_{\text{Inst. Integration Path}} S(Q,\varepsilon)d\varepsilon}{\int_{\text{Const Q}} S(Q,\varepsilon)d\varepsilon}$$

which we will designate as $J(Q_e)$.

For the same conditions as designated before and also with $Q = 10\ \text{Å}^{-1}$ we find $J(Q_e) = .96$. A comparison of $I'(Q_e) = .983$ to $J(Q_e) = .96$ shows reasonable agreement as to the magnitude of the inelastic scattering correction. We see that these quantities are close to unity and therefore the effect of inelastic scattering is small.

We will now carry out the comparison at $Q = 2.1\ \text{Å}^{-1}$. To attempt the S&W formalism to $E_o < 100$ meV (and the related small Q) is stretching the Placzek development. It is also a miscarriage of the 1/v detector law. The results may nevertheless be of interest. For $Q = 2.1\ \text{Å}^{-1}$ we find $E_o = 4.56$ meV. At this energy E_o is

clearly not less than the level spacing $\Delta = \epsilon_{max} \sim 30$ meV.

We will temporarily ignore this constraint. The quantity n is chosen to be n = -1 because at these low energies the neutron spectrum is approximately proportional to E. Thus

$$\phi(E) \alpha \frac{E}{E_T^2} \exp(-E/E_T) \alpha E = 1/E^{n=-1}$$

for $E/E_T << 1$, where E_T is approximtely the mean thermal energy of the reactor. Under these conditions we find $I'(Q_e = 2.1\ \text{Å}^{-1}) = 1.018$ which we compare to $J(Q_e = 2.1\ \text{Å}^{-1}) = 1.054$. The comparison does not show close agreement, but considering the aforementioned restrictions, the results may be considered to be similar.

Finally, we do the comparison at $Q = 20\ \text{Å}^{-1}$. In the large E limit, the value of n(E) as graphed by S&W is inappropriate for the Maxwellian neutron energy distribution produced by a reactor. We may estimate the value of n by assuming a Maxwellian distribution with characteristic energy $E_T = 25$ meV. By setting

$$\frac{d}{dE}\left[\frac{E}{E_T^2} \exp(-E/E_T)\right] = \frac{d}{dE}\left[\frac{1}{E^n}\right]$$

and solving for n at a value of E = 414 meV (which correspond to $Q = 20\ \text{Å}^{-1}$) we find $n \underline{\sim} + 2.5$.

This analysis leads us to the result of $I'(Q_e = 20\ \text{Å}^{-1})$ = .924, which we may compare with $J(Q_e = 20\ \text{Å}^{-1})$ = .931. These two values are in amazingly good agreement.

The overall result of these comparisons is that the corrections are in the same general directions in the two models. The agreement breaks down most in the limit of small E. This is reasonable as the Placzek derivation is not designed for this region and also because the 1/v detector law assumed by S&W is in severe error at this energy.

References

Bellissent, R. and Tourand, G., Journal de Physique, No. 12, Tome 37, p. 1423 (1976).

Bischoff, F.G., "Generalized Monte Carlo Methods for Multiple Scattering Problems in Neutron and Reactor Physics," Ph.D. Thesis, Rensselaer Polytechnic Inst., 1970.

Breitling, G. and Richter, H., Mater Res. Bull., 4, 19 (1969).

Brillouin, L., Wave Propagation in Periodic Structures, (Dover, New York, 1953) (1946).

Carlson, D.E. and Wronski, C.R., Appl. Phys. Lett. 28, 671 (1976).

Carpenter, J.M., Nucl. Inst. & Methods 47, 179 (1967).

Carpenter, J.M. and Sutton, J.D., Nucl. Inst. & Methods 99, 453 (1972).

Carpenter, J.M., Mueller, M.H., Beyerlein, R.A., Worlton, T.G., Jorsensen, J.D., Brun, T.O., Watanabe, N., Kimura, M. and Gunning, J.E., "Neutron Diffraction Measurements on Powder Samples Using the ZING-P Pulsed Neutron Source at Argonne National Laboratory," Proceedings of the Neutron Diffraction Conference, Petten, August 5-6, 1975, Reactor Centrm Nederland, RCN-234, p. 192-208.

Carpenter, J.M. and Pelizzari, C.A., Phys. Rev. B 12, 2391 (1975).

Carpenter, J.M. and Pelizzari, C.A., Phys. Rev. B 12, 2397 (1975).

Carpenter, J.M., private communication (1977).

Copley, J.R.D., Comp. Phys. Commun. 7, 289 (1974).

Dore, J.C. and Clarke, J.H., Nucl. Inst. & Methods 136, 79 (1977).

Duggin, M.J., J. Phys. Chem. Solids 30, 1267 (1972).

Egelstaff, P.A., Thermal Neutron Scattering, Academic Press, London, N.Y.

Elliot, S.R. and Davis, E.A., Structure and Excitations of Amorphous Solids, AIP Conference Proceedings #31 (Williamsburg, Va., 1976), p. 117.

Geiling, S. and Richter, H., Acta Cryst. 2, 305 (1949).

Greaves, G. N. and Davis, E. A. "Continuous Random Network Model for Amorphous Arsenic" 12th Int. Conf. on Physics of Semiconductors Stuttgart (B. G. Teubner) (1974).

Greaves, G. N. and Davis, E. A. Phil. Mag. 29, 1201 (1974).

Greaves, G. N.,Davis, E. A. and Bordas, J. Phil. Mag. 34, 265 (1976).

Greaves, G. N., Knights, J. G. and Davis, E. A. "Electronic Properties of Amorphous Arsenic" Amorphous and Liquid Semiconductors edited by J. Stube and W. Brenig (London: Taylor & Francis) (Proc. of 5th Int. Conf., Garmisch) (1973).

Holas, A., Holas J., Maliszewski, E. and Sedlakova, L. Nucl. Inst. & Methods 69, 173 (1969).

Holas, A. Nukleonika 13, 871 (1968).

Joannopoulos, J. D. and Pollard, W. B. Solid State Comm 20, 947 (1976).

Kaplow, R., Strong, S. L. and Averbach, B. L. Phys. Rev. 138A 1336 (1965).

Kelley, M. J., and Bullett, D. W. Solid State Comm. 18, 593 (1976).

Knights, J. Solid State Comm 16 515 (1975).

Knights, J. C. and Mahan, J. E. Solid State Comm. 21, 938 (1977).

Konnert, J. H. and Karle, J. Acta Cryst. A29, 702 (1973).

Krebs, H., J. Non-crystalline Solids 1, 455 (1969).

Krebs, H and Steffen, R. Z. anorg. allg. chem. 327, 224 (1964).

Krogh-Moe, J. Acta Cryst. 9, 951 (1956).

Lannin, J. S., Eno, H. F. and Luo, H. L. Solid State Comm. 25, 81 (1978).

Leadbetter, A. J., Smith, P. M. and Seyfert, P. Phil. Mag. 33, 441 (1976).

Marshall, W. & Lovesey, S. W., Theory of Thermal Neutron Scattering (The International Series of Monographs on Physics) Oxford at the Clarendon Press.

Mueller, M. H. Advances in X-Ray Analysis, Vol. 15, p. Plenum Press, N. Y., (1972).

Mildner, D. F. R., "Neutron Time of Flight Diffraction and Structural Analysis of Glassy Carbon", University of Michigan, Ann Arbor, Michigan, 1974.

Mildner, D. F. R., Pelizzari, C. A. and Carpenter, J. M. Acta Cryst. A33, 954 (1977).

Mildner, D. F. R. and Carpenter, J. M. Acta Cryst. A33, 962 (1977).

Narten, A. H. and Levy, H. A. Science 165, 447 (1969).

Pace, N. G., Saunders, G. A. and Sümengen, Z. J. Phys. Chem. Solids 31, 1467 (1970).

Pelizzari, C. A., Ph.D. Thesis, "Neutron Diffraction and Inelastic Scattering by Vitreous Beryllium Fluoride" University of Michigan, Ann Arbor, Michigan, 1974.

Placzek, G. Phys. Rev. 86, 377 (1952).

Prael, R., private communication (1977).

Rahman, A., private communication (1977).

Reichardt, W. and Rieder, K. H. "Lattice Dynamics of Arsenic" Proc. of Conf. on Neutron Scattering, Gatlinburg, Tenn. June, 1976 CONF-760601-P1, p. 181.

Reynolds, M. B. Trans. Am. Soc. Metals 45, 839 (1952).

Sinclair, R. N. and Wright, A. C. Nucl. Inst. & Methods 114, 451 (1974).

Sjolander, A. Ark Fys 14, 315 (1958).

Smith, P. M., Leadbetter, and Apling, A. J. Phil. Mag. 31, 57 (1974).

Spear, W.E. and LeComber, P.G., Solid State Commun. 17, 1193 (1975).

Spear, W.E., LeComber, P.G., Kinmond, S. and Brodsky, M.H., Appl. Phys. Lett. 28, 105 (1976).

Stohr, H., Z. anorg. allg. chem. 242, 318 (1939).

Turchin, V.F., Slow Neutrons, Daniel Davey & Co., Inc., N.Y., 1965.

Van Hove, L., Phys. Rev. 95, 249 (1954).

Vineyard, G.H., Phys. Rev. 95, 249 (1954).

Vineyard, G.H., Phys. Rev. 110, 999 (1958).

Wick, G.C., Phys. Rev. 94, 1228 (1954).

Wilde, D.L. and Guttman, L., "Computer Modeling of Amorphous Arsenic," Argonne National Laboratory Undergraduate Research Participant Project, unpublished.

Wright, A.C., Advances in Structure Research by Diffraction Methods, Vol. 5, 1974.

Wu, C.T. and Luo, H.L., J. Non-Crystalline Solids 13, 437 (1973/4).

Yarnell, J.L., Katz, M.J. and Wenzel, R.G., Phys. Rev. A 7, 2130 (1973).

Zemach, A.C. and Glauber, R.J., Phys. Rev. 101, 118 (1956).

Zemach, A.C. and Glauber, R.J., Phys. Rev. 101, 129 (1956).

Zernike, F. and Prins, J.A., Z. Phys. 41, 184 (1927).